UNIVERSITÀ DEGLI STUDI DI PADOVA

UNIVERSITA' DEGLI STUDI DI PADOVA

Sede Amministrativa: Università degli Studi di Padova

Dipartimento di Innovazione Meccanica e Gestionale

SCUOLA DI DOTTORATO DI RICERCA IN INGEGNERIA INDUSTRIALE
INDIRIZZO: INGEGNERIA DELLA PRODUZIONE INDUSTRIALE
CICLO XXII

TRIBOLOGICAL PERFORMANCE OF ENVIRONMENTALLY FRIENDLY SOLID LUBRICANT COATINGS FOR SHEET METAL WORKING

Direttore della Scuola: Ch.mo Prof. Paolo F. Bariani
Supervisore: Ch.mo Prof. Paolo F. Bariani
Correlatore: Ch.mo Prof. Stefania Bruschi

Dottoranda: Francesca Borsetto

A mia madre

TABLE OF CONTENTS

ACKNOWLEDGEMENTS

The present work has been carried out under the supervision of Professor Paolo F. Bariani to whom I express my sincerest gratitude.

A special thanks is for Dr. Andrea Ghiotti and Professor Stefania Bruschi who have always being able to support and to give me valuable advises, suggestions and teaching and most of all their friendship.

I would like to thank my colleagues at DIMEG for the friendly and bright atmosphere all through my Phd period.

A thanks is also for the students who contributed with their work to the results here presented.

Last but not least I would like to thank my gorgeous family that had the patient to support me in these years, any goal could not be reached without them

ABSTRACT

In a society becoming more and more conscious of the effect of human activities on environment, it is not possible to neglect impacts caused by manufacturing. Not only environmental but particularly economical and legislative reason oblige industry to respond. Besides, it must be a technological objective to optimize production towards environmental compatibility or cleanness respectively.
Sheet metal forming is assessed to consume quite few energy, related to the weight of a finished component, and to yield a high degree of material efficiency. However due to the earth's decreasing resources and the pollution caused by energy and material consumption further reductions of consumptions are required.
The transformation of energy, material and supplies into a finished or semi-finished piece is only one aspect of metal forming. Besides the piece to be produced, all production steps of material's pre-treatment, forming and post-treatment also produce unwanted and more or less harmfull residual materials and emissions. referring to the forming step oil based lubricants play a key role as they are environmentally hazardous and pose a danger both directly to the production personnel, which are in daily contact with the products. In addition they force to use unhealthy degreasing agents to remove the oil from the formed parts. The possible strategies for how to handle residual lubricants are:

- disposal
- recycling
- reduction
- substitution
- avoidance

Nowadays, the disposal of the exhausted oil is still a very widespread method even if it does not represent an ecologically nor economically attractive solution for the future, but reduction and especially substitution are required wherever possible. Pursuing the reduction/avoidance strategy, in recent years different types of solid lubricant coatings deposited mainly on the tool side have been proposed and their frictional behaviour investigated. Scientific literature presents results from several tests performed on these materials through commercially available friction testers, but they usually reproduce testing conditions far from the real process ones.
Therefore, the objective of the present work is to investigate the friction behaviour of three different types of solid lubricant coatings deposited either on the tool side or on the sheet metal side, under process conditions.
Two different case studies have been analyzed: deep drawing of stainless sheets and hot stamping of quenchable boron high strength steels.
With respect to the first tribological system the friction coefficient μ is determined as function of the main process parameters: normal pressure, sliding speed, tool and sheet metal specimen temperatures by means of an ad hoc experimental device, designed and set-up during the Phd period at The Department of Manufacturing, University of Padova. The results obtained for two different inhorganic coatings (tool side) and two types of organic coated sheet were compared with the performance of a

deep drawing conventional oil (considered as reference). While the inorganic coated dies performed worse than the non coated ones (due especially to their surface morphology) the organic film coated specimens showed a high potential to perform dry sheet metal working operations being their coefficient of friction comparable with the one of the traditional oil.
In the case of the hot stamping process Al-Si coated high strength steel sheet where studied in terms of the film evolution with thermal parameters. The coating tribological performance as function of testing temperature, normal pressure, sliding speed tool surface roughness was investigated by means of high temperature pin on disc test. As main result it was found that the interaction between the testing temperature and the normal pressure did influence the friction at the sheet metal die interface thus allowing an optimization of the process parameters.

SOMMARIO

In una società che diventa sempre più consapevole delle conseguenza che l'attività umana ha sull'ambiente, non è possibile ignorare l'impatto dovuto alle aziende manifatturiere. Queste ultime devono rispondere non solo a delle esigenze ambientali ma anche a degli obblighi di tipo economico e legislativo.
Nello specifico, lo stampaggio di lamiera viene considerato come un processo che consuma non poca energia se viene considerato il peso del componente finito, al tempo stesso si tratta di un processo caratterizzato da un livello elevato di efficienza per quanto riguarda l'utilizzo di materia prima. Nonostante ciò l'esaurirsi delle risorse presenti in natura ed il livello preoccupante di inquinamento causati dal consumo di energia e di materia prima impone un'ulteriore riduzione dei consumi.
La trasformazione di energia, materia prima e utenze in un prodotto finito o semi-finito è solo un aspetto dello stampaggio di lamiera. Oltre al pezzo da realizzare, tutte le fasi di produzione dal pre-trattamento del materiale, alla formatura, al post-trattamento producono anch'esse materiali residui o emissioni non voluti o pericolosi. Con particolare riferimento alla fase di formatura i lubrificanti di tipo liquido giocano un ruolo fondamentale essendo per la maggior parte nocivi nei confronti dell'ambiente e pericolosi da utilizzare da parte del personale. In aggiunta sono necessari agenti sgrassanti, solitamente nocivi, per pulire il pezzo finito. Al fine di ridurre l'impatto ambientale degli olii lubrificanti, e possibili strategie sono:

- smaltimento
- reciclaggio
- riduzione
- sostituzione
- eliminazione

Attualmente la pratica più diffusa è quella relativa allo smaltimento anche se non rappresenta una soluzione vantaggiosa né dal punto di vista economico né dal punto di vista ecologico; la riduzione ed ancora di più l'eliminazione dei lubrificanti liquidi dovrebbero essere perseguite laddove possibile.
Sostenendo una politica di eliminazione negli ultimi anni sono state proposte diverse tipologie di rivestimenti solidi atti alla riduzione dell'attrito nello stampaggio di lamiera. In letteratura si trovano diversi risultati sperimentali relativi al loro comportamento tribilogico, in condizioni però tendenzialmente diverse da quelle tipiche di processo.
Il presente lavoro di tesi si pone pertanto come obiettivo la caratterizzazione tribologica, in condizioni di processo, di tre sistemi di lubrificazione di tipo solido.
Sono stati presi in considerazione due diversi casi industriali, imbutitura di acciaio inossidabile e stampaggio a caldo di acciaio altoresistenziale al boro.
Con riferimento al primo sistema tribologico si è determinato il coeffciiente d'attrito in funzione di pressione normale, velocità di scorrimento, temperatura sia dell'utensile che della lamiera tramite test simulativo di tipo trip drawing. L'attrezzatura sperimentale in grado di realizzare tale tipologia di test è stata interamnente progettata e realizzata durante il periodo di dottorato presso i laboratori del DIMEG, Università di Padova.

I risultati ottenuti per i due rivestimenti di tipo inorganico (CrN, CrN-DLC) depositati sul lato stampo sono stai peggiori di quelli ottenuti con gli stampi non rivestiti e lubrificati solo con olio. Ciò è stato probabilmente dovuto alla morfologia della superficie rivestita che va ottimizzata una volta effettuato il deposito del rivestimento stesso.
Per quanto riguarda i rivestimenti organici, uno in particolar modo, ha dimostrato di essere un ottimo candidato per operazioni di stampaggio a secco dal momento che presenta un coefficiente d'attrito paragonabile a quello dell'olio.
Con riferimento invece al sistema tribologico presente nelle operazioni di hot stamping, si è inizialmente studiata l'evoluzione sia chimica che morfologica del rivestimento Al-Si (depositato sulla lamiera) con i parametri termici di proceeso. Quindi si è analizzato il comportamento tribologico dello stesso in funzione di parametri quali la temperatura di test della lamiera, la pressione normale, la velocità di strisciamento e la rugosità dello stampo. Si è messo in evidenza come l'interazione tra pressione normale e temperatura abbiano un'influenza significativa sull'attrito all'interfaccia lamiera/stampo permettendo così un'ottimizzazione dei parametri di processo.

CHAPTER 1

INTRODUCTION

1.1. Industrial and Scientific background

In a society becoming more and more conscious of the effect of human activities on environment, it is not possible to neglect impacts caused by manufacturing. Sheet metal forming is assessed to consume quite few energy, related to the weight of a finished component, and to yield a high degree of material efficiency. However due to the earth's decreasing resources and the pollution caused by energy and material consumption further reductions of consumptions are required.

Besides the piece to be produced, all production steps of material's pre-treatment, forming and post-treatment also produce unwanted and more or less harmful residual materials and emissions. Referring to the forming step oil based lubricants play a key role as they are environmentally hazardous and pose a danger both directly to the production personnel, which are in daily contact with the products. In addition they force to use unhealthy degreasing agents to remove the oil from the formed parts. Nevertheless surface finish is an important aspect in sheet forming, for this reason scratches, scoring, die pick up and galling should be avoided by proper selection of lubricants and lubrication technique. [1] Unhomogeneousbor poor lubrication can lead to wrinkling and folding, and significant die wear because of the material transfer from the blank to the die as shown in the following image.

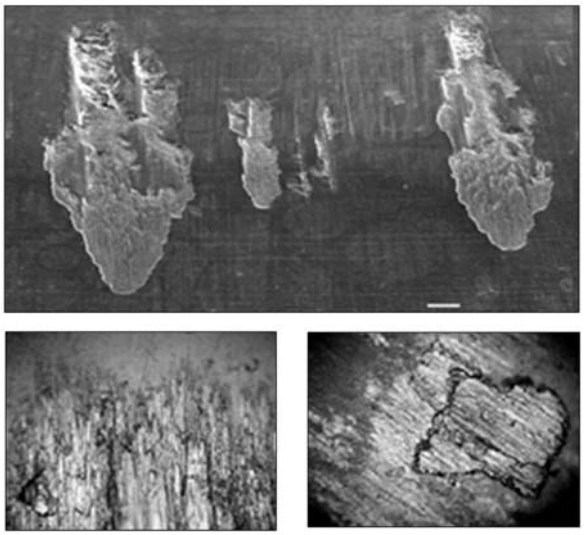

Figure 1.1. *Example of material transfer from the blank to the die.*

The lubrication aspect is even a more critical issue when it comes to sheet metal forming operations carried out at elevated temperature (typically above 300°C). Tribological contacts cannot be lubricated by conventional means, i.e liquid lubricants, since they will rapidly decompose and deteriorate. Thus other types of lubricants must be used such as lamellar structured solid lubricants (e.g. graphite and molybdenum disulphite), self-lubricating surface coatings or even making use of the tribochemical layers (oxides etc.) formed during operation if their properties are beneficial.

Among the possible industrial strategies to be pursued in order to reduce the environmental impact of liquid based lubricants the disposal policy is nowadays the most widespread method even if it does not represent an ecologically nor economically attractive solution for the future. Reduction and especially substitution are required

wherever possible. Pursuing the reduction/avoidance strategy, in recent years different types of solid lubricant coatings deposited mainly on the tool side have been proposed and their frictional behaviour friction was investigated. Scientific literature presents results from several tests performed on these materials through commercially available friction testers, but they usually reproduce testing conditions far from the real process ones.

1.2. Objective and organization of the work

Despite the many works that can be found in literatures, the objective of the present work is to investigate the friction behaviour of three different types of solid lubricant coatings deposited either on the tool side or on the sheet metal side, under process conditions.
Two different case studies have been analyzed: deep drawing of stainless sheets and hot stamping of quenchable boron high strength steels.
With respect to the first tribological system the friction coefficient μ is determined as function of the main process parameters: normal pressure, sliding speed, tool and sheet metal specimen temperatures by means of an ad hoc experimental device, designed and set-up during the Phd period at The Department of Manufacturing, University of Padova. The results obtained for two different inhorganic coatings (tool side) and two types of organic coated sheet were compared with the performance of a deep drawing conventional oil (considered as reference). While the inorganic coated dies performed worse than the non coated ones (due especially to their surface morphology) the organic film coated specimens showed a high potential to perform dry sheet metal working operations being their coefficient of friction comparable with the one of the traditional oil.
In the case of the hot stamping process Al-Si coated high strength steel sheet where studied in terms of the film evolution with thermal parameters. The coating tribological performance as function of testing temperature, normal pressure, sliding speed tool surface roughness was investigated by means of high temperature pin on disc test. As main result it was found that the interaction between the testing temperature and the normal pressure did influence the friction at the sheet metal die interface thus allowing an optimization of the process parameters.

CHAPTER 2

LITERATURE REVIEW

2.1. Fundamentals of tribology

Tribology is the science and technology of interacting surfaces in relative motion. It includes the study and application of the principles of friction, lubrication and wear. The word "tribology" derives from the Greek τρίβω ("tribo") meaning "rub" (root τριβ-), and λόγος ("logos") meaning 'principle or knowledge'.

Historical review

Leonardo Da Vinci (1452-1519) historically was one of the first scholars to study friction systematically. He realized how important friction is for the workings of machines. He focused on all kinds of friction and drew a distinction between sliding and rolling friction. In Figure 2.1 his original sketches for friction experimental set up are shown. Leonardo stated the two basic laws of friction 200 years before Newton even defined what force is. Da Vinci simply stated that:

- the areas in contact have no effect on friction, the frictional resistance was the same for two different objects of the same weight but making contacts over different widths and lengths
- if the load of an object is doubled, its friction will also be doubled.

Leonardo defined a friction coefficient as the ratio of the friction divided by the mass of the slider.

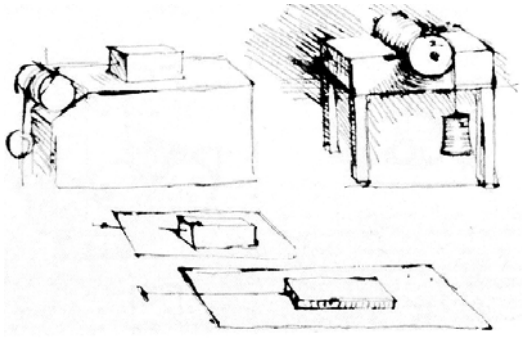

Figure 2.*1*. *Drawings of the tribological experiments suggested of by Leonardo da Vinci.*

Experimentally, he found a universal friction coefficient 0.25 independent of the material. This universal friction coefficient of 0.25 is called Bilfinger value. Many other friction scientists after Leonardo believed in the existence of a universal material independent friction coefficient. However, most of them found another value but all in the range 0.1 - 0.6. Leonardo made the observation that different materials move with different ease. Leonardo Da Vinci did not publish his theories, so he never got credit for his ideas. The only evidence of their existence is in his vast collection of journals.

Guillaume Amontons (1663-1705),rediscovered the two basic laws of friction that had been discovered by Leonardo Da Vinci:

- The force of friction is directly proportional to the applied load. (Amontons 1st Law)
- The force of friction is independent of the apparent area of contact. (Amontons 2nd Law)

Amontons speculated that friction was caused by the interaction of surface roughness peaks. For hard surfaces, he envisioned that the asperities would be forced to slide up and down over one another; for more "elastic" materials, he suggested that the sliding would push aside the surface irregularity peaks. He believed that friction was predominately a result of the work done to lift one surface over the roughness of the other, or from the deforming or the wearing of the other surface. For several centuries after Amontons' work, scientists believed that friction was due to the roughness on the surfaces.

Charles August Coloumb (1736-1806) confirmed Amontons' laws experimentally almost a hundred years after they were first expounded. Coloumb added a third law (Amontons-Coulomb Law) to the already existing Amontons laws:

- Kinetic friction is independent of the sliding velocity

He suggested that friction was caused by mechanical interlocking of asperities and that the actual surface material on the individual asperities was functionless. Although his explanation was wrong, his name lives in quite prominently: the term "Coulomb friction" is still used for dry friction under most conditions (except where heavy plastic deformation is involved, as in bulk metalforming)

F. Philip Bowden and David Tabor in the 40s and 50s, established the basis for understanding friction mechanisms in metals. [2] When two metal surfaces are brought into contact with each other they will touch on their highest points and these areas of contact will grow as the load increases. In a metal working process, the tool is normally very hard and smooth, compared to the workpiece (Figure 2.2.)

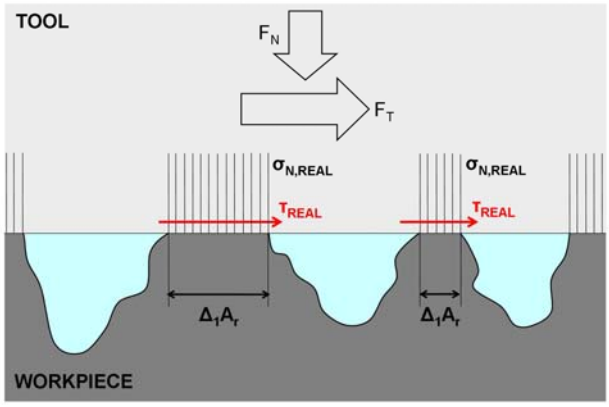

***Figure 2.2**. Real area of contact between smooth, hard tool and rough, soft workpiece.*

The total area of contact A_r is called the real area of contact, to distinguish from the apparent area of contact A_a which is the total, macroscopic tool/workpiece interface.
The stress situation in the flattened asperities is such that a plastic deformation occurs very much in the same way as in a hardness test. In a hardness test of the workpiece, an indenter is forced into the material, and the hardness is measured as the load divided by the horizontal projection of the area or the curved area depending on which hardness definition is used. The value of the hardness is very close to the normal pressure needed to flatten the asperity, namely around HB = $3\sigma_0$ where σ_0 is the material yield stress. At light and moderate loads, the plastic deformation of each

workpiece asperity can be treated individually and so a static equilibrium for the normal force F_N gives:

$$F_N = \sum_{i=1}^{n} \Delta_i A_r * HB = A_r * HB \tag{2.1}$$

Now it is assumed that a tangential force F_T is applied, and that some kind of resistance towards sliding exists on the top of the asperities, Bowden and Tabor assumed an adhesion in this place. This resistance against sliding can be set at f*k per unit area, where f is a constant between 0 and 1and k is the shear strength of the material. Horizontal equilibrium than gives:

$$F_T = \sum_{i=1}^{n} \Delta_i A_r * f * k = A_r * f * k \tag{2.2}$$

For the friction coefficient we get:

$$\mu = \frac{F_T}{F_N} = \frac{A_r * f * k}{A_r * HB} = \frac{f * k}{HB} \tag{2.3}$$

If the normal pressure σ_N and the friction stress τ are calculated from equations (2.1) and (2.2) the following is obtained:

$$\sigma_N = \frac{F_N}{A_a} = \frac{A_r * HB}{A_a} = HB * \alpha \tag{2.4}$$

$$\tau = \frac{F_T}{A_a} = \frac{A_r * f * k}{A_a} = f * k * \alpha \tag{2.5}$$

where α is the ratio between real and apparent area of contact. In the forging processes very high normal pressures occur, pressures reaching 3-4 times the yield stress of the workpiece. For such high pressure α will be a considerable fraction of 1. Then the plastic zones beneath each area of contact will begin to interact, and it will become increasingly difficult to flatten the surface. If a diagram depicting the relative area of contact α as function of normal pressure σ_N is drawn, the result will be the one shown in Figure 2.3 (a). If, equation (2.5) is now used, remembering that f and k are constants, a curve showing the connection between friction stress and normal pressure (Figure 2.3 (b)) can be obtained.

(a) (b)

Figure 2.3. (a) *Relative area of contact as a function of normal pressure.* ***(b)*** *General trend of friction stress versus normal pressure. [2]*

The classical approximations to this curve can be seen in Figure 2.4:

- Figure 2.4(a) shows the oldest friction model, suggested by the French engineer G. Amonton, assuming proportionality between τ and σ_N, which is very well obeyed at normal pressures well below the yield stress of the material.
- Figure 2.4(b) shows a more recent friction model where τ=mk, 0≤m≤1. This has many merits including mathematical simplicity and is often used in theoretical analysis of metal forming problems.
- Orowan introduces the combined model of Figure 2.4(c), where it is assumed that Amonton's law is obeyed when $\mu\sigma_N<k$. If the product of the coefficient of friction and normal pressure reaches the shear strength of the workpiece material, the surface of the workpiece will stick to the tool and the tangential displacement relative to the tool will take place beneath the surface.

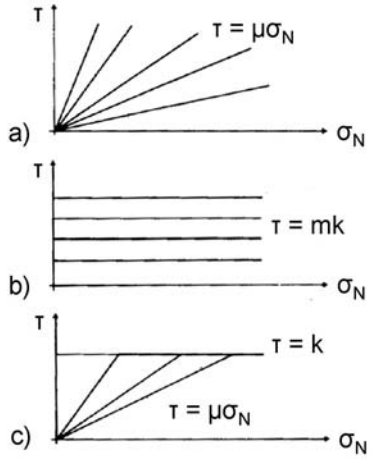

***Figure 2.4**. **a)** Amonton's law **b)** Constant friction law **c)** Orowan's friction model. [2]*

T. Wanheim, N. Bay and Petersen have suggested a friction model that takes the more complicated behaviour of Figure 2.4 into account. This is based on a slipline field analysis of ridge asperities (Figure 2.5) where the shape of the slipline field depends on friction factor f describing the tangential stress on top of each asperity. From such slipline fields the graphs in Figure 2.6 can be constructed, showing the real area of contact as a function of the normal pressure and the nominal friction stress and τ/k as function of the normal pressure and the friction factor.

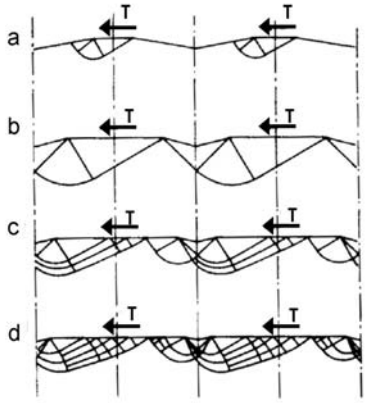

***Figure 2.5.** Slipline fields of flattened asperities in sliding against tool. [2]*

It can be seen from Figure 2.6 that α increases proportionally with σ_N/σ_0, as long as σ_N/σ_0 is below a certain value. This limit is marked by the dotted line, which is roughly approximated by σ_N/σ_0=1.5. Furthermore α approaches unity asymptotically as σ_N/σ_0 increases, and approaches this value faster for a higher friction factor.

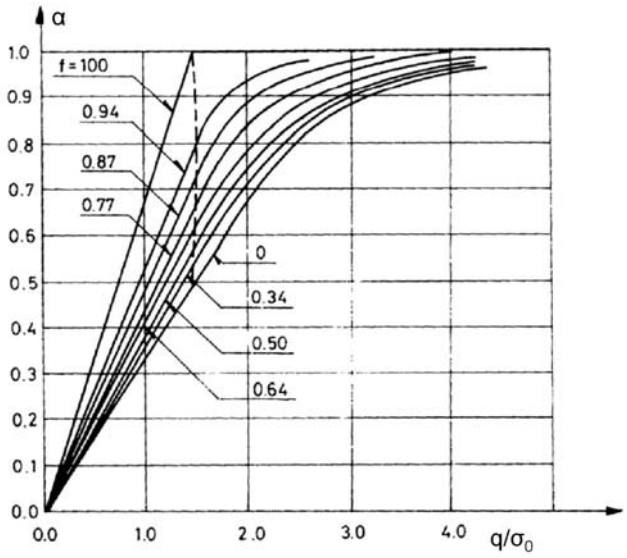

***Figure 2.6**. Real area of contact as a function of the normal pressure. [2]*

In Figure 2.7 the nominal friction stress is plotted as function of the normal pressure. The limit of proportionality between τ/k and σ_N σ_0 is represented by the dotted line. It is seen that τ increases with increasing σ_N/σ_0 and approaches a limiting value asymptotically. This limit is given by:

$$\tau/k = f \tag{2.6}$$

For low normal pressures Amonton's law applies, and for high normal pressures the law of constant friction stress is valid. It is noted that τ = f*k.
The intermediate pressure range $1.5<\sigma_N/\sigma_0<3$, which is of special interest in many forging operations, is a transition range where neither of the two friction laws apply.
The model can be defined by the following equations. The limit of proportionality between friction stress and normal stress:

$$\frac{\tau}{k} = (1-\sqrt{1-f}) \tag{2.7}$$

$$\frac{\sigma_N'}{\sigma_0} = \frac{2+\pi+2\arccos(f)+2\sqrt{1-f^2}}{2\sqrt{3(1+\sqrt{1-f}}} \tag{2.8}$$

The friction curves can be approximated by:

$$\frac{\tau}{k} = (1-\sqrt{1-f})\,\frac{\sigma_N/\sigma_0}{\sigma_N'/\sigma_0} \qquad \text{for } \frac{\sigma_N}{\sigma_0} < \frac{\sigma_N'}{\sigma_0} \tag{2.9}$$

$$\frac{\tau}{k} = \frac{\tau'}{k} + (f - \frac{\tau'}{k})\ 1 - \exp(\frac{\sigma'_N/\sigma_0 - \sigma_N/\sigma_0) * \tau'_0/k}{(f - \tau'/k)\sigma'_N/\sigma_0}) \qquad \text{for } \frac{\sigma_N}{\sigma_0} > \frac{\sigma'_N}{\sigma_0} \tag{2.10}$$

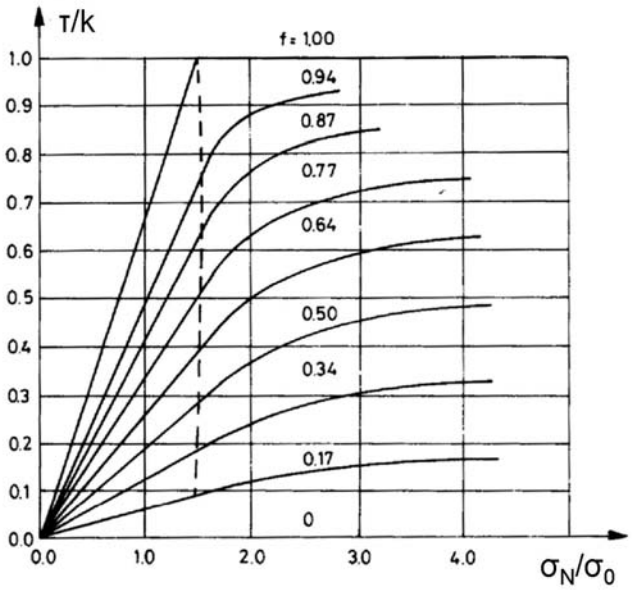

Figure 2.7. *Nominal friction stress τ/k as a function of the normal pressure and the friction factor.[2]*

2.2. Nature of surfaces

Friction is caused by forces between the two contacting bodies, acting in their interface. These forces are determined by two factors besides the load; the *properties* of the contacting material and the *area* of contact. The friction forces are usually not directly predictable because both of these factors depend very much on the particular conditions. For example, the properties may be significantly different than expected from bulk values because the surface material is deformed, contains segregations, is covered by an oxide layer, and so on. Also, the real area of contact is usually much smaller than the apparent area of the bodies because real surfaces are not smooth on an atomic scale. Because of this close dependence of friction on the surface topography and on the properties of the surfaces and the near-surface layers, a brief discussion of the relevant characteristics will be presented. [3]

2.2.1. Surface topography

The geometric shape of any surface is determined by the finishing process used to produce it. There will be undulations of wavelengths that range from atomic dimensions to the length of the component. These often result from the dynamics of the particular finishing process or machine used. There may be additional peaks and valleys caused by local microevents such as uneven deformation of hard microstructural constituents, local fracture, or corrosive pitting. Even after a surface has been carefully polished, it will still be rough on an atomic scale. It is useful to distinguish among macrodeviations, waviness, roughness, and microroughness relative to an ideal flat surface (Figure 2.8).

Macrodeviations are errors from irregular surface departures from the design profile, often caused by lack of accuracy or stiffness of the machine system.

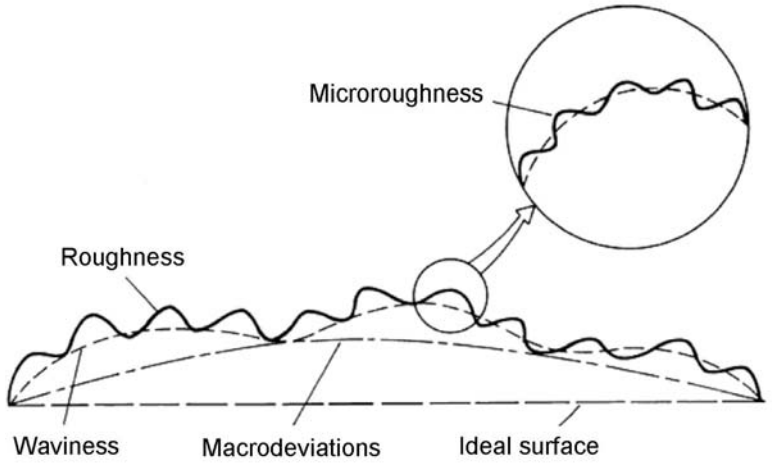

***Figure 2*.8.** *Schematic showing selected types of surface deviations relative to an ideal solid surface. [3]*

Waviness is periodic deviations from geometric surface, often sinusoidal in form and often determined by low-level oscillations of the machine-tool-workpiece system during machining. Typically, wavelengths range from 1 to 10 mm and wave heights from a few to several hundred micrometers

Roughness is the deviations from the wavy surface itself, caused by geometry of the cutting tool and its wear, machining conditions, microstructure of the workpiece, vibrations in the system, and so on. Surface roughness changes as a surface goes through the wearing-in process, but may then stabilize.

Microroughness is finer roughness super-imposed on the surface roughness. It may extend down to the near-atomic scale and may be caused by internal imperfections in the material, nonuniform deformation of individual grains at the surface, or corrosion and oxidation processes that occur while the surface is being generated or during its exposure to the environment.

2.2.2. Composition

A surface is usually not completely clean, even in a high vacuum. Some of the events that can take place at surfaces are segregation, reconstruction, chemisorption, and compound formation (Figure 2.9).

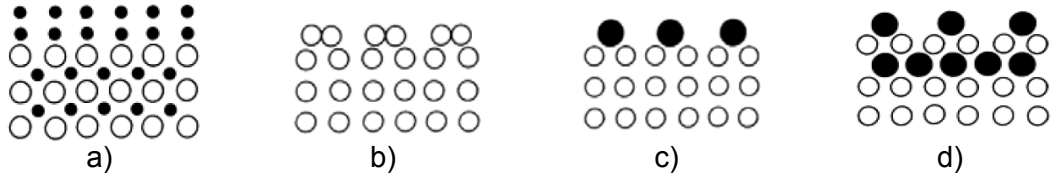

***Figure 2.9**. Effect of composition on surface roughness defects. **(a)** Segregation**, (b)** Reconstruction, **(c)** Chemisorption, **(d)** Compund formation. [3]*

Segregation of alloy species to grain boundaries is a well-known phenomenon that may profoundly affect mechanical properties (Figure 2.9(a)). Segregation to the surface may also take place. This generally occurs for small, mobile alloy or impurity atoms, such as interstitial carbon and nitrogen in iron, during processing or heat treatment. In some cases, the segregation of as little as 1 at.% of alloy element to the surface can completely dominate adhesion between contact surfaces. Significant changes in friction properties have been observed for ferrous surfaces with segregation of carbon, sulfur, aluminum, and boron, and for copper surfaces with segregation of aluminium and indium. The nature of the changes friction due to surfaces segregation depends on the nature of the changes that the specific segregation in question causes in surface mechanical properties, adhesion, oxide film formation, and so on. For example, if certain metallic glasses containing boron are tested at increasing temperature, μ increases first with temperature, from about 1.0 - 1.5 at room temperature to 1.8-2.5 at 350°C. Above 500°C, drops drastically (to about 0.25), a change that has been associated with the formation of boron nitride on the surface.

Reconstruction takes place when the outermost layers of atoms undergo a change in crystal structure (Figure 2.9(b)). Examples include evaporation of silicon from a SiC surface upon heating, leaving behind a layer of carbon, and conversion of diamond surface layers to graphite or carbon during rubbing. Reconstruction may result in substantial changes in friction coefficient, but the fact that reconstruction has taken place may be evident only after careful characterization of the surface layers.

Chemisorption readily occurs on clean surfaces (Figure 2.9(c)). Adsorbed species include water molecules from atmospheric moisture and carbon compounds also derived from the atmosphere or from lubricants used during operation or manufacture. The adsorbed species may also be components of various salts originating from the environment of from human handling of the component. The amount of adsorbed species, the degree of surface coverage, and the nature of the adsorbed molecule can substantially affect the adhesion between two surfaces, thereby directly or indirectly influencing friction behaviour. For example, when a monolayer of ethane is introduced on a clean iron surface, the adhesive force drops from a value of greater than 400 dynes to 280 dynes. If the monolayer is acetylene force drops to 80 dynes. For a vinyl chloride monolayer, the force drops to 30 dynes that is to only 7 to 8% of the value for the clean surface.

Chemical compound formation may take place when surface comes into contact with a different solid, a gas, or a chemisorbed species. Without any tribological contacts, a surface will readily acquire a layer of oxide or hydroxide due to reactions with ambient moisture and oxygen. When two surfaces rub against each other, they may adhere at local spots that can reach elevated temperatures by frictional heating; interdiffusion may then take place, resulting in local compound formation in the surface layers (Figure 2.9(d)). This can strongly affect friction. It is well known, for example, that friction between two metals that can form alloy solutions or alloy compounds with each other generally is greater than if the two are mutually insoluble. This fact has been used by Rabinowicz to develop a generalized "map" showing which metals can safely slide against one another and which metal couples should be avoided (Figure 2.10).

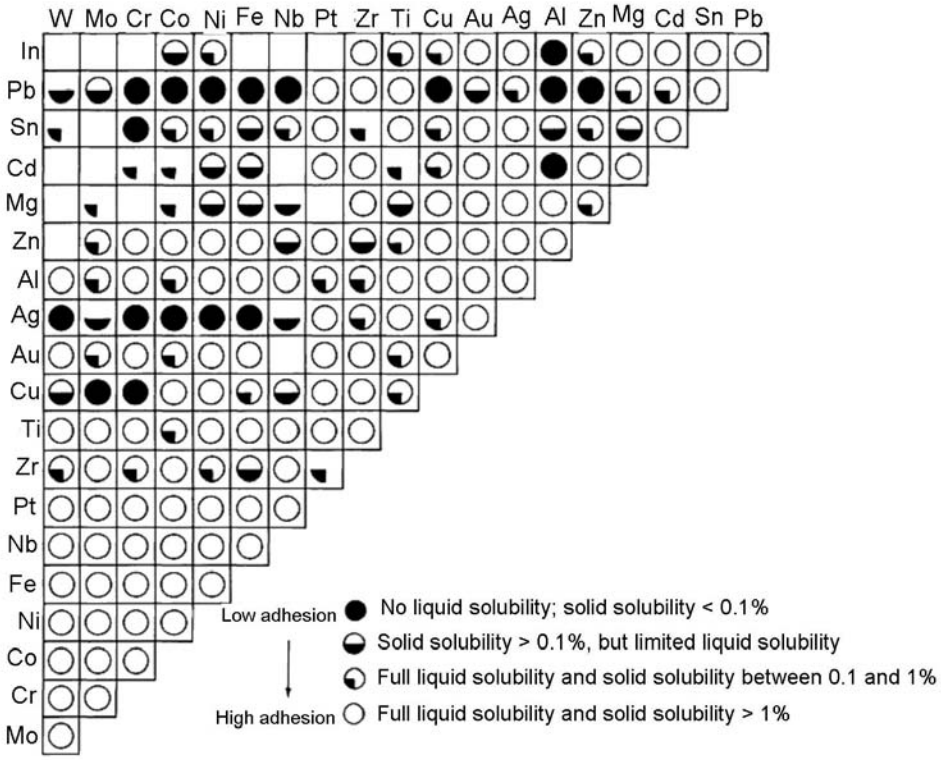

Figure 2.*10*. *Compatibility chart developed by Rabinowicz for selected metal combinations derived from binary equilibrium diagrams. [3]*

2.3. Tribology in sheet metal forming

In the case of metal forming operations, tribological effects appearing in the tool/workpiece interface are subjected to relative sliding, contact pressures, thermal energy transfer and metallic adhesion mechanisms [4]. When considering the presence of a lubricant, additional considerations regarding chemical reactions, lubricant retention and permeation should be taken into account (Figure 2.11).

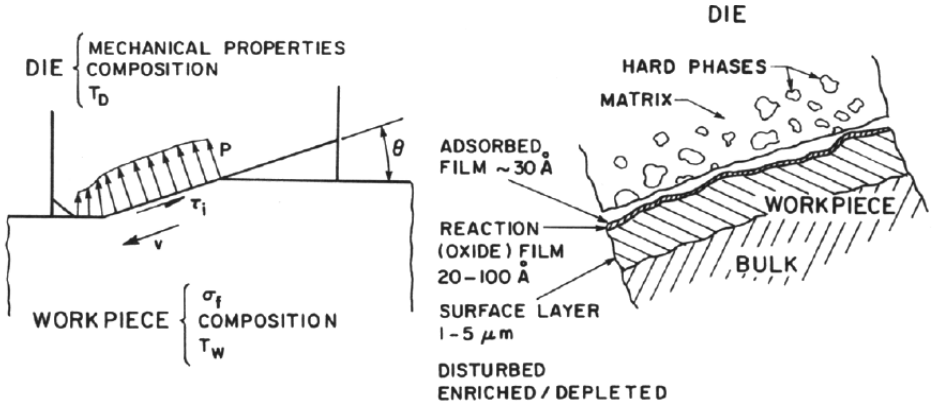

Figure 2.11. a) *Macroscopic and* ***b)*** *microscopic schematic of the contact boundary between tool and workpiece in a metalforming operation [5]*

In the case of metalworking operations the formation of new fresh and chemically very active, virgin workpiece surfaces due to surface expansion caused by material plastic deformation represents an exceptional tribological condition. [5,6] The freshly exposed metal may be very reactive especially in cases, where high contact pressures occur at the interface sealing off the access of oxygen, thus impeding oxide layer formation. This can cause cold welding between the two contacting surfaces, which is usually avoided by the presence of a lubricant. Consequently the role of a lubricant is mainly to prevent the contact between “old” and “new” surfaces with tools. The lubricant ability of separating the contacting surfaces has significant consequences in terms of final product quality, wear and thermal loads on tool, energy requirements and in some cases the very possibility of the plastic deformation. To fully understand the mechanisms in metalworking tribology the contact interface between tool and workpiece at the microscale should be examined. [4] The workpiece surface usually consists of peaks and valleys while the tool counter face is typically ground and often polished thus appears smother then the former.
Different conditions may appear at the interface as a consequence of the microstructure in terms of directionality and magnitude, which has a decisive influence on establishing and sustaining a lubricant film.
In order to avoid too severe tribological conditions, surfaces should be held as far apart as possible. This is generally done by metalworking lubricants, which may be solid, semisolid or liquid-based lubricants.

2.4. Fluid film lubrication

The choice of an appropriate lubricant depends on system needs and cost, as well as on health, safety, and environmental considerations. Lubricant properties depend on the base oil (or blend of base oils) and on any additives that are used. Additives are chemicals that enhance the properties of an oil. They are added to base oils in concentrations that range from the order of tens of ppm to as much as 25%. Additives generally fall into three groups: polymers, polar compounds, and compounds containing active elements, such as sulphur and chlorine.
Viscosity is the most important property characterizing the performance of a liquid based lubricant. It is a measure of the resistance of a fluid which is being deformed by either shear stress or extensional stress. It relates directly to the ability of the lubricant to separate relative sliding surfaces and often correlates with other performance characteristics. In general, in any flow, layers move at different velocities and the fluid's viscosity arises from the shear stress between the layers that ultimately opposes any applied force (Figure 2.12).
Isaac Newton postulated that, for straight, parallel and uniform flow, the shear stress, τ, between layers is proportional to the velocity gradient, $\partial u/\partial y$, in the direction perpendicular to the layers:

$$\tau = \eta \frac{\partial u}{\partial y} \tag{2.11}$$

where η is the dynamic viscosity expressed in Ps s according to the SI system. The cgs physical unit for dynamic viscosity is the poise (P), named after Jean Louis Marie Poiseuille. It is more commonly expressed, particularly in ASTM standards, as centipoise (cP): 1 P = 1 $g \cdot cm^{-1}s^{-1}$.

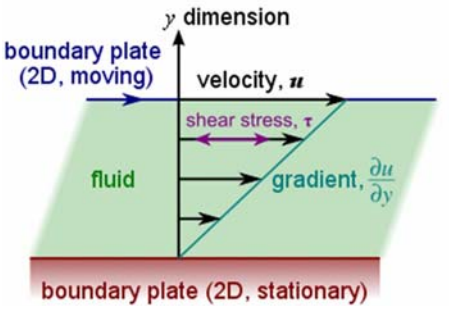

Figure 2.12. *Viscosity scheme. 76]*

The kinematic viscosity is instead defined as the ratio between η and the fluid density ρ:

$$v = \frac{\eta}{\rho} \tag{2.12}$$

The cgs physical unit for kinematic viscosity is the stokes (St), named after George Gabriel Stokes. It is sometimes expressed in terms of centistokes (cSt or ctsk). In U.S. usage, stoke is sometimes used as the singular form:

1 St = 1 $cm^2 \cdot s^{-1}$ = 10^{-4} $m^2 \cdot s^{-1}$.

1 cSt = 1 $mm^2 \cdot s^{-1}$ = $10^{-6} m^2 \cdot s^{-1}$.

The viscosity of oils depends strongly on temperature as shown in Figure 2.13. The rate of change with temperature depends primarily on viscosity level, varying from about 0.5%/°C for a 1mm^2/s (1cSt) oil to about 6-10°C%/°C for 105 mm^2/s (105 cSt). The dependence of viscosity on temperature can be represented over a considerable range of temperature by the MacCoull-walther equation:

$$\log [\log (cSt + 0.7)] = A - B (\log T) \tag{2.13}$$

where A and B are constants and T is the absolute temperature in units of Kelvin. The constant 0.7 is valid for viscosities ranging from 210^7 down to 2m^2/s. The constant increases as viscosity decreases below this latter value.

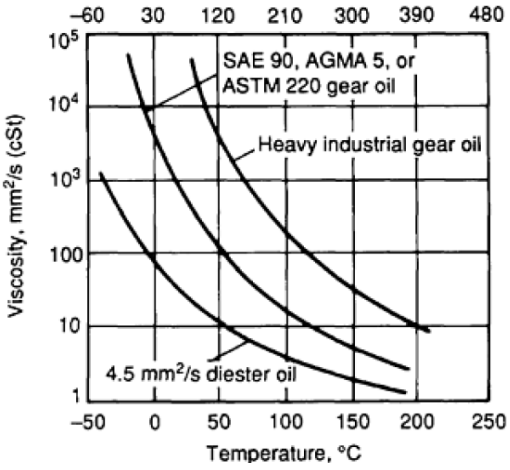

Figure 2. 13*. Viscosity-temperature dependence. [3]*

Pressure increases viscosity, and the effect becomes appreciable for mineral oils at pressure above the order of 10 MPa. Classically the barus equation expressed the pressure effect:

$$\eta_{t,P} = \eta_{t,0} e^{\alpha P} \qquad (2.14)$$

where P equals the gage pressure, $\eta_{t,P}$ equals the dynamic viscosity at temperature T and gage pressure P, $\eta_{t,0}$ equals the dynamic viscosity at temperature T and atmospheric pressure, and α is the viscosity-pressure coefficient.

2.4.1. Lubrication regimes

Basically, four regimes of lubrication are relevant to metalworking processes and shift between different lubrication mechanisms is well explained by the so-called Stribeck-curve (Figure 2.14). The curve shows the relation between coefficient of friction μ as function of the parameter H=(ηv/p), where η is the lubricant viscosity, v the relative velocity and p the contact pressure. The H parameter is often referred as the Hersey or Sommerfield parameter. the corresponding lubricant film thickness is also shown.

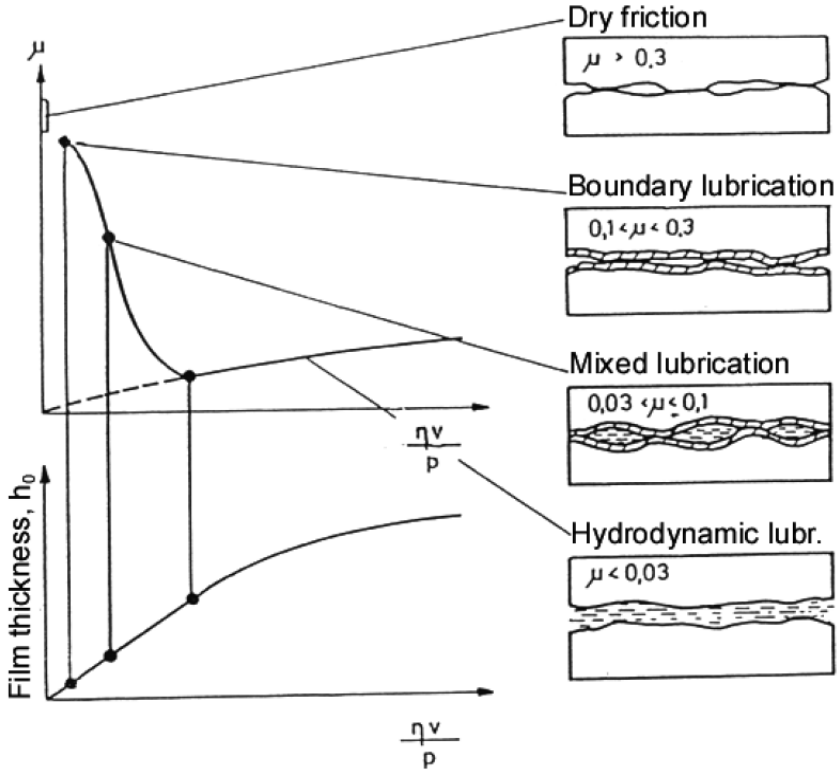

Figure 2.14. *The Stribeck curve. [4]*

- **Thick film** [3]: The surfaces are completely separated by a fluid film having a thickness h_0 about one order of magnitude greater than the surface roughness ($h_0 >> R_a$); thus there is no metal to metal contact. The film is thick enough to cause complete separation of the surfaces, relative motion occurs by shearing of the fluid film and the resisting force is that caused by the lubricant viscosity. A thick lubricant film can be generated by tangential and normal relative motion between two surfaces. this

mode is known as hydrodynamic lubrication. The effectiveness of such lubrication depends directly on relative speed and lubricant viscosity. For highly loaded contacts, elastic deformation of the surfaces can redistribute and broaden the contact area and lubricant pressure, thus greatly increasing the load capacity and lubricant film thickness compared with those generated by rigid contact. Such thick-film lubrication resulting from the surface flattening effects of elastic deformation is known as elastohydrodynamic lubrication (EHL). In many metalforming operations, a thick lubricant film can also be formed at the interface between the rigid die surface and the plastically deformed surface of the workpiece. This mode of thick-film lubrication is often referred to as plastohydrodynamic lubrication (PHL).

Hydrodynamic lubrication

When fluid lubricant is present between two rolling and/or sliding surfaces, a thick pressurized film can be generated by the surfaces velocities to reduce friction and wear. Hydrodynamic film thickness can be formed by wedging the lubricant through a convergent gap with the tangential surface velocities, known as wedging film action, or by squeezing the lubricant out of contact area with the relative normal velocity between the contacting surfaces, known as squeeze film action. A pure hydrodynamic lubrication strongly relies on continuous high sliding velocities and subsequently pressures and temperatures remain low. Hence the mechanism only appears in case of ideal conditions. The coefficient of friction is low, usually ranging from between 0.001 and 0.02.

Elastohydrodynamic lubrication

When lubricant pressure causes elastic deformation of the surfaces that is on the same order as the lubricant film thickness, the influence of deformation on lubrication performance becomes a significant parameter. Contacts operating under this condition are in the regime of elastohydrodinamic lubrication (EHL). In EHL, lubricant film thickness is the most important variable. It is formed by the wedging action at the inlet region between an elastically deformed contact under a steady load. As in hydrodynamic lubrication, it increases with speed, lubricant viscosity and decreases with load.

Plastohydrodynamic lubrication

In metalworking processes, a thick lubrication film can be generated hydrodinamically between the workpiece and the die to control friction and wear. The lubrication behavior between a rigid surface and a plastically deformed surface is known as plastohydrodynamic lubrication. The discovery of this mechanism was only realised in the early eighties by Japanese researchers. It was found, that in a special case of mixed lubrication, permeation of lubricant occurred in the microstructure of a surface by dragging lubricant from reservoirs to flatten asperity plateaus. This implies that the surrounding contact pressure can be exceeded by the pressure acting on the edges of the lubricant pockets thus the lubricant move from high to low pressure occurring on the asperity plateaus. As a result, a very thin lubricant film separate the asperities from the tool surface, hence shear stress in these regions does not appear. The important factors controlling the micro-plasto mechanisms are geometry of lubricant reservoirs, viscosity, sliding velocity and the appearing pressure gradients across the individual lubricant pockets. [4,8]

- **Thin film/Mixed lubrication** [3]: as the normal load increases, or as the speed and viscosity of the fluid decrease, the film thickness is reduced to about three to five times the surface roughness. There may be some metal-to-metal contact at the higher asperities; this contact increases friction and leads to slightly higher wear. The load is shared by the hydrodynamic pressure and the asperity contact pressure. For this reason, thin-film lubrication is sometimes referred to as mixed, partial hydrodynamic or elastohydrodynamic lubrication.

The boundary between the thick-film and the thin-film regimes can be identified by a film parameter: Λ, the ratio of the average lubricant thickness to the composite surface roughness, for surfaces with a Gaussian height distribution. Λ=3 separates the thick-film and thin-film regimes. The thin-film and boundary lubrication regimes are separated more conveniently by the load ratio, that is, the ratio of the load borne by the fluid pressure to that borne by the asperity contact pressure. Because of the presence of asperity contacts in thin-film lubrication, the lubrication variables, including film thickness, pressure, shear stress, and surface temperatures, are no longer well-behaved, but instead contain local fluctuations caused by the asperity interactions. The tribological integrity of thin-film lubrication depends on how well the asperities are protected by various modes of lubrication. Figure 2.15 shows that sliding asperities are protected by three types of lubricating films:

- Micro-EHL and friction polymer films
- Physically adsorbed and other surface films
- Oxide films

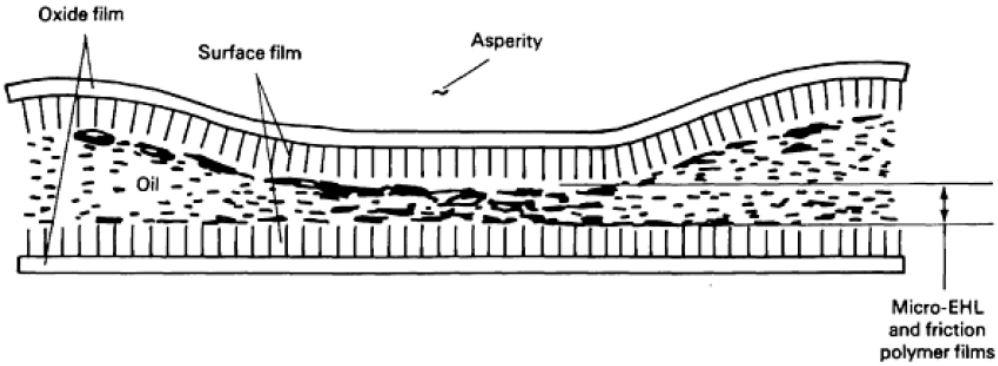

***Figure 2.15**. Three layer lubricating film that typically protects an asperity from friction and wear. [3]*

Micro-EHL and friction polymer films.

A very thin film of oil can be developed at the asperities of an EHL contact by the normal approaching action of an asperity at the entrance region of conjuction, by the sliding action of the asperity within the conjuction, and by collision between two sliding asperities. Such films are known as micro EHL oil films. If the geometry of these contacts can be approximated as ellipsoidal tips, these thin oil films can be estimated using existing macro-EHL theories. The thickness of a micro-EHL film is critically dependent on the lubricant viscosity around the asperity tips. If this viscosity is greatly enhanced by high lubricant pressure generated by the macro-EHL action, then an effective micro-EHL film can be generated otherwise, the micro-EHL oil film will be too

thin. For most mineral oils, the average lubricant pressure must reach approximately 300 to 500 MPa to generate an effective micro-EHL film for protection against scuffing.
Another type of polymeric film can also be generated when the asperity temperature becomes excessive because of heating from the sliding friction. This type of film is known as frictionally induced polymeric film. In this process the lubricant undergoes a primary oxidation and forms a product that, under further oxidation, can polymerize into high molecular weight polymers. The polymeric film offers additional protection, but continues to polymerize and finally becomes insoluble sludge and deposit, impeding lubrication.

Physically adsorbed and other surface films
A nanolayer or multilayer surface film is formed by adsorption of polar lubricant molecules onto the surface, providing an effective barrier against metal-to-metal contact. This process is reversible. At high temperatures, the adsorbed molecules return to the bulk fluid. When the temperature is lowered, the molecules again become adsorbed on the surface.
The effectiveness of the physically adsorbed surface film ceases when the asperity temperature reaches a level at which desorption dominates the process. For most mineral oils, the critical surface temperature at which half of the surface becomes desorbed is around 150°C. This critical surface temperature appears to depend on the ambient pressure around the sliding asperities (Figure 2.16). The breakdown of a physically adsorbed surface film generally occurs when the fractional coverage of the adsorbate drops below 0.5.

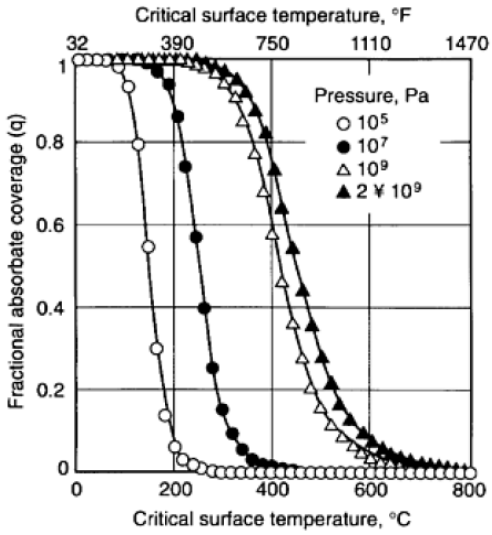

***Figure 2.16**. Plot of fractional adsorbate coverage versus critical surface temperature as a function of lubricant pressure. [3]*

In addition to adsorbed surface films, other types of surface films can be generated by chemisorption and chemical reaction of the surface with lubricant additives.

Oxide films
They are formed by oxidation of the surface with oxygen present in the atmosphere or dissolved in the lubricant. The breakdown mechanism of oxide films by gradual

depletion or by sudden transition from mild to severe wear are only partially understood. The critical condition for transition from mild to severe wear wear appear to be associated with critical speed rather than a critical load.

- **Boundary lubrication** [3]. Boundary lubrication lies in the regime of extremely low Λ for case of very low speed, low viscosity, and very high load. In this regime, the frictional coefficient is usually insensitive to speed, viscosity or load. The load is totally supported by the asperity contact. Friction and wear behavior is completely governed by any film that happens to be on the surface, either planned or unplanned. Depending on the boundary film thickness and its strength, the friction coefficient ranges from about 0.1 to 0.4. Three types of surface films are commonly known to be effective in boundary lubrication: physically adsorbed, chemically adsorbed, and chemically reacted surface films. Adsorbed films are usually monomolecular and have thickness in the range of nanometers. Reactive films can be quite thick and are much more stable and durable than adsorbed films. they are enhanced by the additives in the base lubricants that form sulfides, chlorides, or phosphates with the solid surfaces, providing effective surface films for protection of sliding asperities under extreme conditions

In sheet metal forming operations, deformation takes place typically by biaxial tensile stresses and, unlike in bulk deformation processes, it involves minor changes in thickness except in ironing. The forming speeds are relatively low, as are contact stresses; however, there can be considerable relatively sliding and the contact area at the die-workpiece interfaces can be very large. [1] In most sheet forming processes the prevailing lubrication mechanism is of boundary lubrication, mixed or micro-plasto hydrodynamic lubrication thus depending on the topography and contact pressure. Figure 2.17 summarises the different regimes. [4]

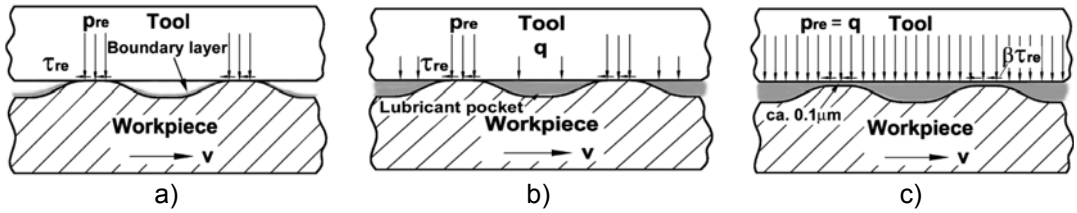

Figure 2.17. *Typical regimes of lubrication in metal forming:* ***a)*** *Boundary lubrication,* ***b)*** *mixed boundary-hysrostatic lubrication and* ***c)*** *micrp-plasto hydrodynamic lubrication. [4]*

2.5. Solid lubrication

Liquid lubricants allow heavily-loaded counterfaces to slide over each other with minimum tangential resistance. Any solid material which performs the same function can be considered a solid lubricant. A solid lubricant, therefore, should ensure that the two counterfaces separate in the vicinity of the lubricant and do so with the lowest friction coefficient possible. Several inorganic materials (molybdenum disulfide, graphite, hexagonal boron nitride, boric acid) can provide excellent lubrication. Most of these solids owe their lubricity to a lamellar or layered crystal structure. a few others (soft metals, polytetrafluoroethylene, polymide, certain oxides and rare –earth fluorides, diamond and diamond like carbons, fullerenes) can also provide lubrication although

they do not have a layered crystal structure. In fact, DLC films are amorphous, but provide some of the lowest friction coefficient of all the solid materials.
Main drawback of solid lubricant include [9]:

- Except for soft metals, most solid lubricants are poor thermal conductors and, hence, cannot carry away heat from sliding interfaces.
- Depending on test environment and contact conditions, their friction coefficients may be high or fluctuate significantly
- They have finite wear lives and their replenishment is more difficult than that of liquid lubricants
- Oxidation and aging-related degradation may occur over time and present some problems with transition-metal dischlogenides

Upon exposure to high temperatures or oxidative environments, they may undergo irreversible structural chemistry changes that in turn lead to loss of lubricity and the generation of some abrasive, nonlubricious by-product

2.5.1. General characteristics of solid lubricant

As illustrated in Figure 2.18 the layered crystal structure solid lubricants are such that while the atoms lying on the same layer are closely packed and strongly bonded to each other, the layers themselves are relatively far apart, and the forces that bond them (Wan Der Waals) are weak.

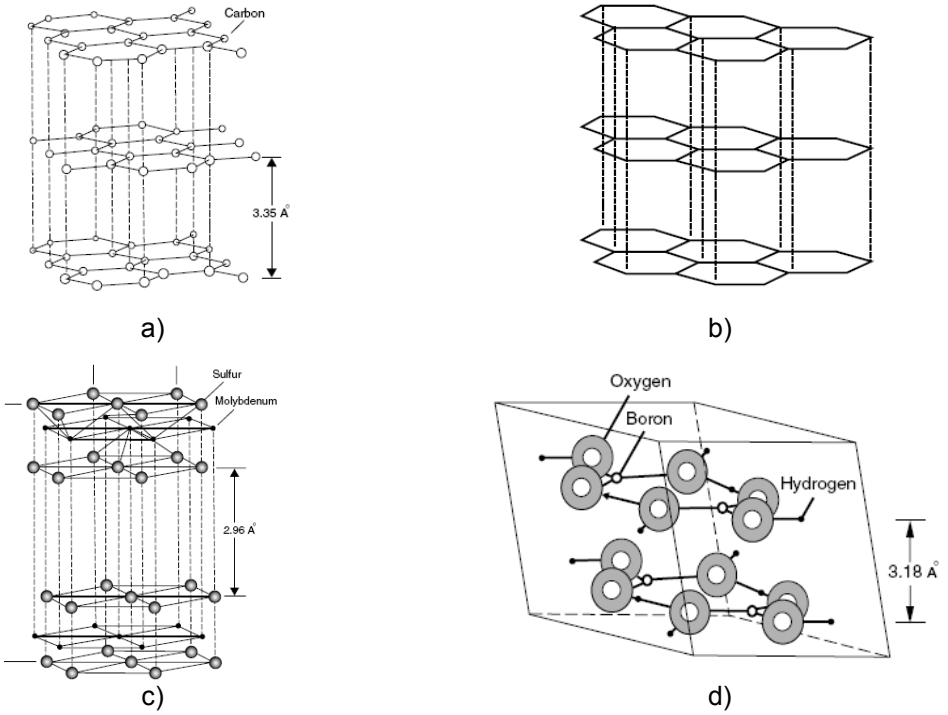

***Figure 2.18**. Schematic illustration of layered crystal structures of **(a)** graphite, **(b)** hexagonal boron nitride, **(c)** molybdenum disulfide (representing transition metal dichalcogenides), and **(d)** boric acid. [9]*

When present between sliding surfaces, these layers can align themselves parallel to the direction of relative motion and slide over one another with relative ease, thus providing low friction. While this mechanism is largely responsible for low friction and is essential for long wear life, a favourable crystal structure in itself is not sufficient. For effective lubrication the presence or absence of certain adsorbates is also needed for providing easy shear in most solids. Solid lubricants can be applied to a tribological surface in a variety of forms. The oldest and simplest method is to sprinkle, rub, or burnish the fine powders of solid lubricants on surfaces to be lubricated. Certain solid lubricants have been blended in an aerosol carrier and sprayed directly onto the surfaces to be lubricated. Powders of solid lubricant can be strongly bonded to a surface by appropriate adhesive and epoxy resins to provide longer wear life.
However, in most modern applications, thin films of solid lubricant are preferred over powders or bonded forms. They are typically deposited on surfaces by advanced vacuum deposition processes (sputtering, ion plating, and ion-beam-assisted deposition) to achieve strong bonding, dense microstructure, uniform thickness, and long wear life. Recent developments in PVD and CVD deposition techniques have led to the synthesis of a new generation of adaptive, self-lubricating coatings with composite or multilayer architectures.

2.5.2. Mechanism of lubrication by solid thin film

In general, the lubricity and durability of a solid lubricant are controlled by a mechanism that involves *intrafilm flow*, *interface sliding* and *interfilm sliding* as shown in Figure 2.19. [9]

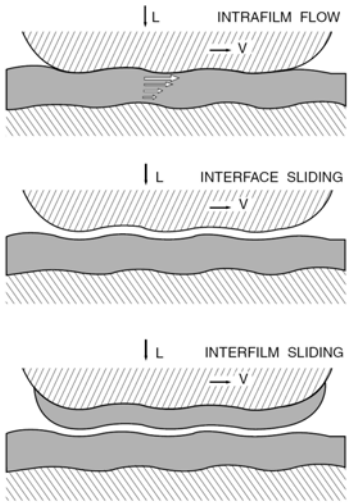

***Figure 2.19**. Schematic representation of three ways by which sliding can be accommodated between an uncoated and a coated surface.[9]*

- Intrafilm flow occurs when the film adheres to both surfaces and flows like a viscous fluid to accommodate relative displacements of the two surfaces. Although normally associated with noncrystalline materials, viscous like shear flow can also take place with crystalline materials at relatively high temperature. The friction behaviour of Ag, shown in [10], would be such an example; the correlation of shear strength with friction coefficient clearly indicates that the Ag undergoes plastic flow to

accommodate motion, and the shear strength of the film itself determines the friction coefficient. Platelelets of lamellar materials can also exhibit flow by intercrystalline slip.

- Interface sliding allows the two original surfaces to slide over one another only if there is no adhesion to the rider.

- Interfilm sliding occurs when the lubricant adheres to both surfaces but separates into two distinct films (at least for a moment or so) that slide across one another. In this case neither of the two original surfaces is in contact. The shear strength is, therefore, that of the two films sliding against one another.

2.5.3. Tribological contact mechanism in coated surfaces

According to K. Holmberg et all. [11] the tribology of a contact involving surfaces in relative motion can be understood as a process with certain input and output data (Figure 2.20).

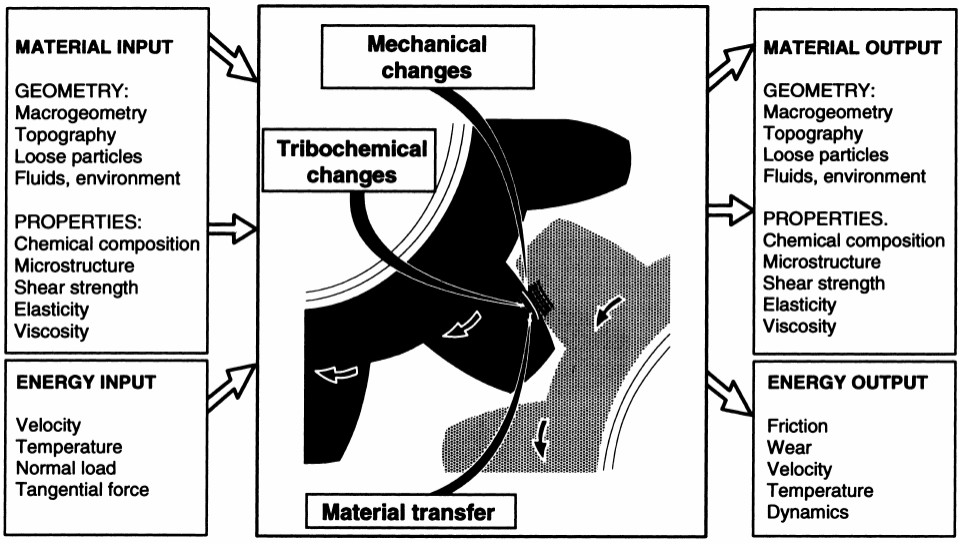

Figure 2.20. *The tribological process in a contact between two surfaces includes mechanical and tribochemical changes as well as material transfer. [11]*

Input data that are used as a starting point for the analysis of a tribological contact are:

- geometry of the contact, both on a macro and micro scale
- material properties based on the chemical composition and structure of the different parts involved, and the environmental parameters
- energy parameters such as the normal load, velocity, tangential force and temperature.

The complete tribological process in a contact in relative motion is very complex because it involves simultaneously friction, wear and deformation mechanisms at different scale levels and of different types. To achieve a holistic understanding of the complete tribological process taking place and to understand the interactions, it is

useful to analyse separately the tribological changes of four different types (Figure 2.21):

- the macro- and micro-scale mechanical effects
- the chemical effects
- the material transfer taking place

In addition, there has recently been an increasing interest in studying tribological behaviour on a molecular level; i.e. nanomechanical effects.

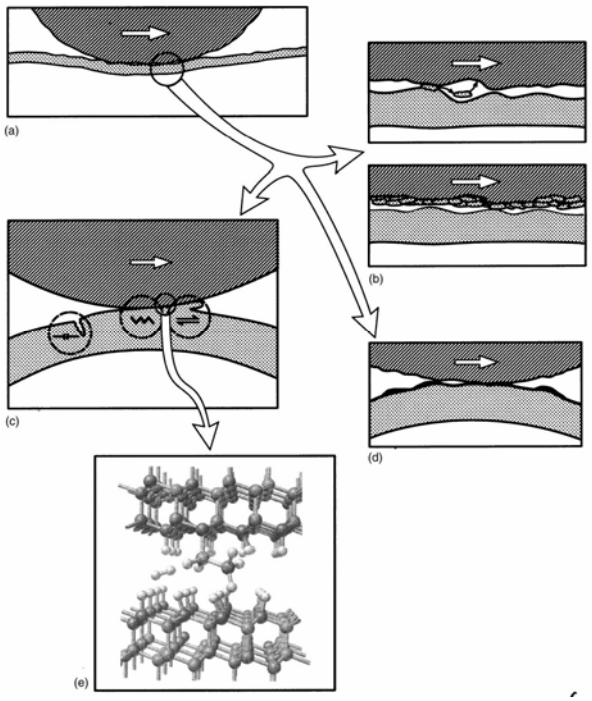

***Figure 2.21**. Tribological contact mechanisms: **(a)** macromechanical, **(b)** material transfer, **(c)** micromechanical, **(d)** tribochemical and **(e)** nanomechanical contact. [3]*

2.5.3.1 Macromechanical friction and wear mechanism.

The macromechanical tribological mechanism describes the friction and wear phenomena by considering the stress and strain distribution in the entire contact, the total elastic and plastic deformations they result in, and the total wear particle formation process and its dynamics. In the case in which one of the two surfaces in contact or both of them are coated, four main parameters can be defined that control the tribological contact behaviour:

a) coating to substrate hardness relationship
b) Thickness of the coating
c) Surface roughness
d) Size and hardness of any debris in the contact, which may originate from external sources or be produced by the surface wear interaction themselves.

The combination of these four parameters will result in a number of different contact conditions characterized by specific tribological contact mechanism. Figure 2.22 shows schematically 12 such very typical tribological contacts, with different mechanism influencing friction, when a hard spherical slider moves on a coated film surface. the corresponding wear mechanisms have been described in a similar way and are presented in Figure 2.23. [9]

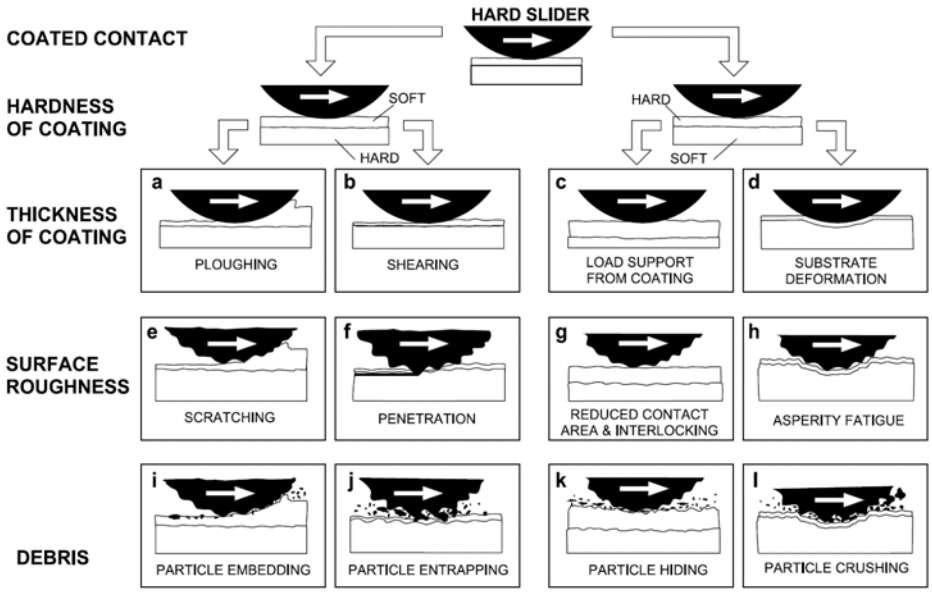

***Figure 2.22**. Macromechanical contact conditions for different mechanisms that influence. [9]*

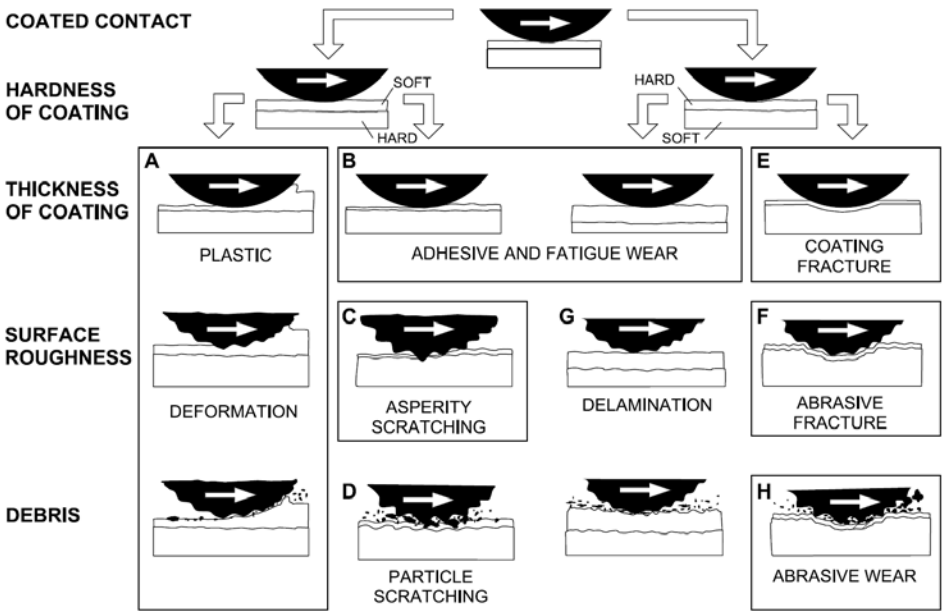

***Figure 2.23**. Macromechanical contact conditions for different mechanisms that influence wear when a hard spherical slider moves on a coated flat surface. [9]*

Soft coating on hard substrate

For soft coatings, the thickness of the coating influences the ploughing component of friction. when the film is thin enough, the effect of ploughing on the film is small (see Figure 2.22) The friction is thus determined by the shear strength of the film and the contact area, which is related to the deformation properties of the substrate. For very thick soft coatings the mechanism of ploughing will be very similar to that of soft materials scratched by a hard indenter. The formation of grooves in the coated surface by plastic deformation (see Figure 2.23(a)) is the main wear effect; but with thinner films, continuous sliding can result in coating compaction as well as adhesive and fatigue wear (see Figure 2.23(b)). The surface substrate roughness has an almost negligible influence on friction if the roughness is considerably smaller than the thickness of the soft coating and the coating is stiff enough to carry the load as shown in Figure 2.22(e). However, when the roughness of the slider is higher than the coating thickness, coating penetration will take place (Figure 2.22(f)) and the friction is considerably increased due to scratching of the substrate material.

Hard coating on softer substrate

The hard coating can provide good wear protection and with a suitable choice of material and surface layer design the friction can be very low as well. With a very thin hard layer on top of a softer substrate (see Figure 2.23(e)), it may be that neither the coating nor the substrate is able to support the load. However, the function of the coating is to separate the substrate form the counter-surface and to prevent ploughing by increasing the hardness of the top layer of the surface. Increased substrate hardness results in decreased contact area, where the shear takes place, and decreased friction, which is indicated in the results obtained by Ronkainen et all. [12] the prevention of ploughing reduces both frictional and wear; however, the higher shear strength introduced at the contact interface by the hard coating can, on the other hand, have the effect on increasing friction in sliding if no microfilms are formed (see Figure 2.21). That is why very high coefficients of friction often occur in sliding contacts with hard coating. The increase in friction caused by increased shear generally seems to be more dominant than the reduction in friction due to decreased ploughing. For very soft substrates, the indentation deformation will be considerable and this will thus add a ploughing effect on friction (Figure 2.22(d)). The deflection increases the stresses in the coating and also at the interface between the coating and the substrate, possibly resulting in fracture or fatigue cracks that may harm the coating or the substrate material. With a soft substrate, cracks may occur in the coating, both within the contact area and outside at the substrate material pile-up area, as shown in Figure 2.24. The harder the substrate the higher the loading that the coating can resist without failure by fracture. [9]

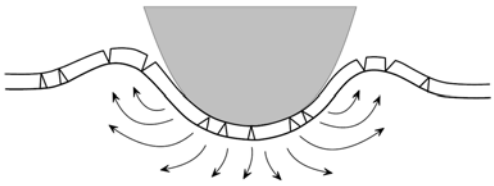

***Figure 2.24**. Fracture of a hard brittle coating on a soft substrate takes place in the contact area and at the material pileup area around the contact. Directions of material flow are indicated by arrows. [9]*

Increased loads can be resisted with thicker hard coating because of their load-carrying capacity, which reduces deflection, as shown in Figure 2.22(c).

2.5.3.2 Micromechanical interactions: material response

The micromechanical tribological mechanisms describe the friction and wear phenomena by considering the stress and strain at the asperity level, the crack generation and propagation, material liberation, and single particle formation. in typical engineering contacts, these phenomena are at the size level of about 1 μm or less, down to the nanometer level. Friction can be generated by adhesion between the two surfaces, by ploughing, or by asperity deformation as shown in Figure 2.25. The elasticity, hardness, and fracture toughness of the material influence friction and wear, both on a macroscale and on a microscale. On a macroscale, the rough surface of an elastic material deforms with the applied load and the load is thus spread more widely over the two surfaces, resulting in a lower surface pressure for the materials to respond to, as shown in Figure 2.26(a) and (b).

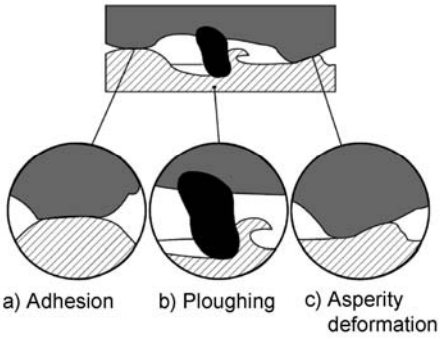

***Figure 2.25**. The three components of sliding friction are **(a)** adhesion, **(b)** ploughing, and **(c)** asperity deformation. [9]*

In sliding and rolling, the hardness of the material indicates its ability to carry a load. When a counterface such as a sphere slides on a soft flat surface, indentation and ploughing may take place, with high friction and wear as a result. For a harder material the ploughing action decreases, with less friction and wear as a result, as shown in Figure 2.26(c) and (d).

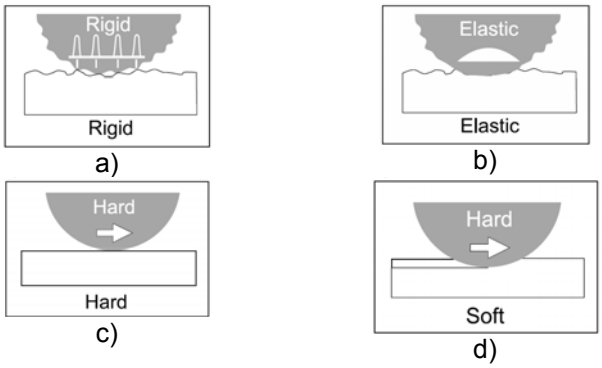

***Figure 2.26**. The deformation and contact pressure for a rough sphere on a rough plane in the case when both are **(a)** rigid and **(b)** elastic. The substrate deformation when a hard sphere is sliding on **(c)** a hard substrate and **(d)** a soft substrate. [9]*

The basic wear mechanism can be described by studying the material response effects in a simplified situation when a sphere is sliding over a flat surface (energy accommodation concept) as shown in Figure 2.27. At stage 1, point A on the upper surface is in contact with point B at the lower flat surface. When the upper surface moves to stage 2 some distance to the right, point B will follow point A because of the adhesion or interlocking between the surfaces. This movement of point B is allowed by the material response in the lower surface. This material response can be split up into three components: elastic deformation, plastic deformation, and brittle fracture. In the elastic case, B will follow A; and when the contact is release, B will elastically move back to its original position. The main parameter indicating the material response is the Young's modulus of elasticity (E).
In the situation of plastic behaviour, point B will follow point A in the same way, but after the contact release, the deformation of the flat surface will not return to its original shape but remains deformed. In this case a key parameter indicating the material response is the shear strength, τ. Third, in the situation of brittle fracture behaviour, point B again moves with point A and now the movement is allowed by the material cracking on the left-hand side of the contact. The moving contact has created a crack in the surface. The parameter indicating the material response is the fracture toughness or, more specifically, the critical stress intensity for microstructurally short cracks, K_{Ic}. The fracture toughness can more conveniently be expressed in the form of critical strain energy release rate, G_c.

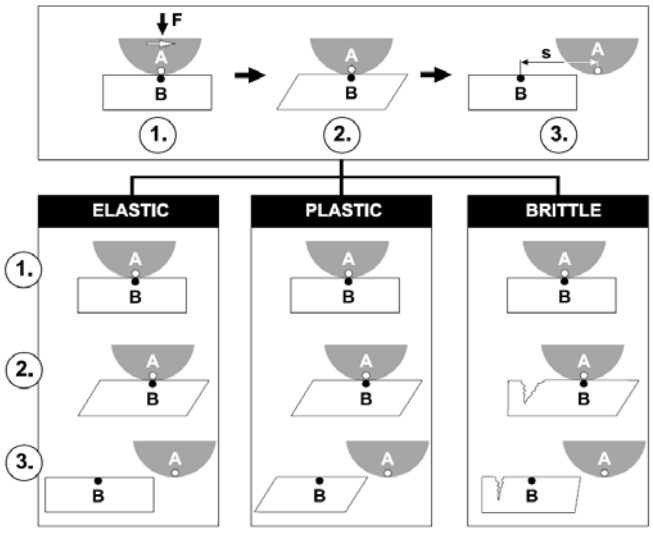

***Figure 2.27**. The three modes of energy accommodation in a sliding contact are elastic deformation, plastic deformation, and brittle fracture. [9]*

Thus far, it has been assumed that both materials are homogeneous and defect-free. Now assume that the flat material has cracks at the surface perpendicular to the surface itself, created, for example, from earlier sliding situations that are now repeated. Figure 2.28 shows how the surface in the elastic case is modified and returns after each contact to its original shape. However after a certain number of repeated contacts, fatigue cracks will be created in the surface that result in material release. In the fully plastic situation, the contact will result in a modified surface, and when this is repeated, the modification will continue, and finally this process will also result in

material release from the surface. In the brittle fracture situation, the repeated contacts will result in more new cracks. In all the three cases, material will be released from the surface and wear particles will be formed.

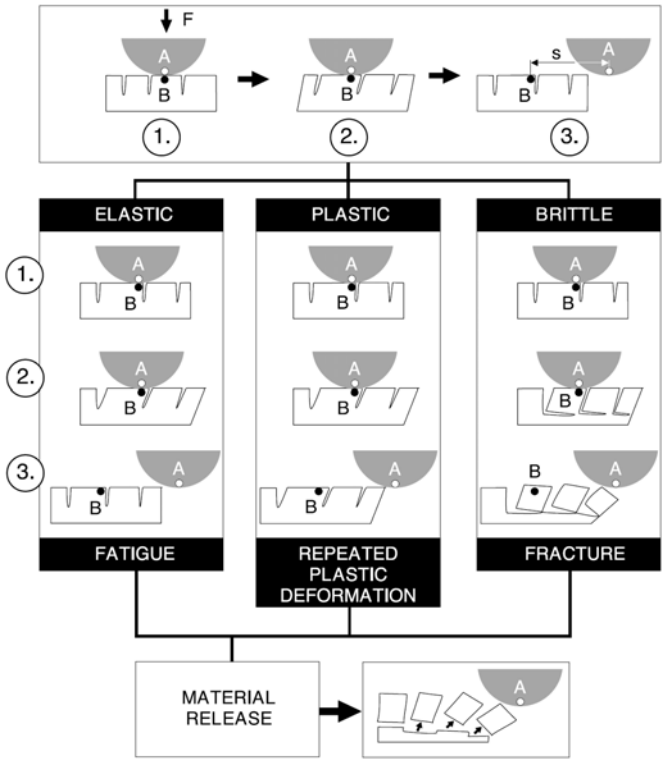

***Figure 2.28**. Material release and particle formation mechanisms in the elastic, plastic, and brittle energy accommodation modes. [9]*

The discussion has thus far been limited to a sphere sliding on a smooth surface. The situation is basically the same even if the lower surface is not considered flat due to surface roughness, curvature, or ploughing, as shown in Figure 2.29.

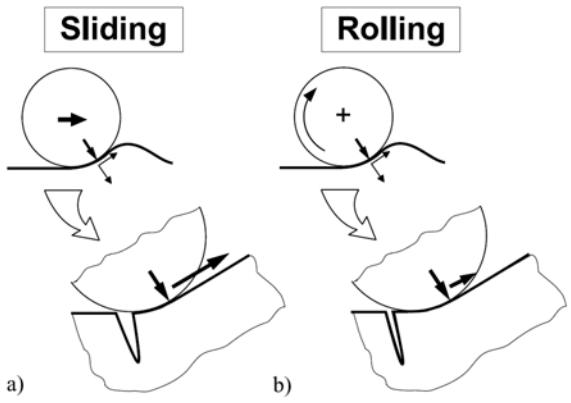

***Figure 2.29**. Energy accommodation geometry in **(a)** sliding and **(b)** rolling, with curved surfaces or asperities. [9]*

It is concluded that the Young's modulus of elasticity, shear strength, and fracture toughness are basic important material parameters influencing the friction and wear behaviour of the contact. To control the wear and friction situation, the values of this parameters in the coating, at the asperities, and in the bulk of the substrate, should be known.

2.5.3.3 Tribochemical mechanism of coated surfaces

The chemical reactions taking place at the surfaces during the moment of sliding contact and also during the periods between repeated contacts, change the composition of the outermost surface layer and its mechanical properties. This has a considerable influence on the friction and wear properties because they are determined to a great extent by the properties of the surface, where phenomena such as shear, cracking and asperity ploughing take place. [9]

Formation of thin microfilms on hard coatings

Formation of low-shear microfilms on the hard coating or perhaps only on the asperity tips of the coating significantly reduces the coefficient of friction. Thus, if the contact is considered on a micro scale, there is effectively a soft coating on a hard substrate, although now the coating (e.g. diamond) plays the role of hard substrate and the soft microfilm formed plays the role of a coating. It is obviously advantageous if the substrate under the hard coating is as hard as possible, to avoid fracture of the brittle coating by deformation, to improve the load support and to decrease the real area of contact.

The very low coefficients of friction of polished diamond and diamond-like coatings are further explained by the extreme smoothness of the surface excluding effects such as interlocking and asperity ploughing, as well as of the hard coating reducing the ploughing component of friction. A transfer layer is soon built up on the conterface when a steel or ceramic surface slides against a diamond-like hard carbon coating. The explanation for the low shear strength between the two surfaces is, however, the formation of an extremely slippery microfilm between the surfaces. Erdemir *et al*.[13], Liu *et al*.[14] have published convincing evidence in the form of Raman spectra of the surfaces and the wear products which indicate that graphitization is taking place and a low-shear-strength graphitic microfilm is formed between the surfaces. Perhaps the difficulty in finding the low-shear-strength film is associated with it occurring mainly in the form of graphitic wear products or third bodies present in the moment of sliding but partly disappearing thereafter. Erdemir *et al*. [13] showed that long-term sliding is needed before a more distinct graphitic layer can be detected and they measured coefficients of friction as low as $\mu = 0.02$. Higher sliding velocities and loads improve the graphitization process and result in decreased friction and wear. The DLC coatings can afford the low friction in temperatures up to 300°C. Decreased friction and wear properties are generally reported for decreasing environmental humidity.

In experiments carried out in dry N_2 with ceramic surfaces sliding on diamond coatings, Erdemir *et al*. [15] have shown that micrographitization takes place and results in extremely low friction down to $\mu = 0.0447$. In open air, evidence on interface graphitization has not yet been found.

Singer [16] presents a three-stage nanoscale model for the formation of reaction layers and for the building up of transfer layers in the case of sliding contacts with MoS_2 and Tin coatings.

In environments containing oxygen, such as air, a thin (about 1- to 10 nm thick) oxide layer is formed very quickly on most metal surfaces. Some oxygen layers (e.g copper oxide) are sheared more easily than a metal, while others (e.g. aluminium oxide) form a very hard layer. There are a number of reports describing studies on different aspects of oxide layer formation on tribological properties. [17]
In contacts with alumina (Al_2O_3) surfaces, Gee and Jenett [18] found that the tribologically formed hydroxide films are much softer than the remaining alumina, and that the films are liable to fracture under concentrated load conditions. The formation of environmentally stable and smooth third-body films on wear surfaces was believed to be responsible for the improvements in room-temperature tribological performance of nanocrystalline zinc oxide (ZnO) films. Friction, in the beginning was sensitive to load and sliding speed, but once a smooth wear scar was formed, it was very stable and the test conditions had no significant effect on it. Experiments with steel sliding against a chromium nitride (CrN) coating resulted in the formation of a chromium oxide (Cr_2O_3) surface film with very good wear resistance [19]. Increasing the applied load or the sliding velocity heleped to form a thicker Cr_2O_3 film, thus reducing wear.

2.5.3.4 Material removal and change interactions: debris and surface layers

The process of wear and friction results in both geometrical and structural changes in the surfaces of the contacting bodies. these changes will influence future contact conditions and friction and wear generated in the same contact

Surface and subsurface cracks

Based on macroscale experimental observations in rolling contact tests Nèlias et all [20] reported that the cracks are either initiated from subsurface inclusions or surface microcracks. Under the load is a stress concentration built up around inhomogeneities like inclusions and primary carbides. This is due to the elasto-plastic mismatch between the inhomogeneities and the martensitic matrix. Once the yield stress is reached, a plastic strain is induced in a small volume surrounding the inclusion. Under repeated action, the dislocations will move back and forth and accumulate. This process leads to localized changes in the steel microstructure and a crack is nucleated in this domain once a critical density is reached. Surface microscale are typically generated in the discontinuities of the surface topography, such as grinding marks or large wave-length surface roughness. The process of initiation of surface microcracks and formation of microspalls along grinding marks is shown schematically in Figure 2.30(a). Microcracks can also propagate parallel to the surface at a few microns depth along the machining direction, leading to the formation of microspalls, as shown in Figure 2.30(b). The cracks are mainly located on the top of large roughness peaks, as shown in Figure 2.30(c). There are indications that the local friction coefficient at the top of asperities may be large enough to initiate transverse microcracks. Depending on the combination of load movement, friction direction, and crack orientation, a lubricant may help propagate surface cracks by hydraulic pressure effects. Recent studies of the stress intensity factor at the tip of a surface breaking crack in a layered surface indicate that compressive stresses may tend to prevent crack propagation. There is a strong influence on both the fracture load and the fracture pattern by the mismatch of elastic properties between the layer and the substrate [21] Variations in coating properties and coating thickness may change the fracture loads by up to a factor of ten.

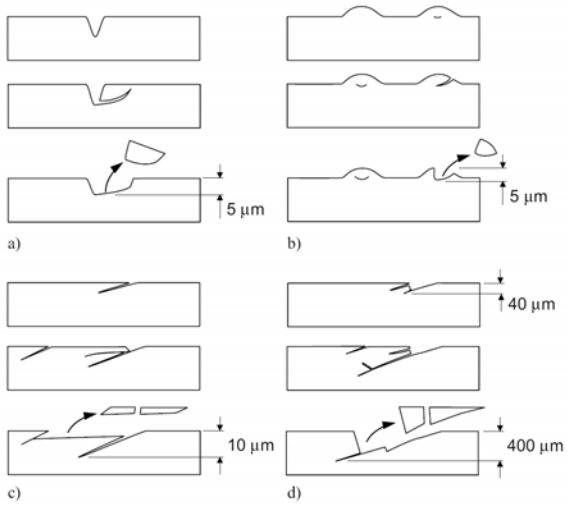

***Figure 2.30**. Schematic stages of **(a)** microspall formation along grinding marks (transverse cut), **(b)** microspall formation below longitudinal roughness of large wavelength (transverse cut), **(c)** microcrack and microspall formation (longitudinal cut), and **(d)** surface initiated deep spall formation (longitudinal cut). [9]*

Tribological influence of wear debris

Debris that have been generated by the wear process or loose particles originating from the surrounding environment may be present in a tribological contact. It has been observed that the coefficient of friction rises significantly once the wear particles are formed at the sliding surface, and particles present in the contact affect the instantaneous coefficient of friction and the wear. The friction coefficient can be altered by removing wear particles or by inserting particles in the interface, as shown by Hwang et all [22], who also found that the particle size influences friction but not so much as the number of particles present in the contact. In experiments with sliding surfaces of materials with different hardnesses (Pn, Zn, Al, Cu, Ni, Ti and AISI 1045 steel) they found a clear difference between soft and hard surfaces: soft and ductile surfaces produced larger wear particles with a stringer tendency to agglomerate, while hard surfaces produced smaller wear particles with weaker agglomeration tendency.

Particle embedding

Considering the sliding situation shown in Figure 2.22 (i), hard particles are present in the contact, the particles having a diameter significantly smaller that the thickness of the soft coating on a hard substrate. The particles are pressed into the soft coating and embedded into it without ant further contact with the slider as long as the soft coating remains thicker then the particle diameter. In this case, the particles have no great effect on friction, which is primarily controlled by the ploughing mechanism described earlier. The slider will produce a main groove by ploughing in the soft coating, and the surface asperities or trapped debris may cause microploghing and microgrooves within the main groove.

Particle entrapping

For thin surface coatings where the dimensions of the particles are of the same magnitude or larger than the coating thickness and the surface roughness, as shown in

Figure 2.22(j), their influence on friction can be considerable. If the particles are harder than the coating but softer than the substrate, then they are easily caught by the roughness of the counterface or partly sink into it and scratch grooves in the soft coating. An increase in friction may follow if the slider and the substrate are of equal hardness and the loose particles in contact have a higher hardness. Then the particles may partly sink through the coating into the substrate, as well as into the counterface by a kind of anchoring mechanism resist motion. Even if the particles are fairly spherical in shape, it is not probable that they will decrease friction by rolling because they will be stuck into the soft coating. Sin et all. [23] have shown that the contribution of ploughing on the friction coefficient is very sensitive to the ratio of the radius of curvature of the particle to the depth of penetration. The particles are free to rotate in the contact and they are often considerably sharper than the asperity angles of engineering surfaces. The wear rate depends on the particles size. If the particles in the contact are soft with low shear stress, they can carry part of the load and inhibit direct substrate-to-counterface contact, thus reducing both wear and friction. A similar effect has been observed by Yamada et all [24], who found that polymer particles can act very effectively to reduce wear and friction

Particle hiding

The introduction of small particles into the sliding contact of a hard and rough surface, as shown in Figure 2.22(k), does not necessarily make the tribological contact more severe. The particles can be hidden in the valleys formed by the asperities, while the sliding takes place at the asperity tops. Thus, the particles will have no great effect on either friction or wear. It is important to notice that reduced surface roughness can increase both friction and wear if the particles cannot hide in the valleys and instead interact with the surfaces by scratching and interlocking.

Delamination

When a hard rough slider moves over a hard rough surface as shown in Figure 2.23(g), the sliding action takes place at the top of the contacting asperities. They mainly deform plastically, although the overall contact stress may be less than the yield stress of the contacting materials, because the local stresses at the small asperity areas are much higher. High contact stresses can generate dislocations, pile-up of dislocations, and crack nucleation very near the surface, as described by Suh et all [25] in the delamination theory of wear and shown in Figure 2.31.

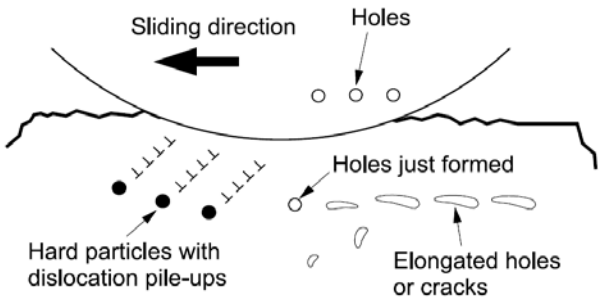

***Figure 2.31**. The initial stage of the delamination process of wear particle formation by shear deformation of voids in the material near the surface. [9]*

Because of the small plastic deformation of the surface, a large number of cracks must be nucleated before a loose particle can form. The delamination particles are flake-like and may be some hundred micrometers long.

Particle crushing

When particles, large in relation to the surface roughness, are introduced between two hard surfaces, the result can be particle crushing, scratching, or rolling, as shown in Figure 2.22(i). If the particles have lower hardness than the surfaces, then they will be crushed and destroyed under the load of the contact, with smaller debris and some increase in friction as a result. If the particles have a higher hardness than the surfaces, they will be caught by the roughness of the surfaces, resulting in ploughing and scratching. The scratching particles carry part of the load, which results in concentrated pressure peaks on both surfaces as they try to penetrate them. The high pressure peak may be the origin of crack nucleation in the coating.

The presence of hard particles between hard surfaces may in some cases reduce the coefficient of friction. If the particles are fairly round in shape, hard enough to carry the load, and at least one of the surfaces is smooth, the particles may act as rollers and reduce the friction.

Debris agglomeration

Particles that have been liberated from a surface by wear may still have an influence on the future friction and wear behaviour and wear behaviour of the contact. In sliding contact with different materials of different hardness (lead, zinc, aluminium, copper, nickel, titanium, and steel), Hwang et all. [22] observed different wear particle agglomeration behaviour, depending on hardness and sliding directions. Smaller wear particles had a stronger tendency to join together and form larger ones, and particles of soft and ductile metals had a stronger tendency to agglomerate than of hard and brittle metals. Particles agglomeration was not just limited to one location but occurred simultaneously over a distributed area, and the observed particle or flake sizes were in the range of 100 to 600 μm. The mechanism of agglomeration is complicated and probably due to adhesion and/or mechanical interlocking. The agglomerated particles can act as larger particles in the contact, detach to either of the surfaces, or be rejected from the contact. [26]

Transfer layers

The material transfer mechanism (Figure 2.21(b)) is well known for polymers (e.g. polytetrafluoroethylene [PTFE]), sliding on steel. Surface material from the the polymer wears off and attach by adhesion to the steel counterface to form an extensive PTFE film. Consequently after some time of sliding, the tribological pair is actually PTFE sliding against a thin PTFE film on steel, which has very low friction.

A typical building-up process of a transferred surface layer in contacts with steel and hard coatings such as TiN, CrN, and (TiAl)N has been described by Huang et all. [27]. As a result of the ploughing action of hard coating asperities, slider material fragments were first removed and then adhered to some preferential sites on the sliding track of the coating. The preferential sites were the highest asperities that made earliest contact with the counter-surface. Repeated sliding resulted in accumulation of fragments, which then united and formed discontinuous layers on the coating surface.

After some sliding the highest asperities were covered with transferred material, which was deformed and flattened under continuous sliding and a transfer layer built up.

2.5.4. Role of the film-substrate interface stresses in the tribological performance of surface coatings

The phenomena that take place in a tribological contact are influenced by the force pressing the two surfaces together.
A useful approach to calculating the coating/substrate interface stresses has more recently been used by Ramalingam and Zheng et all. [28] to assess the problems that may be encountered when hard coatings are applied on substrates with lower or higher compliance than the coating. Numerical solutions are obtained for different stress distributions on the coated surface. It is reasonable to represent the coated part as a semifinite solid with a thin film of thickness *h*, as shown in Figure 2.32.

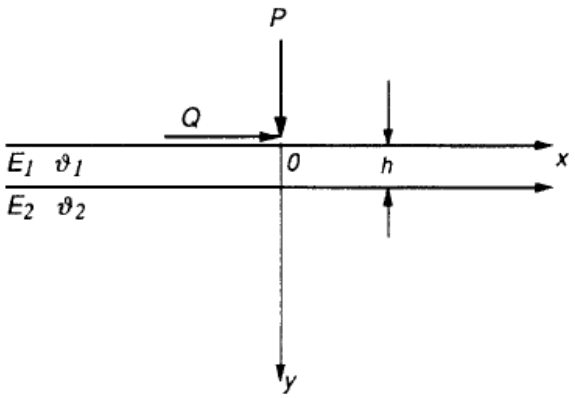

***Figure 2. 32**. Schematic of the problem geometry for plane strain modelling of a layered semi-infinite solid to determine stresses within the composite for line loads applied at the origin. [28]*

Films and substrates are taken to be isotropic and homogeneous with elastic constants E_I and E_2, and Poisson's ratios θ_1 and θ_2. Stresses in the film and at the film-substrate interface are of particular interest. Lamè equations, which for the plane strains assume the form given by equations (2.15, 2.16, 2.17), are then used to determine the stresses in terms of the derivatives of displacements:

$$\sigma_X = 2G\frac{\partial u}{\partial x} + \lambda\left(\frac{\partial u}{\partial x}+\frac{\partial v}{\partial y}\right) \qquad (2.15)$$

$$\sigma_Y = 2G\frac{\partial v}{\partial y} + \lambda\left(\frac{\partial u}{\partial x}+\frac{\partial v}{\partial y}\right) \qquad (2.16)$$

$$\tau_{XY} = G\left(\frac{\partial u}{\partial y}+\frac{\partial v}{\partial x}\right) \qquad (2.17)$$

Where:

- $G = E/[2(1 + \theta)]$, $\lambda = \theta E/[(1 + \theta)(1 - \theta)]$ are the Lamè constants (2.18)
- u, v are the displacements along x and y respectively

For a layered solid with a single layer, two sets of displacements $u_i(x,y)$ and $v_i(x,y)$; i = 1, 2 will have to be determined, one set for the coating (1) and the other for the substrate (2). Stress solutions for particular cases are obtained by first determining the response of the layered material to a loading qcos(αx) acting on y = 0 along x = $-\infty$ to $+\infty$ using the displacements u_i and v_i; i = c, s given by equations (2.19 - 2.22):

$$u_1(x,y) = [e^{-\alpha y} (A_1 + A_2 \alpha y) + e^{\alpha y} (A_3 + A_4 \alpha y)] \sin(\alpha x) \quad (2.19)$$

$$v_1(x,y) = [e^{-\alpha y} (B_1 + B_2 \alpha y) + e^{\alpha y} (B_3 + B_4 \alpha y)] \cos(\alpha x) \quad (2.20)$$

$$u_2(x,y) = [e^{-\alpha y} (C_1 + C_2 \alpha y)] \sin(\alpha x) \quad (2.21)$$

$$v_2(x,y) = [e^{-\alpha y} (D_1 + D_2 \alpha y)] \cos(\alpha x) \quad (2.22)$$

Here, $u_1(x,y)$ and $v_1(x,y)$ are the displacements along x and y respectively in the film, while $u_2(x,y)$ and $v_2(x,y)$ represent the displacements in the substrate. Equations (2.21) and (2.22), contain only two terms each, since the stresses and displacements vanish in the substrate for y = ∞ . The displacements contain 12 constants (written in capitals), and once they are determined, the stresses are calculated with the Lamè equations given by equations (2.15), (2.16), (2.17). With displacement formulation, calculating the stresses in a layered solid reduces to one of first solving a set of algebraic equations to determine the coefficients of displacements (2.19) to (2.22). To determine the unknown coefficients, the two stress equilibrium equations (for the plain problem):

$$\frac{\partial \sigma_x}{\partial x} + \frac{\partial \sigma_{xy}}{\partial y} = 0 \quad (2.23)$$

$$\frac{\partial \sigma_{xy}}{\partial x} + \frac{\partial \sigma_y}{\partial y} = 0 \quad (2.24)$$

are first written in terms of displacements u(x,y) and v(x,y) using Lame equations. Two equations are obtained for the film with $u_1(x,y)$ and $v_1,(x,y)$ and two more for the substrate with $u_2(x,y)$ and $v_2(x,y)$. Note, however, that u(x,y) and v(x,y) contain both positive and negative exponential terms. To satisfy the equilibrium equations everywhere in the film, it is necessary to equate the coefficients of positive and negative exponential terms also to zero so that the two equilibrium equations for the film give four algebraic relations between the unknown coefficients. Two more algebraic relations are obtained from the equilibrium requirement in the substrate. Thus, a total of six algebraic relations among the coefficients are obtained from the stress equilibrium equations. The requirements for displacement continuity at the film-substrate interface:

$$u_1=u_2 \text{ and } v_1=v_2 \text{ at } y = h \quad (2.25)$$

yields two additional relations, and local continuity of stresses σ_Y and τ_{XY} provides two more relations (these four requirements hold for perfectly adherent films).
When only normal loads are applied, at y = 0, the film surface must be free from shear tractions, i.e.τ_{xy} = 0. This provides yet another relation between coefficients for a total of 11 equations. The normal load applied on the upper surface of the film of the layered solid gives the final equation necessary to make the problem determinate.

2.5.4.1 Stresses due to normal loads applied at the film surface

A load or loads applied over a part of the coated surface can be written as a Fourier cosine integral given by:

$$F(x) = \frac{2}{\Pi} \int_0^\infty d\alpha \int_0^\infty f(\eta)\cos(\alpha\eta)\cos(\alpha x)d\eta \qquad (2.26)$$

where η is a dummy variable. Refer to Figure 2.33 and consider a normal strip load of constant intensity $p(x) = p_0$. applied over a width *a* along y = 0. Then:

$$p(x) = p_0 \qquad 0 \le x \le |a/2| \qquad (2.27)$$

$$p(x) = 0 \qquad x \ge |a/2| \qquad (2.28)$$

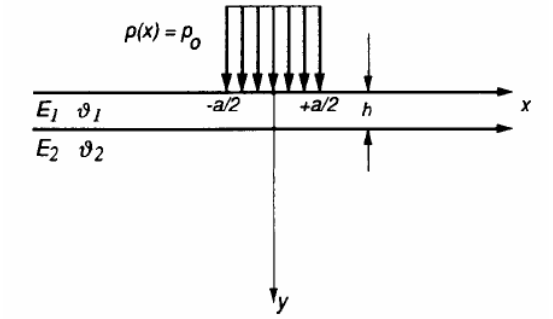

***Figure 2.33**. Schematic of the problem geometry for plane strain modelling of a layered semi-infinite solid to determine stresses within the composite due to a distributed load of constant intensity p_0 applied at the origin. [28]*

The strip load, written as a Fourier cosine integral becomes

$$p(x) = \int_0^\infty p_\alpha \cos(\alpha x)d\alpha \qquad (2.29)$$

Where:

$$p_\alpha = \frac{2p_0}{\alpha\pi} \sin \alpha\frac{a}{2} \qquad (2.30)$$

For normal strip loading, the applicable stress boundary condition for σ_Y is then:

$$\sigma_Y\big|_{Y=0} = -\int_0^\infty p_\alpha \cos(\alpha x)d\alpha \qquad (2.31)$$

For normal line loading having a magnitude equal to the total force due to the strip load, p_α is given by – P/π. The last equations required to determine the constants of the displacement functions, equations (6-3) to (9-3), for a uniformly distributed normal load acting over a width a or a normal line load with a magnitude equal to the total force due to the strip load are obtained by replacing (q/a) for the cosinusoidal load q cos(αx) with p_α of equation (2.19-2.22) or -P/π. The coefficients of the displacement functions may be determined for any other loading applied to the film surface in a similar manner. Once the coefficients are determined, Lame equations are used to calculate the stresses at any point (x,y) within the coated body. Since the load applied over the film surface is represented in terms of a Fourier integral, stress solutions are obtained by

numerical integration between the limits α = 0 and ∞ . The upper limit of integration is determined by calculating the stresses on the film surface and checking for agreement with the external load applied. The solution for an isolated line load is particularly useful, since it may be used as an influence curve. Stresses for any distributed load may then be computed as a linear combination of isolated loads, as long as the elasticity requirements are not violated.

Case 1: Normal strip load at the origin

A uniform loading over a contact width *a*, where *a* is a multiple of the film thickness, is considered. In relatively narrow contacts, as when *a*/h = 3, flexural stresses are highly tensile, Figure 2.34(a).

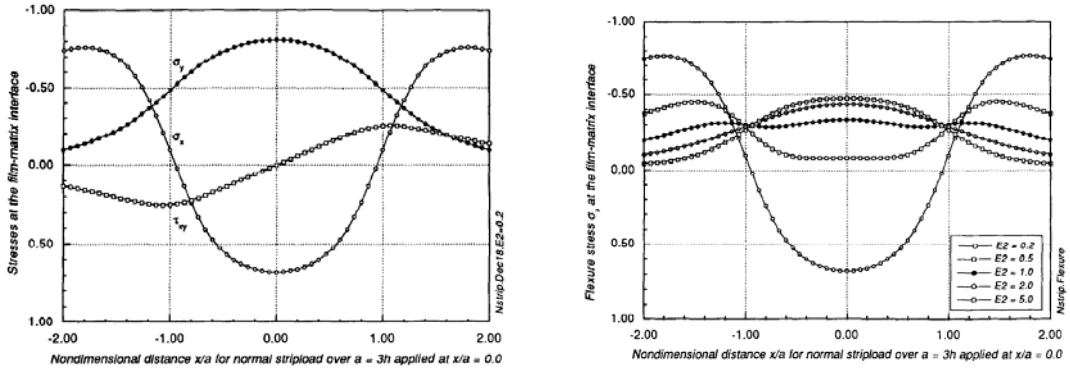

(a) (b)

Figure 2.34. ***(a)*** *Calculated interface stresses σ_X, σ_Y and τ_{XY} due to a unit normal strip load at the origin over a loading width 3 times the film thickness.* ***(b)*** *Sign changes at the substrate modulus E_2 is raised (bottom). [28]*

The results shown apply for $E_{substrate}/E_{film}$=0.2. The bearing stress σ_Y and the shear stress τ_{XY} at the film-substrate interface pose no new problems. The tensile flexural stress problem encountered with more compliant substrates can be overcome with a careful choice of the film thickness. Whenever the contact dimensions are much larger, as when *a*=10 h, film flexural stresses are not tensile within or outside the contact. This is shown in Figure 2.35 for a contact in which width *a*=10h and $E_{substrate}$=0.2E_{film}.

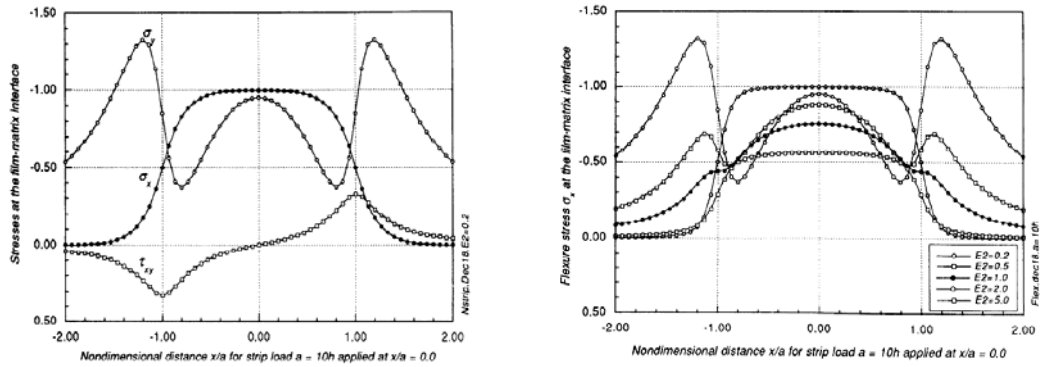

Figure 2.35. ***(a)*** *Calculated interface stresses σ_X, σ_Y and τ_{XY} due to a unit normal strip load at the origin over a loading width ten times the film thickness.* ***(b)*** *Calculated interface stresses σ_X, as function of the substrate elastic modulus. [28]*

Flexural stresses are compressive regardless of the substrate modulus as long as contact occurs over a region much larger than the film thickness.

Case2: Shear strip load at the origin

If transverse forces are applied to a distributed contact to obtain relative motion, a frictional resistance to movement is generated. This appears at the contact as a shear stress with the loading intensity proportional to the normal stress. In a coated part, distributed shear loading gives rise to large, tensile flexural stresses in the film and at the film-substrate interface. Calculated results for *a*/h = 3 and a/h = 10 are shown in Figure 2.36(a) and Figure 2.37(a).

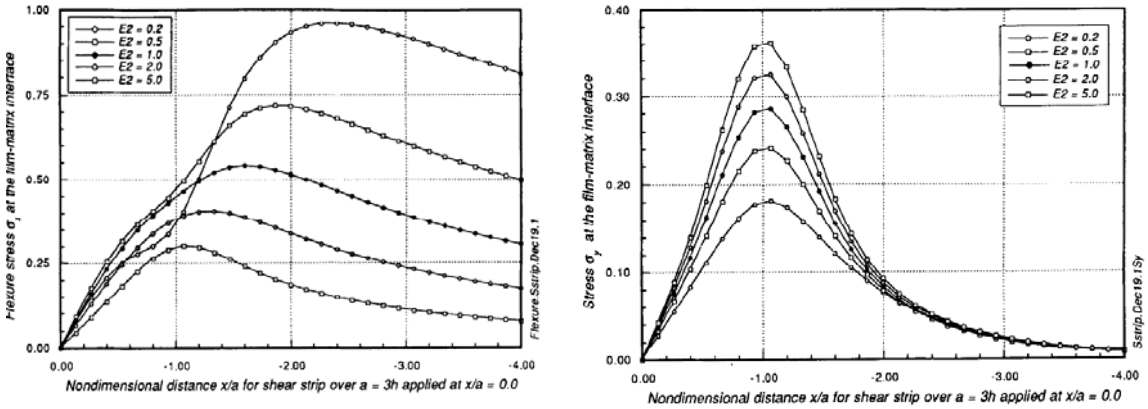

(a) (b)

***Figure 2. 36**. (a) Calculated interface stresses σ_X and σ_Y due to a unit tangential strip load applied at the origin over a loading width three times the film thickness. (b) Calculated interface stresses σ_Y as function of the substrate elastic modulus. [28]*

Stress component σ_Y at the film-substrate interface, tending to separate the film from the substrate, also becomes tensile in the wake of the contact, i.e. for negative x/*a* values, Figure 2.37(a) and Figure 2.37(b). Softer substrates are, however, less hazardous in this regard than stiffer substrates.

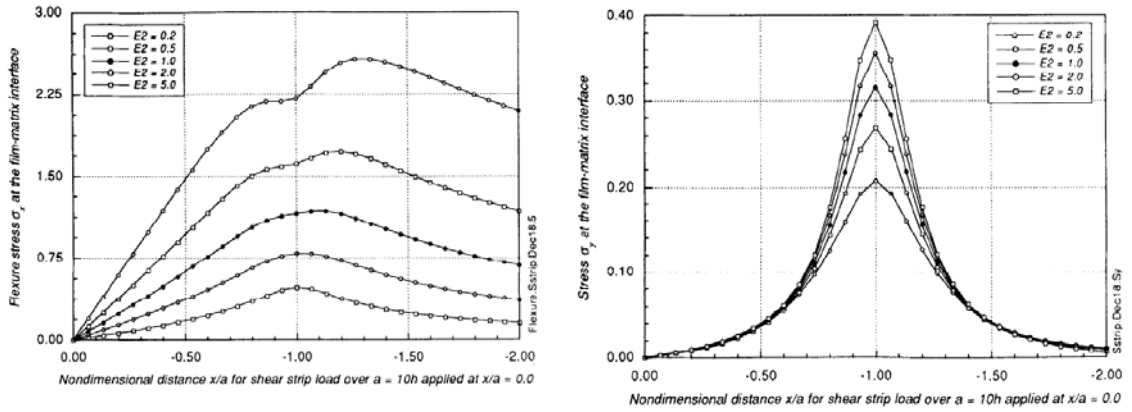

(a) (b)

***Figure 2. 37**. Calculated interface stresses **(a)** σ_X and **(b)** σ_Y due to a unit tangential strip load applied at the origin over a loading width ten times the film thickness as function of the substrate elastic modulus. [28]*

2.5.4.2 The effect of residual stresses on the coatings tribological performance

According to [29], thin coatings are typically subjected to considerable residual stresses caused during the manufacturing process. In some cases these stresses are beneficial for the mechanical and tribological behaviour of the component. In the development of diamond coatings for tool applications the residual stresses have been identified as a major driving force for coating failure. Owing to the relatively high deposition temperatures (600-1000 °C) and the mismatch in coefficient of thermal expansion between coating and substrate, high residual strains are formed in the coating on cooling. The combination of the high Young's modulus of the coating and high residual strain yields large residual stresses. These stresses affect the behaviour of the coating. The model used to consider the effect of residual stresses is the one shown in Figure 2.38 where a coating of thickness *h* is bonded to a substrate with a thickness which is large compared with *h*.

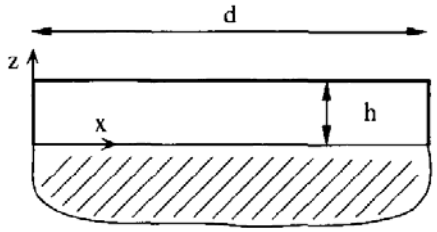

Figure 2.38. *A coating deposited onto a substrate. [29]*

The coating width (distance between edges) is d. The extent of the coating in the y-direction is assumed to be very large compared with *h*, and thus plane strain is assumed. Both materials are assumed to be isotropic and linear thermoelastic. The Young's modulus, the Poisson ratio and the coefficient of thermal expansion for the coating and substrate are (E_c, θ_c, α_c) and (E_s, θ_s, α_s) respectively. The material model is justified since the coating system studied consists of highly brittle materials, which thus deform elastically up to fracture. The assumption of isotropy of the system should be appropriate, despite the fact that the number of crystals across the coating thickness is very limited, since diamond crystals are highly isotropic. The system is considered stress free at the deposition temperature T_d. On cooling to the temperature T_o thermal stresses will develop owing to the mismatch in coefficient of thermal expansion. It is assumed that a uniform temperature is established in the body, both at the processing temperature and at the temperature after cooling, and no transient effects are considered. The temperature dependence of the coefficient of thermal expansion is accounted for by using the mean value, integrated from the stress-free temperature T_d to the final temperature T_o. If the coating was infinitely wide, the only stress present would be a biaxial stress given by:

$$\sigma = [Ec/(1 - \theta_c)](\alpha_c - \alpha_s)\,(T_d - T_o) \qquad (2.32)$$

in the x- and y-directions.
Thermal stresses have been evaluated in three different zones:

- Thermal stresses far from edges
- Thermal stresses at coatings edges
- Thermal stresses in coatings deposited over substrates edges

Thermal stresses far from edges

In Figure 2.39 the stresses at the interface between the coating and the substrate as a function of *x* are shown. In the calculations the geometry was given by h = 10 μm, d= 1.5 and 3 mm, and a substrate thickness of 3 mm.

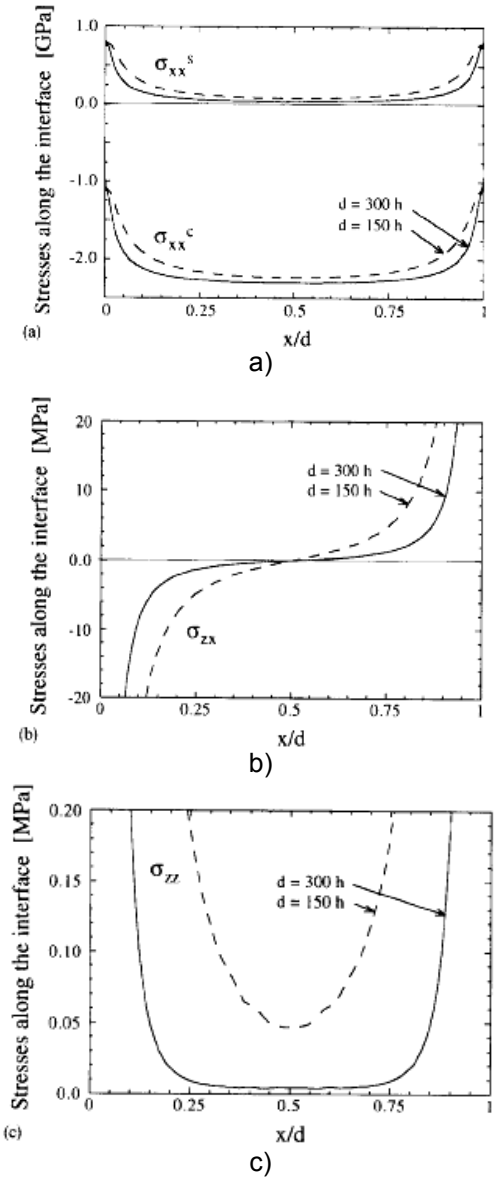

***Figure 2.39**. Stresses at the interface along the coating width; the tangential stress in the coating σ^{c}_{xx} and in the substrate σ^{s}_{xx} (a), the shear stress σ_{zx} (b), and the normal stress σ_{zz} (c). [29]*

However, the results are valid for other geometries with the same thickness to width ratio, *h/d,* provided that the substrate thickness is much larger than h. It can be observed that: σ_{xx} and σ_{zz} are fairly constant far from the edges, but on approaching an

edge all stresses except σ^{c}_{xx} increase.
Far from the edges the shear stress σ_{zx} increases approximately linearly from the centre of the sample.
However, for smaller ratios of *h/d* the edge effects reach farther away from the edge In Figure 2.40 a sample of stresses in cross section of the coating is shown.

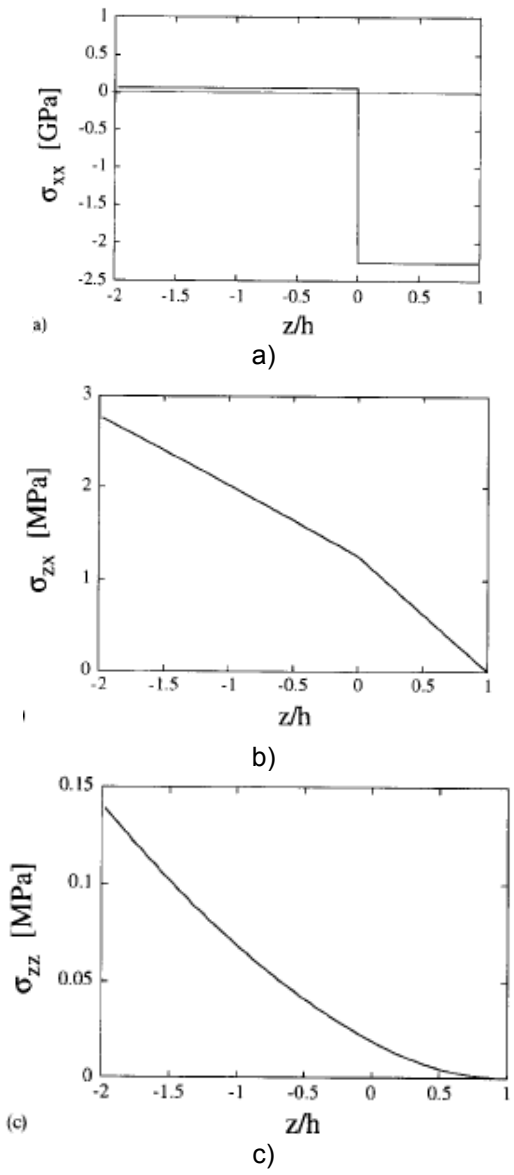

***Figure 2.40**. Typical stresses far from edges (at d/4) as function of depth z. [29]*

The stresses are taken at the distance *d/4* from an edge (h=10 μm and d=3 mm). The stress tangential to the interface is almost constant and compressive at a level of 2.3 GPa in the coating, and tensile at a level of 0.1GPa in the substrate, see Figure 2.40(a). The shear stress σ_{zx} and the stress normal to the interface are zero at the coating surface and increase with increasing depth in the coating, see Figure 2.40(b)

and (c). The thermal stresses at the interface as a function of coating thickness are shown in Figure 2.41. The stresses are taken at *d/4* from an edge.
It is seen that the compressive stress in the coating σ^c_{xx} decreases slightly from a level of -2.3 GPa for *h/d=0.001* to -1.9 GPa for *h/d*=0.025. The tensile stress in the substrate σ^s_{xx} increases.by a factor of 20 when the ratio *hid* is increased from 0.001 to 0.025. The tensile stress in the substrate σ^s_{xx} increases by a factor of 20 when the ratio *h/d* is increased from 0.001 to 0.025. The corresponding increase in the shear stress σ_{zx} and the stress normal to the interface σ_{zz} is almost 3 and 4 orders of magnitude respectively. Thus the very large stress σ^c_{xx} is dominating, but it is seen that for increasing *h/d* the magnitudes of σ_{zz} and σ_{zx} can be significant. Note that σ_{zz} is a tensile stress.
Fracture patterns expected as a result of these stresses are substrate cracks in the z-direction (due to σ^s_{xx}) and (for a weak interface) interfacial debonding (due to σ_{zx} and σ_{zz}). Both cracking modes are promoted by larger *h/d* ratios.

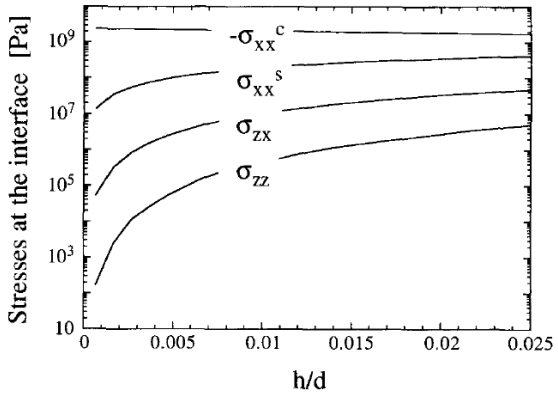

***Figure 2.41**. Typical stresses at the interface, far from edges (at d/4), as function of the ratio hid. Note that σ^c_{xx} is negative. [29]*

Thermal stresses at coating edges
The geometry at the corner of a free coating edge is specified by the angles γ_1 and γ_2.

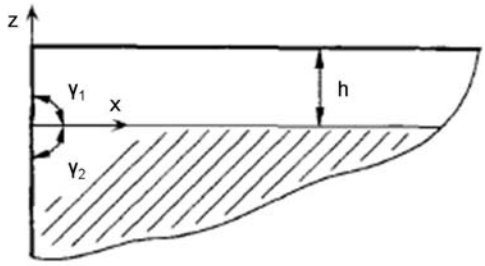

***Figure 2.42.** A coating edge. [29]*

In Figure 2.43 the stresses at the interface close to the free edge are shown.
Three cases are presented:

(i) γ_1 =90 °, γ_2 =90 °, h= 10μm;

(ii) γ_1 =90 °, γ_2 =90 °, h=30 μm;

(iii) γ_1 =90 °, γ_2 =180 °, h=10 μm.

All stresses except σ^{c}_{xx} increase slowly (in magnitude) when approaching the free edge. At a distance of about 2h rapid changes in the stresses occur. It can be noticed that no significant difference in stresses is seen between cases (i) and (ii) when x is scaled by *h*. Thus, the effect of a larger coating thickness is that the high stresses are spread over a larger region. The tangential stress σ_{xx} and the shear stress σ_{zx} are of large magnitudes (at the interface) very close to the edge, but decrease rapidly to zero at the edge (starting at *x/h < 0.1h).* The normal stress σ_{zz} which is tensile far from the edge turns compressive at a distance of about 1.5h from the edge. Very close to the edge it once again becomes tensile. When a corner is formed at the free edge, case (iii), the stresses become even higher at the edge (they are singular in this elastic model). The normal stress σ_{zz} is compressive at the edge, but at a distance of about h from the edge it becomes tensile. The shear stress is very large at the edge.
The strength of the stress concentration (or singularity) is set by the local geometry at the free edge of the interface, i.e. by γ_1 and γ_2 (apart from the materials combination and temperature change). The stresses become higher for higher values of γ_1 and γ_2 (the geometry of the edge approaches that of a crack). The stress state near the intersection of the interface and the free edge can be described by stress intensity factors (similar to at a crack).

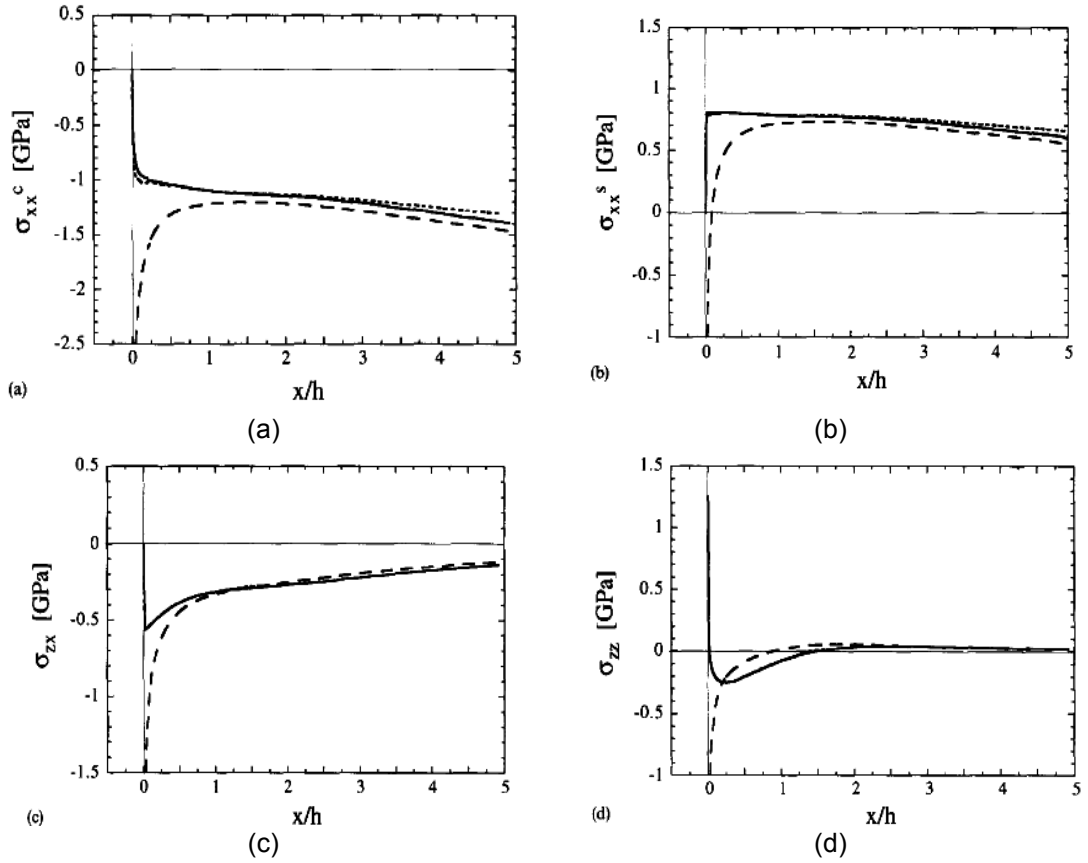

***Figure 2 43**. Stress distribution at the interface as a function of the distance x from the coating edge for three cases: **(i)** γ1 = 90 °, γ2 = 90 °, h = 10 μm **(--); (ii)** γ1 =90 °, γ2 = 90 °, h=30 μm (...); **(iii)** γ1 = 90 °, γ2 = 180 °, h= 10 μm (- -). [29]*

Thermal stresses in coatings deposited over substrate edges

A coating deposited over a curved substrate edge is considered (Figure 2.44).
The radius of the substrate edge is *r*. If the radius is of the same order of magnitude as the coating thickness *h,* large stress redistributions occur at the edge. In Figure 2.45 the stresses at a curved substrate edge are shown for the case *h*=5 μm, *r*=5 μm and a substrate thickness of 2.5 mm.

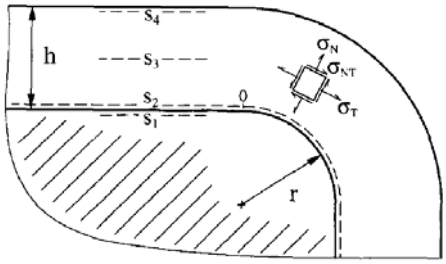

Figure 2.44*. A coating deposited over a substrate edge. [29]*

In Figure 2.45(a) the stress tangential to the interface σ_T is presented for different depths in the compound, along lines parallel to the interface.

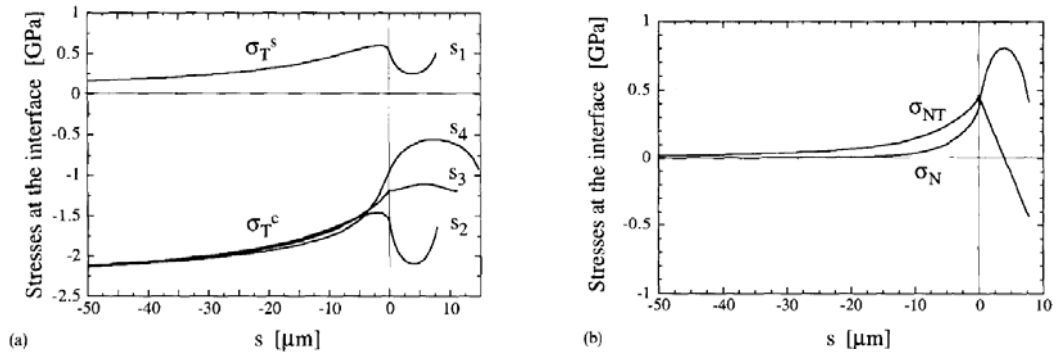

Figure 2.45*. Typical stresses at a coated curved substrate edge (r/h=l); stresses tangential to the interface at different depths in the compound* ***(a)****, and shear and normal stresses at the interface* ***(b)****. [29]*

The tangential stress in the substrate σ^s_T close to the interface (along the line s_l, see Figure 2.45), is tensile and shows a maximum at the beginning of the curved edge. The tangential stress in the coating σ^c_T close to the interface (line s_2) is compressive and has the maximum value at the centre of the edge. However, close to the surface of the coating (line s_4) σ^s_T is seen to decrease appreciably and reaches a minimum at the centre of the edge. Approximately the average value of the stresses along s_2 and s_4 is obtained at the depth *h/2* in the coating (line s_3). Note that the centre of the edge is located at different positions for lines s_2 and s_4 since the magnitude of the radius is different at different depths in the coating. As seen in Figure 2.45(b) the interface is subjected to very high shear and tensile stresses at the curved substrate edge. The shear stress σ_{NT} at the interface has its maximum value at the beginning of the edge and is zero at the centre of the edge. The stress normal to the interface σ_{NT} is tensile and increases to a peak value at the centre of the edge. The magnitudes of σ^s_T, σ_{NT} and σ_N at the interface increase as the edge radius decreases or as the coating

thickness increases. In fact, the ratio *r/h* controls the stress concentration at the edge, provided that the coating width and substrate thickness are large compared with *h*.
In Figure 2.46 the stress concentration at curved substrate edges is presented. The stresses shown are the maximum values at the interface as a function of *r/h.* Furthermore, the minimum value of the tangential stress at the coating surface is shown. Note that for *r/h* < 30 the maximum values of the stresses σ_N, σ_{NT} and σ^s_T all reach the gigapascal range. If the maximum normal stress at the edge for *r/h*=5, as an example, is compared with the normal stress at a distance 10h from the edge, it is typically 700 times larger. A similar comparison for the shear stress and for the tangential stress σ^s_T indicates an intensification of about 30 times and about 3 times respectively.

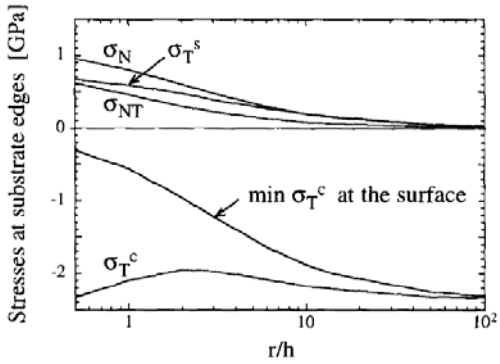

***Figure 2.46**. Stress concentration at coated curved substrate edges as function of r/h. The maximum values of the interracial stresses at the edge and the minimum value of σ^c_T at the coating surface are shown. [29]*

It is a well known experimental fact that coatings with high residual stresses tend to delaminate at edges, as seen in Figure 2.45 and Figure 2.46, it is no surprise that the adhesion problems are concentrated at the edges of coated tools. The interface at the edge is subjected to intense residual stresses in addition to stresses caused by the contact against a workpiece. The tensile normal and the shear stresses at the interface are in the gigapascal range for sharply curved edges, which sets demands on extremely good adhesion. Figure 2.45(b) shows that the maximum levels of the normal and shear stresses occur at different locations. The normal stress has its maximum at the centre of the coating edge whereas the shear stress has its maximum at the beginning of the edge. Since it is the combined effect of the normal and shear stresses that gives the driving force for coating debonding, a larger radius has the additional benefit of separating the peak value of the stress components, and thus lowering the peak value of the combined stress. The conditions for abrasive wear of a coating deposited over a substrate edge are somewhat different from the conditions at a flat surface. At a flat surface far from edges the stress state is dominated by the large biaxial compressive stress. At a substrate edge the tangential stress at the coating surface is lowered as compared to the corresponding stress at the flat surface, e.g. One fourth for *r/h*=1, see Figure 2.40(a). Thus the stresses that prevent crack nucleation and propagation at the coating surface can be considerably lower. In addition, the shear stress and the tensile normal stress are of the same order of magnitude as the compressive tangential stress. The resistance against abrasive wear at the edge is lower compared with at a flat surface. However, as seen in Figure 2.46,

the decrease in σ_T at the surface is controlled by the ratio *r/h.* To avoid coating delamination due to residual stresses, the interface stresses (shear and normal stresses) should be kept low. Further, to increase the resistance against abrasive wear the tangential stress should be kept high. Both these conditions are met by a thin coating: the ratio *r/h* is the stress controlling parameter for frequent substrate edge geometries.

2.5.5. Review of the coating tribological performance

Surface engineering, i.e. techniques and process capable of creating and/or modifying surfaces to provide anhanced performance such as corrosion and wear resistance are today frequently used in the industry. Today, there is an increasing demand for environmental friendly sheet metal forming production processes so therefore great attention is given paid to develop new surface engineered concepts which allow dry/semidry forming operations. In sheet metal forming mainly two such concepts of surface engineering have been proposed, the use of dry lubricants deposited on the sheet metal and the deposition of a low friction anti-sticking coating on the forming tool surface. The common idea is that they are “self-lubricating” which mans that they lower the shear strength within the tribological contact thus lower the friction coefficient. The main differences between theses concepts are hardness and coating ductility which can be related to the chemical composition and structure of the individual coating. Polymers based thin organic coating has a low shear strength and a high material transfer tendency, while PVD-coating has typical ceramic properties like high hardness and high wear resistance.

2.5.5.1 Inorganic coatings tribology

During the last years there has been an increasing interest for development of low friction/high wear resistance PVD coatings which have the potential to form metal sheet under dry conditions.
In the literature, basically two types of PVD coating, CrN and Diamond-like Carbon (DLC) besed coatings, have shown promising results when used in those metal cutting and forming applications where pick-up pf work material on the tool surface should be avoided

B. Podgornik et all [30] investigated the influence of the coating type (film composition and structure) and work material couple on the friction coefficient. Five different PVD coatings: TiN, TiB_2, VN, TaC, DLC were compared in terms of galling properties when applied on forming tool steel and slide against stainless steel. The tribological properties were investigated in a load-scanning rig with a normal load gradually increased under dry conditions. In Figure 2.47 the Coefficient of Friction vs normal load graphs of the five PVD coatings are presented.
It can be seen that low-friction materials, i.e. carbon based coatings (DLC and TaC type) give low and stable friction and excellent protection against galling. However, in order to reduce the pick-up tendency of work material the coated surface should be as smooth as possible. Selection of proper coating or surface treatment plays an important role in the process of obtaining the best galling performance of forming tools. This selection depends greatly on the type of material to be formed. One way of

selecting the optimum technique for surface modification of the forming tools, could be to use adhesion coefficients evaluation (see Chapter 2.2.2).
The same authors found that the coated surface roughness has a crucial effect on the friction level and the ability of a material to prevent pick-up of the counter material, especially in the case of hard wear-resistant coating (TiB_2, TiN), known to generate high friction when sliding against austenitic stainless steel. Polishing of the surface removes irregularities and asperities at the surface, thus eliminating potential sources for initiation of material transfer. The smoother the substrate, the higher the critical load that the coated surface can withstand without stainless steel transfer.
Polishing of the substrate prior to coating deposition will lower the friction and increase the critical load for material transfer. However a post-polishing of a ground and coated surface gives the same or even better galling properties as compared to the finest substrate polishing (Ra≤0.05μm) [31]

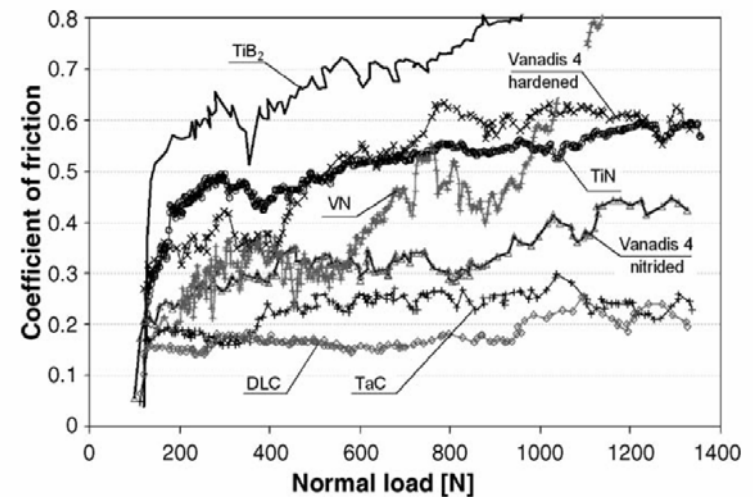

***Figure 2.47**. COF vs Normal load for the five PVD coatings during sliding against Austenitic stainless steel. [30]*

In [32] Podgornik et all. conclude how the optimum solution to providing superior friction and galling properties of forming tools should include the following steps: plasma nitriding to improve the load-carrying capacity of forming tool steel, post-polishing of the contact surface to eliminate any surface asperities and deposition of a hard low-friction coating.

DLC coatings for tribological applications have extensively been investigated for the last 10 years. They consist basically of a mixture of diamond (sp^3) and graphite (sp^2) and are generally divided into hydrogen-free tetrahedral amorphous ta-C DCL coatings and amorphous hydrogenated a-C:H coatings.
K. Vercammenn et all [33] investigated the mechanical and tribological properties of various state-of-the art DLC coatings. The results from that study showed that the tribological properties of the DLC coatings vary strongly depending on the coating composition/configuration and processing conditions (deposition techniques).
Each coating type has specific advantages and the entire range of properties should be studied carefully to select the appropriate coating for a particular application. In dry

atmospheres, the hydrogenated DLC types show lower friction coefficients than the non-hydrogenated, and especially the Si-doped, multilayer. The latter coating and ion beam deposited coatings yield stable, very low friction behaviour under dry sliding conditions. The a-C:H coating coating shows low friction only in humid atmospheres, up to high loads. Wear resistance is high in this case but because of the high hardness, the counterpart is worn rapidly. The 13.56-MHz RF PACVD a-C:H coatings show excellent wear resistance under dry as well as humid sliding conditions, while at the same time protecting the surface of the steel counterbody. High load-carrying capacity is apparent for the magnetron sputtered a-C:H-W multilayer coating, and especially for the PVD C/C-Cr coating, which should prevent failure under high contact stress. The low frequency RF DLC coating does not show peak properties under the given test conditions, but offers a combination of good wear resistance, low friction behaviour and considerable load-carrying capacity.
C. Donnet et all [34] investigated the dependence of friction and wear of DLC coatings on environmental conditions and the nature of the coating as determined by the deposition process. Most DLC films contain a significant amount of hydrogen, depending on the precursor material and deposition method. For varied deposition method, the hydrogen concentration ranges from less than 10% to about 50%. Doping elements such silicon, fluorine, nitrogen and various metals may be incorporated in the film structure.
Friction coefficient of adherent DLC films, typically ranging from 0.01 to 0.5, depending on the nature of the DLC film and the tribotesting conditions are strongly governed by tribochemical effects. However the shearing ability strongly depends on the nature of the surrounding gas present in the contact. DLC coatings are known to be extremely sensitive to the presence of oxidizing species (oxygen, water vapour) during friction, which gives rise to a noticeable tribo-oxidation of the topcoats, generally increasing the friction and wear. (Figure 2.48):

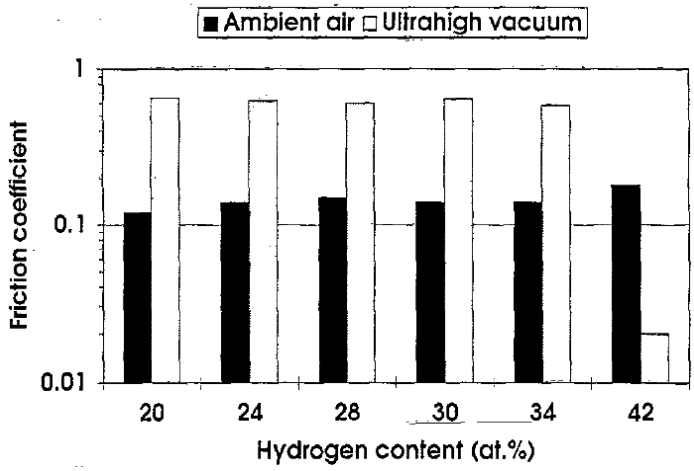

Figure 2.48. *Steady-state friction coefficients in ultrahigh vacuum and in ambient air (RH= 40-60%) for DLC films with different hydrogen content (%). [34]*

The results of the experimental test can be summarized as follows. Whatever the hydrogen content of the films, the friction coefficient is confined in the 0.12 – 0.18 range in ambient air. The friction behaviour in UHV presents two opposite behaviours: steady-state friction coefficients are systematically higher than 0.58 for DLC films with

hydrogen contents up to 34% and near 0.02 for DLC film with the highest hydrogen content (42%).
Murakawa et all [35,36] and Taube [37] investigated the potential of using DLC coated dies in deep-drawing of aluminium sheets. The results show that the DLC coated dies exhibit excellent anti-sticking properties for aluminium under oil-lubricated conditions.
P. Carlsson et all [38] studied the tribological performance of four different types of DLC coatings in sliding against hot dip Zn e and 55% Al-Zn coated steel. The evaluated DLC coatings show potential to work as tool coatings in dry forming of hot dip Zn-coated steel while they do not perform well in case of dry forming of hot dip 55%Al-Zn coated due to severe material pick-up. As already evidenced in [31] the frictional behaviour of the DLC coatings can significantly be improved by a polishing treatment where the surface irregularities originating from the deposition are removed.
Graphite coating of tool steels carried out by pressure spraying for metal-forming applications have been investigated by K. Hanada et all [39]. The pressure-spraying coating method based on a principle of shot peening can coat solid lubricants directly on the substrate at room temperature with pressurized gas, which is a binderless process. Figure 2.49 shows the coefficients of friction of tool steel substrate as-received, as-conventionally coated, and as-sprayed at 0.4MPa for 20s. The as-received substrate and as-conventionally coated substrate indicate about 0.45 and 0.1, respectively, at the initial friction. However those values increase immediately with increasing the friction time. The pressure-sprayed substrate indicated almost the same μ, 0.08-0.1, as the conventional coating substrate at the initial friction. The main point is that a μ value in the range 0.08-0.1 is almost constant with the friction time: the sprayed substrate has a much longer lubrication life time, more than 50 times compared with the case of conventional coating substrate.

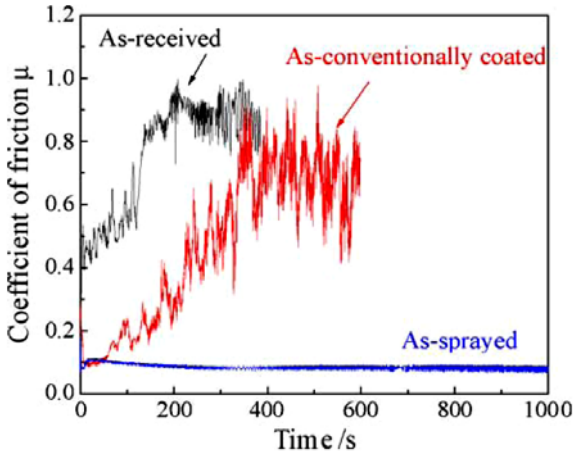

***Figure 2.49**. Coefficients of friction of tool steel substrate as-received, as-conventionally coated, and as-sprayed at 0.4 MPa for 20 s. [39]*

Nickel based coatings have been investigated by C.S. Ramesha et all. [40]. The authors investigated the effects of volume fractions of silicon nitride, fly ash and calcium fluoride, microstructure, load (contact pressure) and sliding velocity on the friction and wear behavior of nickel based composite coatings. Nickel which possess high tensile strength, good toughness and corrosion resistance is a popular choice as

the matrix to disperse both hard and soft reinforcements to improve its wear and anti-friction resistance.
The soft reinforcements have the following properties:

- Silicon nitride possess low friction and high wear resistance combined with good resistance to high temperature oxidation.
- Fly ash is an inexpensive waste material possessing high hardness,
- Calcium fluoride is a good solid lubricant which can be used for high temperature application.

It is observed that nickel composite coatings exhibit lower coefficient of friction when compared with that of the nickel coatings for all the above reinforcements. The coefficient of friction decreases with increased content of the reinforcing phase.
Concerning the effect of contact pressure (loads) on the coefficient of friction of nickel and nickel composite coatings, it is observed that for all studied contact pressures, nickel composite coatings exhibit much lower coefficient of friction when compared with nickel coating. Increase in coefficient of friction of all the coatings on increase in loads can be attributed to larger tendency for plastic deformation at higher loads. This in turn will increase the probability of formation of asperity junctions resulting in higher friction.

CrN coatings offer high thermal stability and oxidation resistance, high corrosion resistance, high wear resistance and a low adhesion to some engineering work materuials such as Cu. Furthermore the relatively low intrinsic stress state and the relatively low deposition temperature make it possible to deposit relatively thick CrN coatings (possible to polish resulting in a very smooth surface) on most steels without any risk for thermal softening. In [38] it is demonstrated how CrN coating results in high friction when sliding against both Zn and 55%AlZn.

2.5.5.2 Organic coatings tribology

Typical polymer based thin organic coating formulations consist of a resin (coating-forming material) and different types of additives, e.g. forming additives and corrosion inhibitors [41] Polymer systems are created of many unlike parts to acquire unique properties for a given application. All polymers have a long chain fatty acid, or monomer. To keep the monomers in the desired suspension surfactants are used. Other additives can be added for various effects, however, the polymer creation process is as important as the ingredients used in the composition. The base of the polymer is the monomer which contains the base hydrocarbon which provides bonding locations for other items to be added. The base monomer controls many of the physical properties of the finished polymer. The choice of monomer influences the glass transition temperature, T_g, and the molecular weight of the system. The T_g has proven to have a strong impact on the lubricity of the system. The lower the T_g the better the lubricating properties. The T_g is controlled by the ability of the molecule to reorient itself in the system. Wider molecules have lower T_g's, however, the larger the free space in the system the more room there is for movement. For this reason under high pressures the T_g's change due to the added restriction due to compression. Experimentation of introducing CO_2 into the polymer emulsion has been able to maintain the free volume during higher hydrostatic pressure on the polymer, however, application at pressures equivalent to cold forming applications has not been tested.

Cross-linking restricts polymer movement so a polymer with little or no cross linking is preferred since material movement is crucial to the performance. Also, branching polymers are unique that the restriction due to wideness is offset by the greater free space associated with the molecule making the change in T_g specific to the individual monomer.
Surfactants, or stabilizers, are used in many different capacities in the polymer creation process. In emulsion polymerization the monomer is mixed with water and a stabilizer is added to make the emulsion remain in its mixed homogenous state. Phosphoric acid is added to react with the metal surface that the polymer will come in contact with, and the phosphoric acid covalently bonds with the monomer as shown in Figure 2.50. For boundary lubrication the long chain fatty acids are good surfactants since they securely hold the material in high stress situations [42]. Additional surfactants are added to the system to ensure stability over time during storage.
There are many additives being used to improve the performance of forging lubricants, and these need to be understood to aid in formulating a new lubricant. The additives of major importance in a cold-forging application are extreme pressure additives, esters or fatty acids, sulfur, salts, phosphorus, silicones, etc. The extreme pressure additives allow for the shearing mechanism to work since the lubricant needs to shear against itself easily. Graphite is a good example of lubricant with low shear stress, however, it does not adhere to the surface well and cannot be applied easily prior to forming. Graphite is commonly used in hot forming where other lubricants cannot operate under the higher temperatures. Materials added to the polymer can tailor the performance in order to meet specific needs.

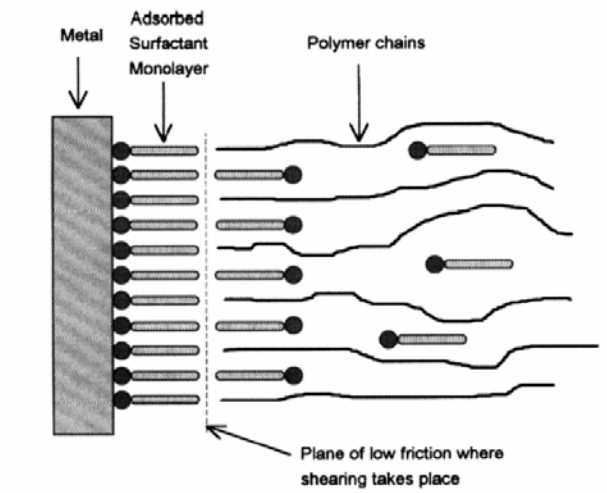

***Figure 2.50**. Surfactant in friction layer. [42]*

Many cold forging lubricant systems use a particulate layer or layers to facilitate shearing during the forming operation. The layers break and the particles are able to slide and redistribute during forming protecting the material underneath. A solid additive to the polymer may allow a similar mechanism for lubrication.
Many tribological investigations have been carried out to understand the wear and friction mechanism of polymers in sliding contact with steel. In particular, great attention has been focused on transfer layer film mechanism in friction. Since most polymers are self-lubricating materials, the transfer film of polymers can act as lubricant [43-47]

In [48-52] P. Carlsson assumes that the coefficient of friction of the organic coating can be controlled by its chemical composition (e.g. by adding forming additives with specific properties) and the coating thickness. Besides the topography of the substrate material also influences the friction characteristics.
The investigated tribological pairs were mainly two, thin organic permanent coatings deposited on hot-dip coated mild steel (pure Zn and 55%Al-Zn) while the counter material was steel. In [48] the friction behaviour of three different types of organic coatings characterized by a different amount of organic part and different chemical composition of the same was studied. Three experimental tests were performed: modified scratch testing, ball on disc testing and bending under tension testing. As the results obtained showed that all tests yielded consistent information concerning the friction and wear properties of the material the ball on disc one was utilized in [49-51].
Of the permanent coatings investigated, a pure organic coating showed the lowest coefficient of friction (μ close to 0.1) and the highest wear resistance offering excellent anti-galling properties. In contrast, a mixed organic inorganic coating displayed a relatively high coefficient of friction (μ close to 0.3) and a significantly lower wear resistance.
The friction characteristics were classified into different groups of performance (Figure 2.51). Typical friction characteristics for well performing organic coatings (Figure 2.51(a)) include a low initial steady-state friction level followed by a sudden increase at a critical number of revolution. The initial friction corresponds to an intact organic coating thus separating the steel sheet from the steel ball surface. The rapid increase and subsequent scatter in friction corresponds to a breakthrough of the organic coating followed by microwelding and subsequent material transfer of soft metal coating to the steel ball. Poor performance (Figure 2.51(b)) appears by an instant increase in friction from start of the test. The bad performing organic coating had a high tendency to form relatively large loosely attached organic coating fragments within the wear spots. These fragments are easily detached from the sliding interface in a multiple sliding event which explains the poor lubricating properties of the thin organic coatings.
Some coating exhibited a transition in the friction curve (Figure 2.51(c)), for which the transfer of polymer film from the sheet to the ball is more continuous, resulting in a well covering transfer film.

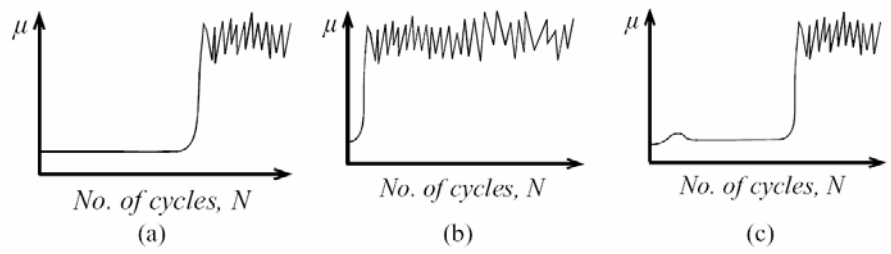

***Figure 2.51**. Schematic illustration showing the three different types of friction characteristics obtained by ball on disc testing. **(a)** Well performing organic coating, **(b)** poor performing organic coating and **(c)** well performing organic coating but showing a transition in the friction curve.[51]*

Besides a continuous wear (resulting in a continuous reduction of the coating thickness) of the organic coating two different coating failure mechanisms have been observed in the cases were galling occurred (Figure 2.52):

- adhesive failure
- plastic flow and ridge formation

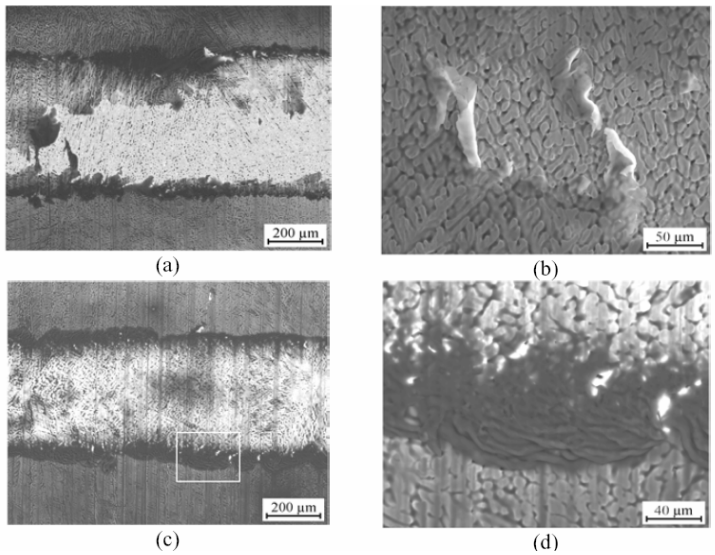

Figure 2.52. *Coating failure mechanism observed in the modified scratch test. Adhesive failure resulting in complete substrate exposure (**a** and **b**) and plastic flow and ridge formation due to low load carrying capacity (**c** and **d**). Scratch direction from left to right.[52].*

The former mechanisms is promoted by a poor adhesion between the coating and the substrate, while the latter mechanism is promoted by a low hardness (low load carrying capacity) of the coating. In general the tendency to adhesive failure and plastic flow/ridge formation will increase with coating thickness above 1.5-2.0µm.
According to the Authors, experimental evidenced the wear characteristics of the thin organic coating are also strongly influenced by the substrate surface topography.
Both the two different substrates were characterized by a long and a short range waviness resulting from the stretch levelling of the steel strip after the hot dip coating process. the organic coated samples displayed a less pronounced wavy surface profile with increasing film thickness since the low level regions tend to be filled with the organic substance during the coating deposition process. In [48] analyses of the as deposited coatings confirmed that the coating thickness is strongly influenced by the surface topography and that the coating thickness on the asperities is only about 5-10% of the nominl thickness value (i.e. 50-100nm). In a sliding contact between a rough surface topography and a smooth tool surface the real contact area corresponds to a few contact points representing the highest asperities, which in combination with thin thicknesses of the organic coating at the top of the asperities may result in localized wear of the organic coating (Figure 2.53).

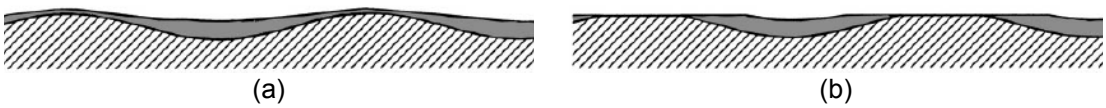

Figure 2.53*. Schematic view of theas deposited organic coating (a) and an example of localized break through of the coating at the asperities. [52]*

2.6. High temperature tribology of High Strength Steels

2.6.1. Introduction

At present the reduction of fuel consumption and CO_2 emissions is one of the most important challenges that the automotive industry is facing. Consequently, the need of limited fuel consumption and pollution emission with eventually constant or improved performances is leading towards a dramatic attention for the car weight reduction. About one-third of a passenger car's total fuel consumption directly depends on its weight: for example, according to industrial estimations, a 100 kg weight reduction implies a fuel saving between 0.3- 0.5 litres for every 100 km driven. High Strength Steels (HSS) show a great potential for meeting these challenges, since their use leads to a reduction of the total weight of the car body-in-white without compromising its structural performances. In the case of the quenchable boron steel 22MnB5 (USIBOR 1500P™), the mechanical and microstructural characteristics required for the formed components have led to the development of a new class of sheet metal forming processes carried out at elevated temperatures, called hot stamping [53-58].
During the hot stamping industrial practice, the steel sheet, whose initial microstructure is a homogeneously distributed mixture of ferrite and pearlite, is heated in a furnace to a temperature in the austenitic range, equal to or higher than Ac_3. The heated steel sheet is then extracted from the furnace, transferred to a pressing machine, where it is simultaneously formed and quenched into cooled dies until the entire steel sheet is transformed into martensite (see Figure 2.54).

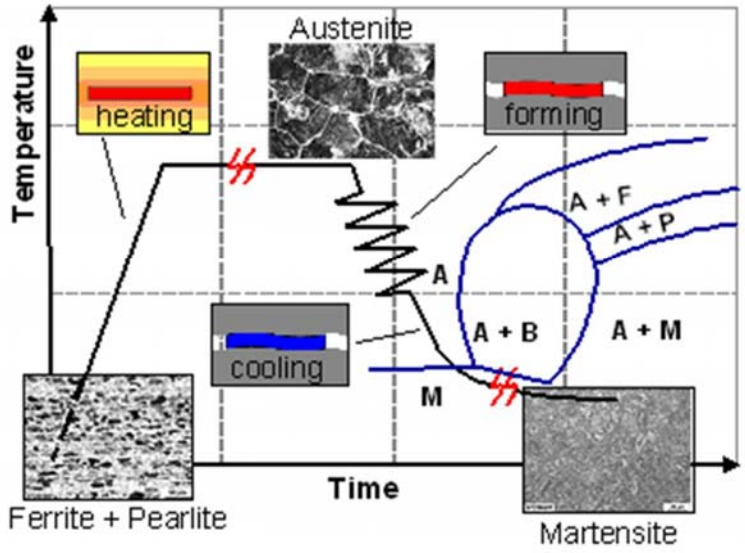

***Figure 2 54**.Thermal cycle and sheet metal microstructural evolution during hot stamping.*

When a steel blank is deformed at elevated temperatures, heating should be carried out in a protective atmosphere to avoid oxidation (scaling) and surface decarburization. However, the hot stamping operations are usually carried out in air, implying surface oxidation and some superficial decarburization, which may have detrimental effects on

both the service life of dies and tools and the surface properties of the final component [59]. The former are due to the extreme hardness of the surface scale, which determines high friction conditions between the dies and the sheet metal in the deformation stage and a relevant die wear, especially in the blanking stage. Moreover, hot formed steel parts usually require an additional operation compared to the traditional stamping process, that is shotblasting or sandblasting, in order to remove the scale layer from their surface. In the last decade, the limits above described have been overcome by Arcelor-Mittal introducing an innovative steel, named Usibor1500P™, whose most relevant characteristic consists in an innovative aluminum-silicon (Al-Si) coating deposed on a 22MnB5 metal sheet capable of preventing surface oxidation during hot stamping process.

2.6.2. High Strength Steel tribology

A survey of the literature shows that the tribological behaviour of the Al-Si coated High Strength Steel sheets, in different hot stamping conditions, has not been completely investigated yet. Up-to-now, many efforts have been spent in the investigation of the material microstructural evolution during the process and in the identification of the proper process parameters, but paying less attention to the material tribological behaviour when subjected to process conditions typical of hot stamping. Very few studies into the tribological behaviour of HSS are available in the open literature. Skåre et al. [60] has looked at the friction and wear behaviour of HSS by the acoustic emission technique. They concluded that the surface quality of the tool is important and that it is possible to use uncoated hardened tools if a good surface of the tool is maintained. They also found that hot-dip galvanised HSS sheets induced less wear on the tools compared to untreated HSS.
J. Hardell et all [61-62] investigated the high temperature friction behaviour of different tool steels during sliding against a 7.9mm thick Al-Si coated HSS sheet by means of ball on disc reciprocating test. The work focuses mainly on investigating the fundamental tribological behaviour of these materials at elevated temperatures and it is not an attempt to simulate the hot-metal forming process. Two sets of experiments were conducted:

I . The friction behaviour of different tool steels and HSS tribological pairs were studied during a temperature ramp from room temperature up to 800°C. These temperature ramp experiments were mainly aimed at studying the influence of increasing temperature on frictional behaviour
II The second set of experiments was conducted at three different constant temperatures with a view to studying the influence of temperature on friction of tool steel and HSS. In this case only the sheet specimen was heated, once it reached the desired temperature the tool specimen was brought in contact and loaded against the sheet metal specimen and the test was started.

The frictional behaviours as a function of temperature in the range 40–800 °C for different tribological pairs are quite similar (Figure 2.55). The initial friction coefficients at the time of commencement of the tests were 0.8. These then quickly decreased to values of 0.6. This trend was observed for all the plasma nitrided tool steels as well as for the untreated tool steels implying that the initial friction coefficients are neither dependent on the composition of the tool steel nor the surface treatment. As the

temperature increased, friction also increased quite rapidly to 1.4. The plasma nitrided tool steels show a rather gradual increase in friction and lower maximum friction coefficients vis-a-vis the untreated tool steels. As the test progressed and the temperature increased, the friction coefficient started to decrease. The temperature at which friction started to decrease was different for different tool steels. The friction continued to drop to a minimum value which was reached at a temperature of 600 °C. Towards the end of the tests, an increase in friction has been observed.

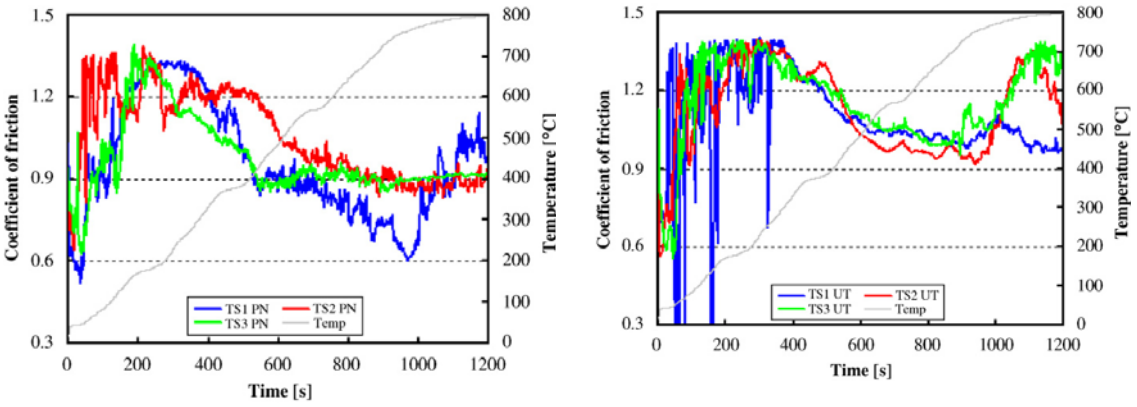

(a) (b)

***Figure 2.55**. **(a)** Coefficient of friction as a function of time for plasma-nitrided tool steel and **(b)** untreated tool steel sliding against and Al–Si-coated high-strength steel during a temperature ramp from 40 to 800 1C (load: 50 N; stroke: 1 mm; frequency: 50 Hz). [61]*

The frictional characteristics of the plasma nitrided tool steels and Al–Si-coated HSS pairs at constant temperatures 40, 400 and 800 °C are shown in Figure 2.56.
The initial friction behaviour at 40°C was similar to that observed in the temperature ramp tests with an initial drop to below 0.6 followed by a sharp increase to about 1.4 and stabilisation at this level thereafter (Figure 2.56 (a)) At 400°C, the initial results were also similar to those observed in the temperature ramp tests with an initial drop but in this case the values were slightly higher (Figure 2.56(b)).
In the case of a testing temperature of 800°C (Figure 2.56(c)), the TS1 PN, friction initially increased from 0.7 to 0.9 then remained at this level before increasing again towards the end of the test to a value of 1.2. The friction in the case of TS2 PN increased from 0.7 to 1.0 after a test duration of 200 s. This was considerably higher compared to that for TS1 PN and also that for TS3 PN for the majority of the test duration. In the case of TS3 PN, friction decreased rapidly from 1.0 to 0.8 during the initial 50s and thereafter gradually increased to a highest value of 1.35 towards the end of the test. It then decreased to 0.9 by the culmination of the test.
In [62] the investigation both on high strength boron steel-plasma nitrided tool steel tribological pairs at elevated temperatures-as well as self-mated hardened high strength boron steel tribological pair has been carried out. The work focused on evaluating the influence of the sheet metal specimen temperature on the friction behaviour y means of a ball on disc reciprocating test. Three temperatures have been considered for the strength boron steel/tool steel tribological couple: 500, 600, 800°C. The tests conducted on AlSi coated boron steel against plasma nitrided tool steel 1-3,

at 500°C have resulted in very high and unstable friction for the first 60s of the test. At 800°C the friction decreases to almost half of its value at 500°C.

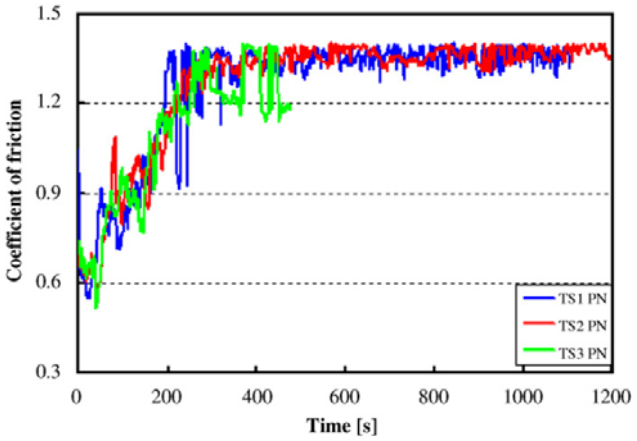

(a)

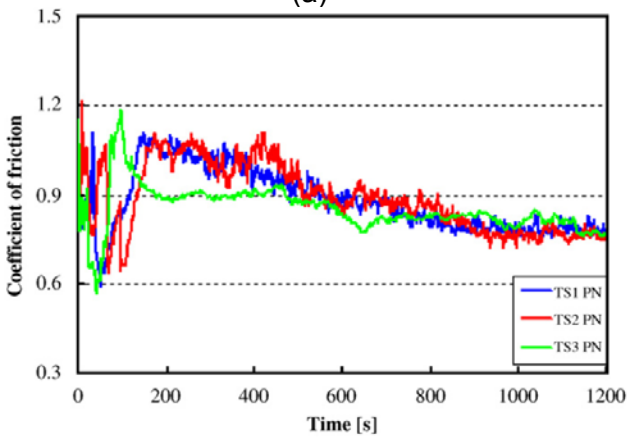

(b)

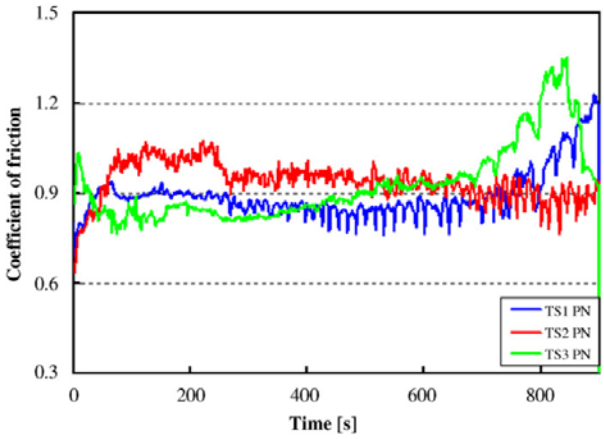

(c)

Figure 2.56. Coefficient of friction as a function of time for plasma-nitrided tool steel and Al–Si-coated high-strength steel at ***(a)*** *800 40°C,* ***(b)*** *400°C and* ***(c)*** *800°C (load: 20 N; stroke: 2 mm; frequency: 50 Hz). [62]*

The steady state friction behaviour was also investigated (Figure 2.57). Friction coefficients obtained from the tests conducted on Al–Si coated boron steel during sliding against the three plasma nitrided tool steels at 500 ◦C are very high and only tests involving plasma nitrided tool steel 3 lasted the entire test duration. The other two seized after a short time as can be seen from Figure 2.57(a). Interestingly, test conducted on Al–Si coated boron steel and plasma nitrided tool steel 1 pair at 800 ◦C resulted in considerably lower friction which increased significantly towards the end of the test, see Figure 2.57(b).

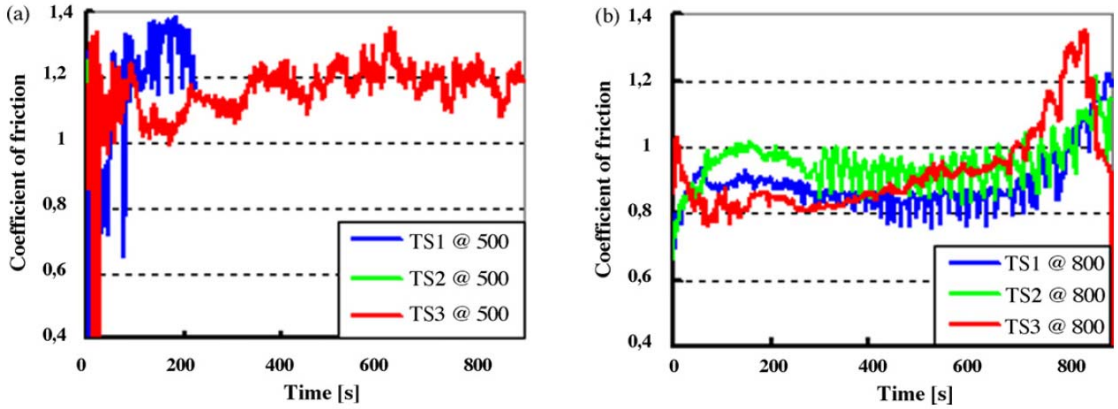

(a) (b)

***Figure 2.57**. Coefficient of friction as a function of time for tests on plasma nitrided tool steels 1–3 against Al–Si coated boron steel pairs at **(a)** 500 ◦C and **(b)** 800 ◦C (load: 20 N; stroke: 2 mm; frequency: 50 Hz). [62]*

The main conclusion concerns the fact that as the sheet metal specimen temperature increases, the coefficient of friction decreases and, according to the authors, this is possibly due to formation of oxides and/or intermetallic compounds that consequently reduce friction. Possibly a lubricious oxide layer forms on the Al-Si coated HSS at elevated temperatures. The Al-Si coated surface undergoes surface morphological changes and their influence on the friction and wear characteristics are unclear and further investigations are necessary to explain the mechanism and their role in determining the tribological behaviour.

The same author investigated different surface treatments/coatings applied on either the tool or sheet surface or both by means of flat drawing test, reproducing the hot stamping thermal cycle. [63] One tool steel composition has been studied in three different variants: untreated, plasma nitrided and nitreded + TiAlN coated. The workpiece material was also studied in three different variants but only the Al-Si coated UHSS will be here considered. The 1.6 mm thick sheet specimen has been heated at 930°C and retained for 390 seconds in order to allow enough time for the diffusion to take place before testing, while the flat dies were kept at room temperature. Once the sheet specimes reached the desired temperature it is then fed into the position between the tool specimens where the target normal load (56 MPa) is applied. The sliding velocity is of 100mm/s while the sliding distance is equal to 280mm. The TiAlN coated tool steel has shown the lowest friction, the initial friction starts at approximately 0.37 and steady state is reached at a level of 0.4. After the running-in, the difference in coefficient of friction is negligible between the different tool steel

variants when sliding against the sheet metal specimen. The higher initial friction values for the untreated and plasma nitrided tool can be attributed to the presence of rough asperities on the milled surfaces of these specimens compared to the TiAlN coated tool steel specimens that were polished prior to deposition of the coating.
The hot flat drawing test has also been performed by A. Yanagida et all. [64] (Figure 2.58). A 2mm thick Al-Si coated 22MnB5 sheet is heated up to 800°C using an infrared image furnace. The temperatures of the workpiece at three point of 150, 300 and 470mm from the exit point of the furnace are of about 800°C, 720°C and 600°C respectively. Once the sheet metal has reached the target temperature it is drawn and compressed by a compression device. According to the authors after heating at a temperature of 720°C a 5 layered structure is observed and the melting point of film does not occur during heating. The heating range of the 22MnB5 steel did not exceed 12-15 K/s to anable a diffusion control alloying reaction between the Al-Si coating and the iron of the bulk material. Also in this case in order to emulated the cold dies condition of the hot stamping the testing dies are kept at room temperature.

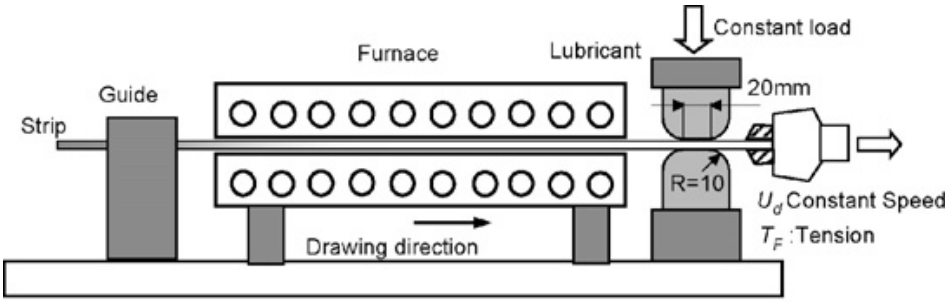

***Figure 2.58**. Schematic representation of simulation testing machine for hot stamping [64]*

The experimental tests have been carried out in order to investigate the friction coefficient dependence on sheet metal temperature, keeping the sliding speed, the stroke and the normal load constant.
Figure 2.59 shows measurement results of the mean coefficient of friction under dry condition in the case of a sheet metal specimen equals to 600°C, 700°C and 800°C: the mean coefficient of friction increases with increasing temperature

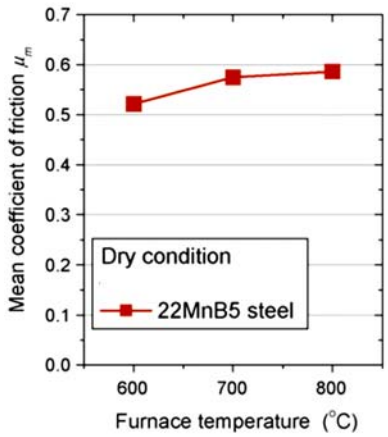

***Figure 2.59.** Effect on temperature on mean friction coefficient. [64]*

This experimental results are in disagreement with what presented in [65-67]. In [65] the hot flat drawing test is again performed. starting with low normal pressure value of 10MPa, three different drawing temperatures: 510°C equal to 20s of transfer time, 700°C for 10s of transfer and 900°C for direct transfer were investigated, the results are presented in Table 2.1.

σ_N [MPa]	Temperature [°C]	μ
10	510	0.44
10	700	0.42
10	900	0.40
25	510	0.45
25	700	0.43
25	900	0.45

Table 2.1. *Different values of friction coefficient for different temperatures and surface pressures.*

Different temperature values have little influence on the frictional behaviour of the tribological system. The directly transferred sheet at a temperature of 900°C shows the lowest value of approximately μ=0.4, increased transfer time and decreasing temperature respectively leads to an increase of the friction coefficient of μ=0.42 for a testing temperature of 700°C and 0.44 for a testing temperature of 510°C. At high surface pressure (25MPa) the same phenomena applies.
It can be observed that there is no or little influence of the contact pressure on the friction behaviour.
The same trends but much more evident has been observed in [66-67]. For the determination of the friction coefficient under process relevant conditions, a modified cup deep drawing test setup was developed (Figure 2.60).

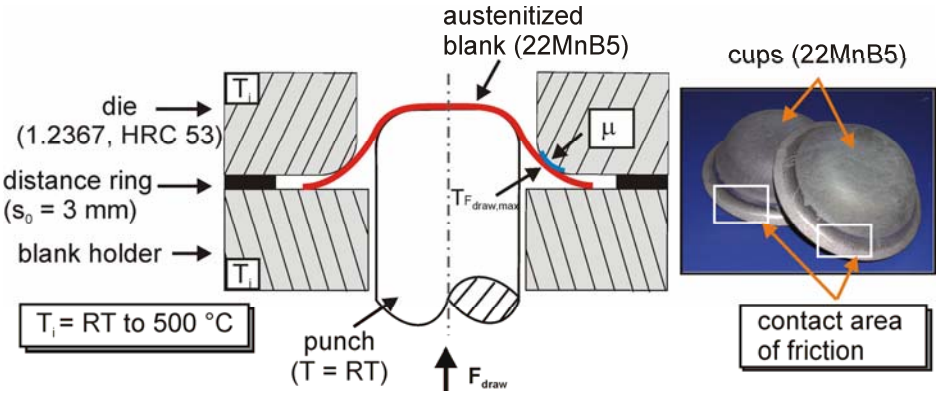

Figure 2.60*. Schematic sketch of the experimental setup of the cup deep drawing test (left) and two drawn cups at elevated temperatures with the contact areas of the main friction between blank and tool pointed out (right.) [66]*

For the experimental reproduction of the hot stamping process aluminium-silicon coated boron-manganese steel 22MnB5 blanks with a diameter between 80 mm and 90 mm had been exposed to a heat treatment of 5 minutes at an austenitization

temperature of 900 °C and 950 °C before being transferred manually to the cold or defined heated tooling device and subsequently being drawn.
Different temperatures at the moment of the maximum punch force were realized by varying the tool temperature in a range between 25°C and 500°C. During the tests, the temperature of the punch was maintained constant at room temperature. All the tests were carried out with a punch velocity of 10mm/s.
In Figure 2.61 the evolution of the friction coefficient of the investigated material is shown as function of the specimen temperature.

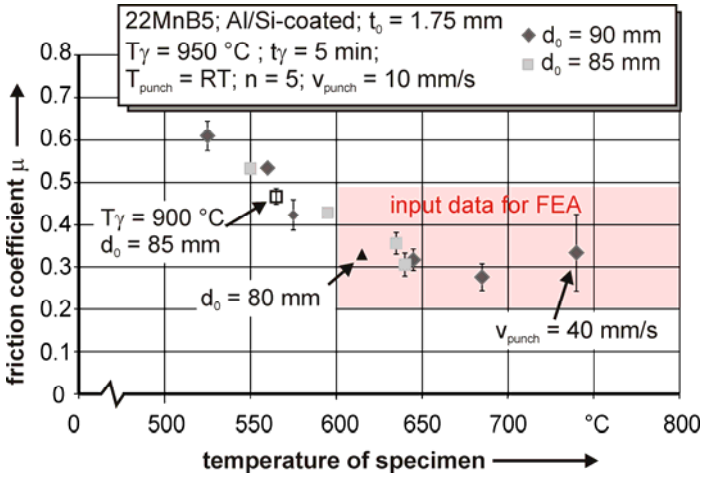

***Figure 2.61**. Evolution of the friction coefficient in dependency of the specimen temperature. [66]*

The coefficients were calculated following Siebel's approach It can be recognized that the frictional characteristic μ exhibits a significant decrease with increasing blank temperature, whereby the values lie in a range between μ=0.6 until μ=0.3. Within hot stamping, the forming operation takes place at about 600-800°C, so the relevant mean friction coefficient in this temperature range can be determined from 0.3 to 0.4. One aspect contributing to the detected evolution could be related to the effect that, with increasing temperature, the aluminium-silicon coating, alloying to a ternary Al-Si-Fe layer system during heat treatment [68] shows a more and more doughty consistency. Hence at elevated temperatures the coating acts as a kind of lubricant, resulting in a decrease of the resistance force of the sliding contact partners and of the friction coefficient respectively. Furthermore, with the aim to find a basic explanation of the determined development of the tribological properties, smoothing effects affecting the real contact area between workpiece and sheet as well as the increased ductility of the blanks' bulk material has to be taken into consideration. The almost linear trend of the friction coefficient μ in Figure 2.61 can be interpreted that in this temperature range the real contact area and the resulting frictional properties are mainly driven by elastic deformations of the involved surfaces according to Greenwood and Williamson.

The wear behaviour of the Al-Si coated HSS sheets was also investigated by J. Hardell et all [61,62]: different types of plasma nitraded treated and untreated tools were investiagted. By performing a Ball on disc reciprocating test (line type of contact) the wear behaviour has been investigated as function of temperature ramp (room

temperature up to 800°C) as well as the case of constant temperature tests (40, 400°C and 800°C) showing a high dependency on testing temperature.
The high friction obtained during tests at 40°C (Paragraph 2.6.1.1) may be attributed to the occurrence of severe adhesion and material transfer from the disc surface to the pin surface. Figure 2.62(a) and (d) show removal of material fragments from the Al-Si coated steel and some material pick-up on the tool steel surface. The low wear of the tool steel may be attributed to the fact that Al-Si alloys are known to form compacted surface layers during sliding. these layers are of protective nature and anhance the wear resistance of the material.

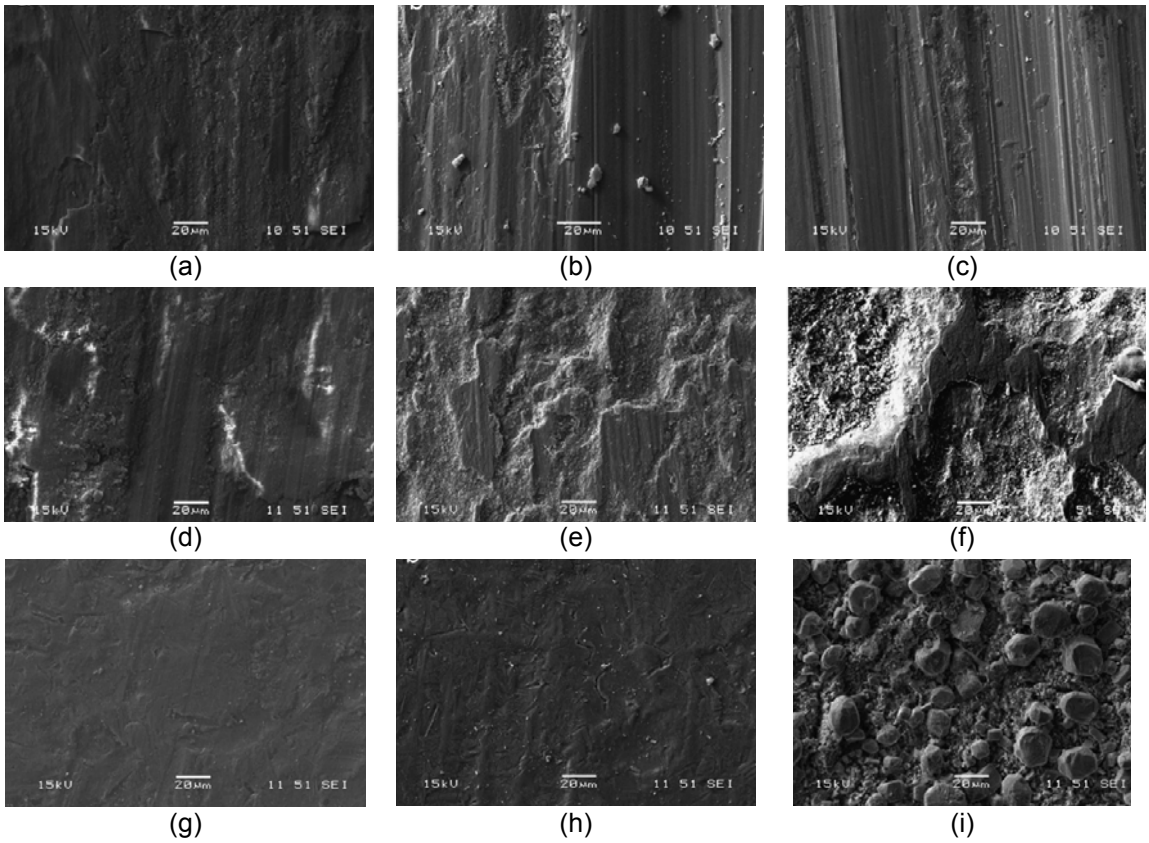

***Figure 2.62**. SEM micrographs of plasma-nitrided tool steel 1 at **(a)** 40 °C, **(b)** 400 °C, **(c)** 800 °C and worn Al–Si-coated high-strength steel at **(d)** 40 °C, **(e)** 400 °C, **(f)** 800 °C (load: 50 N; stroke: 1 mm; frequency: 50 Hz); and unworn Al–Si-coated high-strength steel at **(g)** 40 °C, **(h)** 400 °C, **(i)** 800 1C. [43]*

At 400°C the friction coefficients are lower as compared to those at 40°C. The SEM micrograph (Figure 2.62(b)) shows a relatively clean and smooth tool steel surface. The governing wear mechanism appears to be mainly adhesive accompanied by some abrading action of oxidised wear debris as can be seen from some scoring marks on the tool steel pin specimen surface in Figure 2.66 (b)and some plastically deformed plateaus on the Al–Si-coated disc surface in Figure 2.62(e). Wear of the Al–Si disc specimen at 400 °C seems to be mainly confined to the
coating since an EDS analysis of some of the retained wear debris indicated the presence of Al and Si only. The wear mechanism at 800 °C is predominantly adhesive

as is evident from the SEM micrographs in Figure 2.62(c) and (f). There are also signs of compaction of oxidised wear debris on worn surfaces of both the tool steel pin and Al–Si-coated disc specimens. All tool steel pin specimens are characterised by scoring marks which may result from the abrading action of hard oxidised wear particles.
The features of the worn surface of the disc reveal that sliding occurs on several small plastically deformed plateaus. Also, as observed during the experiments, the valleys are filled with retained wear debris during sliding. This can be supported by the fact that there is a substantial amount of wear debris accumulated in the contact during sliding and that retained wear debris in the valleys are also observed in the SEM micrographsIn [63] the same author has investigate the wear behaviour of Al-Si coated 22Mnb% HSS sheet by means of the hot flat drawing test at a temperature of 930°C. As result the worn surface of the untreated tool steel is characterized by both abrasion and severe adhesive action (galling) as indicated by the pick-up/transfer of the Al-Si coating on the tool steel surface. The nitrided tool steel surface is also characterized by some abrading marks and transfer of the Al-Si coating but to a smaller extent. The severity of abrasion and adhesion is significantly reduced in case of the TiAlN coated tool steel although some transfer of the coating can still be seen.
In [65] the Al-Si coated boron HSS sheet wear behaviour has been evaluated by means of a deep-drawing process simulator (see paragraph 2.6.1.1)
The test sequence was regularly interrupted to characterize and measure the wear evolution. Two wear modes were evidenced: just after the entry of the contact between the strip and the tool die abrasion was predominant and adhesion of Al-Si was observed at the contact exit. these built up layers, formed very early at the beginning of the test are known to form compacted layers at the tool surface during sliding and low wear could be attributed to them.

CHAPTER 3

SHEET METAL FORMING TRIBOLOGICAL TESTS

3.1. Classification of tribological tests

Testing of lubrication is a crucial event in metalworking since insufficient lubrication performance results in severe problems in terms of tool failure and reduced product quality, hence economical loss for industry. Surface quality is of significant importance when forming stainless steel due to expectations of good surface appearance, i.e. scoring is unacceptable in most applications. Lubricant testing is also required in order to find environmental substitutes for hazardous compositions often applied in severe forming operations. However applying untested prototype lubricant directly in a production line imposes large risks of tool failure and damage of machines and other costly equipment.

Tribological testing is of relevance for studies of lubrication mechanisms. It is clear that tribological conditions involve many different parameters implying that prediction of resulting frictional stresses on basis of theoretical calculation is impossible. Therefore experimental testing must be applied in order to evaluate the lubrication effect either in qualitative or quantitative terms. The general process related parameters known to influence a given tribological condition are presented in Figure 3.1. [4]

Workpiece	Tool	Lubricant	Process Parameters	Environment	Equipment
Material	Material	Composition	Sliding Velocity	Air humidity	Stiffness
Initial condition	Condition after manufacture	Amount	Surface expansion	Atmosphere composition	Vibration
Geometry	Geometry	Temperature	Sliding length	Dust	
Surface topography	Surface topography	Viscosity	Contact pressure		
Temperature	Temperature	Compressibility			
		Thickness			

Figure 3.1. *Main tribological parameters. [3]*

Sheet forming is characterized by very varying friction and lubrication conditions depending on the type of process. Thus lubrication performance is more vital for deep drawing than stretch forming operations. The number of tests developed for sheet forming is quite low compared to bulk forming. One reason for this might be that bulk forming is more prone to wear problem due to larger contact pressures, degree of deformation and sliding lengths.

Nevertheless tribological tests for sheet metal forming can be divided into three main categories accordingly to their capabilities in both replicating and controlling the process parameters:

- material testing
- process type testing
- Simulative testing

In the following g chapters the three different typologies of tests will be described and examples will be given.

3.2. Material testing

Material type of testing is usually performed on commercially available friction testers that are configured to realize traditional pin on disk or ball on disc experiment.
The pin/ball on disc experimental set-up (Figure 3.2) consists of a cylindrical pin with a flat/spherical ending surface that is brought in contact with a rotating disc while subjected to a normal load. According to the different geometry the contact will be either a surface or a point type. In the case of a cylindrical pin with a flat ending surface the contact edges should be rounded off in order to avoid effect of concentrated forces. This aspect turns out to be of relevance when the plastic deformation in the areas of contact is not significant (e.g test with high hardness materials, or lubricated tests, characterized by low friction values). [27, 30-31, 32-34, 38-40, 48-52, 61-63]

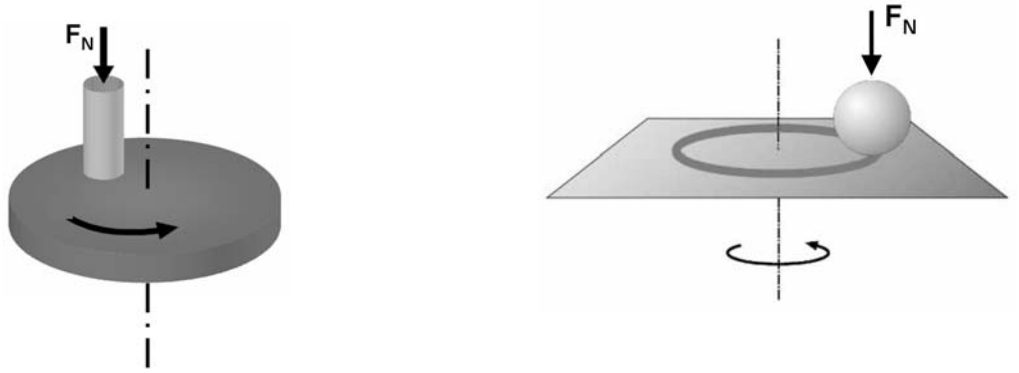

(a) (b)

***Figure 3.2**. **(a)** Pin on disc scheme, **(b)** Ball on Disc scheme.*

As the disc is rotating, a force sensor continuously records both the normal load F_N and the frictional force F_T signals. Consequently the coloumb friction coefficient is calculated as follows:

$$\mu = \frac{F_T}{F_N} \tag{3.1}$$

The continuous monitoring of the normal force F_N is used as feedback for the control of the pin positioning in the vertical direction in order to maintain a constant contact pressure at the pin/disc interface.

Attractive as it may seem for the fast and simple set-up of the test, the first approach presents the main limits in the capability of reproducing the process conditions and its use can only be limited to comparative testing of lubricants.

3.3. Process type testing

It is generally based on equipment similar to that utilised in industry, reproducing sheet metalworking process operations, without changing the basic process kinematics.
Due to their simplicity and immediate information, engineering tests, belonging to the second category, are especially attractive for industry, because of the possibility of reproducing exactly the conditions of the process. The testing procedure seldom does require special equipments and accurate control of the testing conditions. Friction data are usually obtained through the indirect measurement of the specimen deformations.
Examples of process type testing are the drawing of cylindrical cups and the Limited Dome Height (LDH) test (Figure 3.3). [66-67, 69-73]]

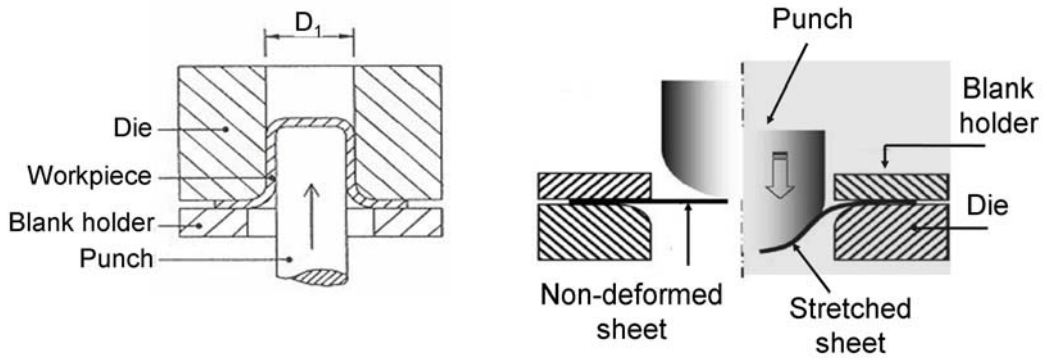

(a) (b)

***Figure 3.3**. Scheme of **(a)** Deep-drawing test and **(b)** Limited Dome Height test.*

In the case of a deep drawing test if the friction is not significantly high the final formed cup will not present tears and/or excessive necking (Figure 3.3(a)).
The method is relatively insensitive to changes in friction regarding the forming force, but the maximum drawing ratio defined as the largest blank diameter possible to draw divided by the punch diameter yields information about the friction level and in this way the lubricant performance may be ranked. Hence in such a case the test method is based on qualitative evaluations. However quantitative measurements have been developed for example based on a divided blank-holder system.
The mechanical buldge test is performed on a square sheet metal, with a hole pierced in its centre. The sheet metal is clamped on its periphery to prevent material drawing into the cavity. The blank is stretched over a hemispherical punch, which replicates the dies utilized in the real deep drawing process both in terms of material and surface finishing. The changes in the hole geometry during the test allow having qualitative information about the friction at the punch-workpiece interface: the bigger the hole diameter at the end of the test the better the lubricating system.
The evaluation of the friction coefficient at the punch-workpiece interface is possible by inverse analysis technique. The same experimental set-up has to be modelled with the FE code. The input data are the blank material flow curve and its anisotropic bahaviour,

punch speed and the friction coefficient at the punch/blank interface.The value of the friction coefficient μ, which minimizes the differences between the measured and the computed hole diameters, corresponds to the tribological condition at the punch-specimen interface.

3.4. Simulative testing

This typology of testing reproduces the tool-workpiece interface conditions taking place during a sheet metalworking operation with the full control of the relevant process parameters such as normal pressure, sliding length, sliding speed, workpiece-tool interface temperature. [61-63, 74-79]
This approach allows reproducing the process conditions, but the simulative testing apparatus has to be designed as a dedicated equipment, embedding the measurement sensors for the test control and the acquisition of the test parameters.
The flat die test and the bending under tension test are probably the most well known simulative type of testing. (Figure 3.4)

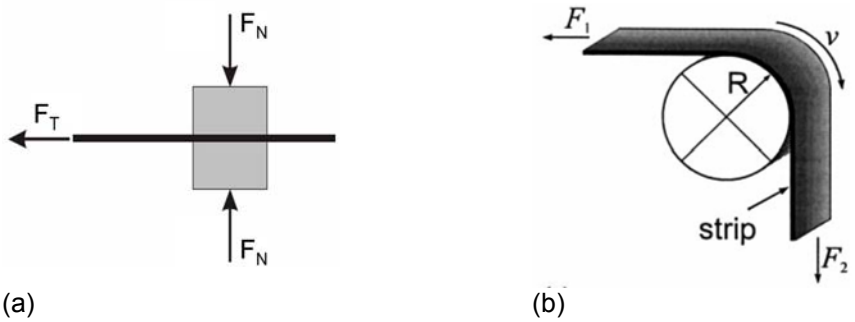

(a) (b)

Figure 3.4. Scheme of the (a) Flat drawing test and (b) Bending under tension test.

The flat drawing test is probably the most well-known method.
The simulating testing machine consists of s compression device and a drawing one. A sheet metal strip is held by the two faces of the two testing tools. They are pressed together with a total force F_N. Once the test starts the sheet metal specimen is pulled through the dies with a certain speed and for a determined stroke. The forces F_N and F_Z are measured, thus the coefficient of friction can be calculated as follows:

$$\mu = \frac{F_T}{2F_N} \tag{3.2}$$

This typology of test allows an independent control of critical process parameters like normal pressure at the sliding interface, sliding speed, interface temperature, surface texture.
Bending under tension is another test method by which conditions in deep drawing can be simulated. In this case the strip is pulled over a circular tool pin equivalent to the die entry radius in deep drawing.
The load conditions can be changed by adding a back tension thus increasing the contact pressure between punch and tool. The coefficient of friction can be evaluated depending on the equipment design. In traditional designs, the measured drawing force is influenced by bending and unbending of the sheet material hence additional tests

using a free rolling tool pin must be carried out in order to accommodate for this when calculating the coefficient of friction.

Often multiple simulative and process type tests are required to analyse complex industrial forming operations since different conditions appear during the process and at different location of the tool geometry as indicated by Figure 3.4.

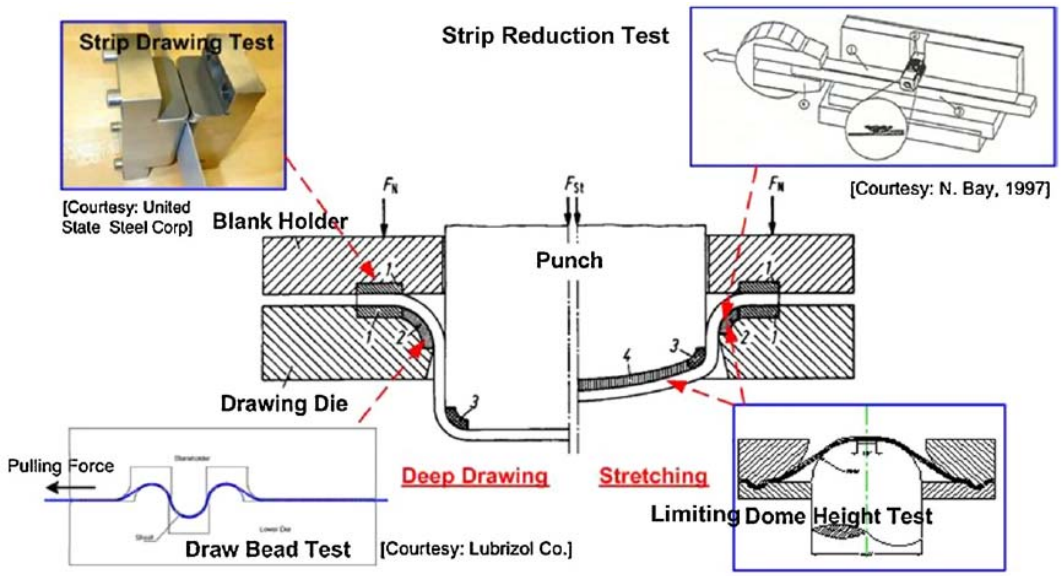

Figure 3.5. *Various tribotests used for evaluating stamping lubricants. [71]*

Both process type and simulative tests may be based on qualitative methods implying evaluation of lubricant performance or quantitative measurements by which frictional stresses are determined.
Friction level and lubricant behaviour may be evaluated by comparison of resulting forces required for the deformation of workpiece. But very often the friction does not contribute more than ~5% to the resulting forming force thus the influence of friction may be disguised by variations due to other factors. Trends yield in many cases more information than absolute values of forces. Trends can be measurements of how forces develop during a process, for Tribological Testing Methods. In case that lubricant breakdown occurs, a change in measured force distribution would appear.
Well-defined measurements of changes of frictional conditions yield the most valuable information regarding lubricant breakdown and can be achieved by designing the test in such a way, that transducers are placed as close as possible to the contact between tool and workpiece. Furthermore, the transducer design plays a significant role in this connection. Since mostfrictional forces are very dynamic, a very fast responding design is often required, which calls for the use of piezoelectric transducers being very rigid and has high natural frequencies.
In case of an appropriate instrumentation friction values are possible to be determined in simple tests without applying calculations based on theory requiring knowledge of stress-strain curve of the workpiece.
Since simulative test equipment is very often designed as dedicated equipment, force

transducers and thermo-couples are more easily implanted than test equipment used for process type tests. Hence simulative tests are often based on quantitative measurements, however there are exceptions.

CHAPTER 4

THE APPROACH

The main object of the present work consists in characterizing from a frictional viewpoint the performance of solid lubricant coatings for sheet metal working.
The lubrication phenomenon both in cold stamping operations and sheet metal forming processes carried out at elevated temperatures was studied.

With reference to the cold deformation theme the case study refers to a stainless steel deep drawing operation actually lubricated with conventional oil lubricant. Two different types of solid lubricant thin films are proposed:

- CrN and CrN-DLC coated tools
- two thin polymer based coated stainless steel sheet (namely coating A and coating B, for industrial confidentiality)

Scientific literature presents results from several tests performed on this type of lubricants through commercially available friction testers (e.g. ball/pin on disc), but they usually reproduce testing conditions far from the real forming ones. The innovative contribute of the present work consists in analyzing the friction behaviour of the proposed solid lubricant coating under process conditions and compare their tribological performance with the one of the more traditional oil lubricant. Experimental values of the friction coefficient μ are determined as function of the normal load, sliding speed, tool and sheet metal temperature. The frictional behavior has been investigated by performing the Flat Drawing Test using an experimental apparatus completely developed at The Department of Manufacturing, University of Padova, within the Phd period. The organic coating adherence behaviour has also been verified through the Modified Limited Dome Height test (MLDH). The following activities were carried out:

In the case of elevated temperature forming processes, the case study refers to hot stamping of quenchable Al-Si coated Boron High Strength Steel. A survey of the literature shows that the tribological behaviour of the Al-Si coating, in different hot stamping conditions, has not been completely investigated yet. Up-to-now, many efforts have been spent in the investigation of the material microstructural evolution during the process and in the identification of the proper process parameters, but paying less attention to the material tribological behaviour when subjected to process conditions typical of hot stamping. It has been outstand a lack of knowledge in the description of the tribological behaviour of such coating during the process and, consequently, in understanding the basic phenomena that rules the effect of Al and Si at the process temperatures in terms of friction behaviour and wear. The originality of the present work consists in investigating the interface conditions simulating the process parameters. In order to fulfil this aim the following target have to be outlined:

- study of influence that hot stamping thermal parameters (i.e. heating temperature, holding time, cooling rate) exert on the Al-Si coating chemical behaviour and surface roughness
- design and implementation of an experimental investigation based on DOE techniques to outline the influence that hot stamping process parameters (i.e. heating temperature, normal pressure, sliding speed and surface rooughness) exert the frictional behaviour

To pursue the first point, the thermal cycle typical of hot stamping operations is experimentally reproduced. The sheet metal specimens are heated at different temperatures from 20°C up to 900°C and then BSE SEM cross sections were measured in order to get information about the coating chemical evolution. For the same specimens, the coating surface roughness evolution was investigated through white light interferometer technique.
For the second purpose high temperature pin on disc testing were performed.

CHAPTER 5

EXPERMENTS

5.1. Introduction

Due to the difficulty of characterizing the tribological behaviour of real forming applications the aim of the present work is to simulate and study the tribological mechanism prevailing at the intimate contact between a forming tool surface and a mating steel sheet surface.
In the case of stainless steel sheet forming operations, PVD coated tools and thin organic coated blanks tribological performance was investigated by means of the Flat Drawing test. The adherence behaviour of the thin organic coated blanks has been evaluated through the Modified Limited Dome Height test.
For the hot stamping operations the Al-Si coating evolution with heating temperature, holding time and cooling rate was analyzed. The frictional behaviour taking place at the AlSi-coated HSS sheet/die interface was investigated by means of the Pin on Disc test.

5.2. Experimental investigation of the alternative solid lubricant coating in the case of stainless steel forming

To investigate the tribological performance of conventional liquid based and alternative solid lubricant coating the Flat Drawing test (Chapter 3.4) was performed. The experimental apparatus was completely developed, at The Department of Manufacturing (University of Padova) within the Phd period. For this reason the experimental device was validated through the comparison of the Flat Drawing test results with the ones obtained by performing Pin on Disc test on a commercially available machine.
In the following paragraphs first the case study is introduced. With respect to the reference tribological pair characterization of the as delivered materials will be presented. Then the experimental set up for friction investigation (Pin on Disc and Flat Drawing test) will be described as well as the apparatus for the coating adherence evaluation. Eventually the experimental strategy will be discussed.

5.2.1. The case study

The reference case is the deep drawing process of an hydraulic bush for quick tubes connection (Figure 5.1). The component is realized started from a 0.38mm thick and 36mm wide sheet metal strip made of stainless steels (x5 CrNi 1810-2R).

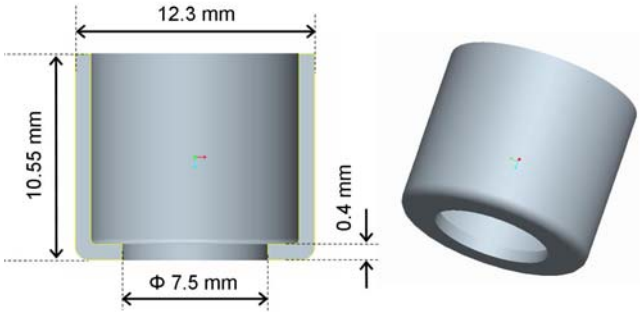

Figure 5.1. *Image of the drawn components.*

The forming sequence that is shown in Figure 5.2 consists on a first blanking operation and by five successively deep drawing operations characterized by a decreasing punch diameters. The last steps consist on a calibration procedure and a final hole blanking.

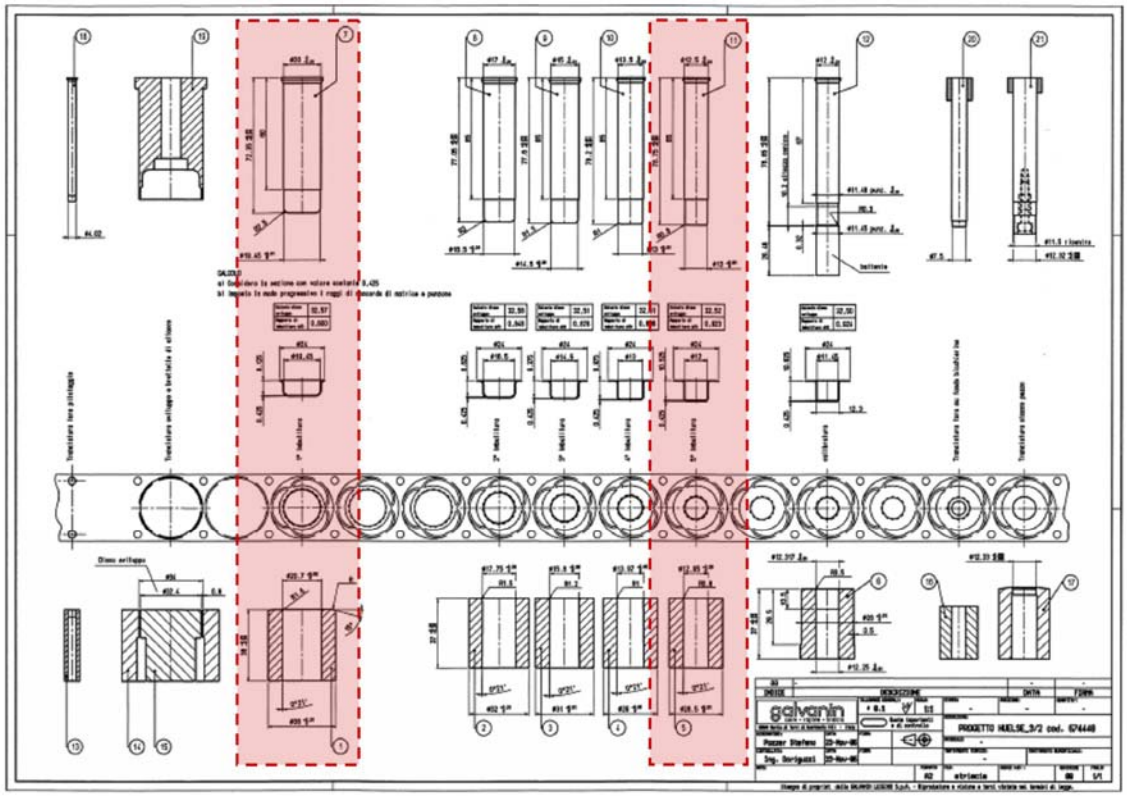

Figure 5.2. *Forming sequence.*

The numerical model of the forming sequence was developed, it evidences that the more critical operations are the first and the last drawing operations especially in terms of normal pressure (Figure 5.3).

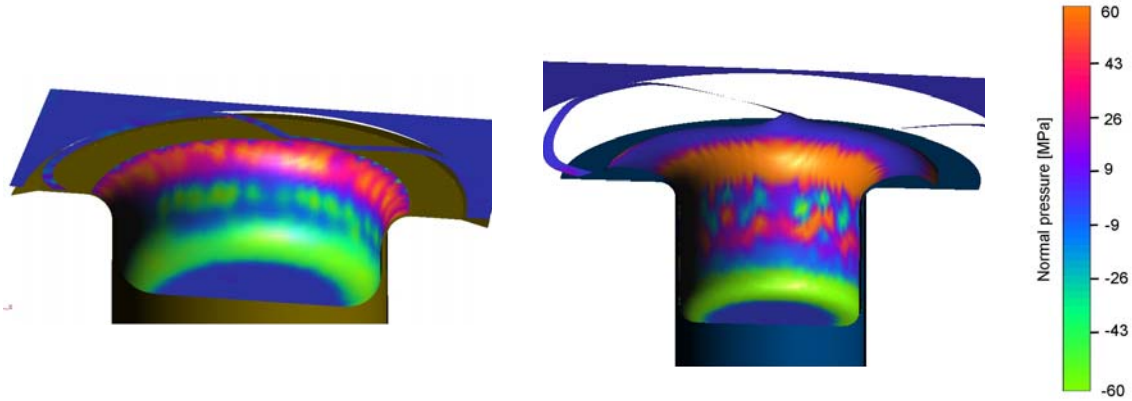

(a) (b)

Figure 5.3. *Numerical results showing normal pressure distribution for the first and the last deep drawing operation.*

As evidenced from infrared images like the one shown in Figure 5.4, the average temperature of the tool, once the production has reached a steady state value, is of approximately 70°C.
It should be evidenced that for the first drawing operation the sheet metal is at room temperature as it does not come from previous forming processes while in the case of the last drawing operation the blank has reached a temperature of about 70°C as well due to both plastic deformation, friction and heat exchange with the tools.

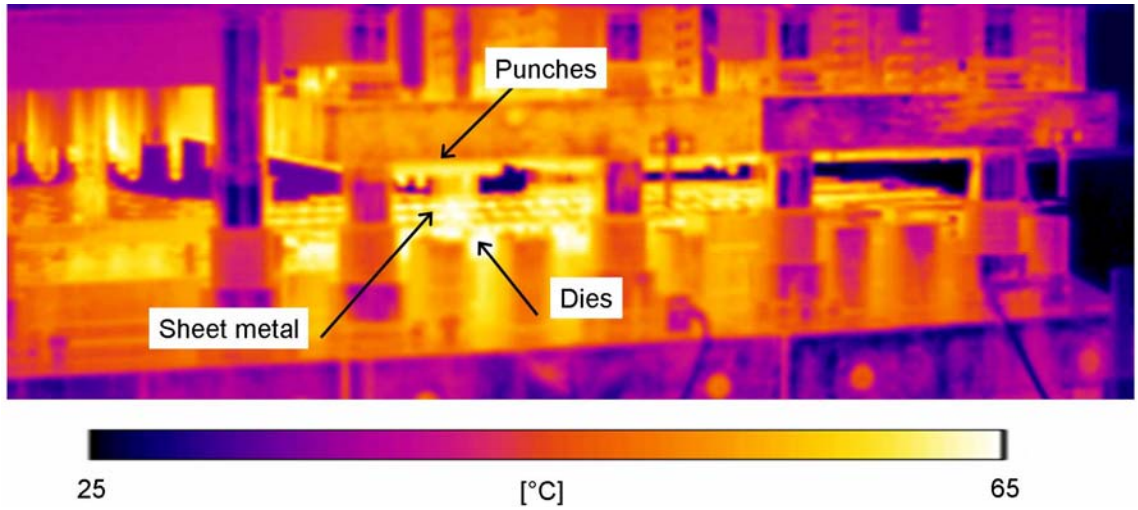

Figure 5.4. *Infrared image of tool assembly during working condition*

Concerning the sliding speed (v), according to industry advises, it should be varying within the range 5≤v≤10 mm/s.

5.2.2. Material characterization

The reference tribological pair is represented by the forming tool and the to be formed sheet metal. The die is made of a cold work tool steel while the sheet metal is 0.38mm thick and 36 mm wide strip of stainless steel. The general material characteristics and surface finishing of both the tool steel and the blank are presented in Table 5.1., while their chemical composition is presented in Table 5.2.

	Die	**Blank**
Material	K340	X5 CrNi 1810
Surface finish	Grinded	2R

Table 5.1. *Die and blank material properties.*

	C	**Si**	**Mn**	**P**	**S**	**N**	**Cr**	**Ni**	**Mo**	**V**
Blank	0.038	0.54	1.12	0.025	0.001	0.02	18.11	11.12		
Die	1.10	0.90	0.40				8.30		2.1	0.5

Table 5. 2. *Chemical composition of the tool steel and the blank.*

The average flow curve at room temperature (Figure 5.5) of the sheet metal was determined through uniaxial tensile tests adopting the GOM Aramis™ system as optical extensometer.

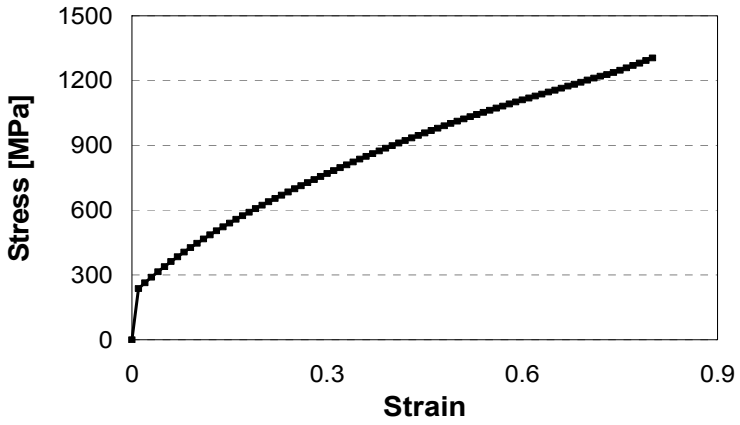

Figure 5.5. *Flow curve of a 0.38mm thick stainless steel (X5 CrNi 1810-2R) sheet metal specimen.*

In order to evaluate the sheet metal anisotropic behaviour, tensile tests were carried out utilizing specimens realized at 0°, 45° and 90° with respect to the rolling direction. Test repeatability was equal to three. In Table 5.3 the values of anisotropy are reported.

R_0	R_{45}	R_{90}	$\bar{R}$	ΔR
0.77	1.15	1.03	1.02	-0.12

Table 5.3. *Sheet Metal anisotropy parameters.*

In the following the different investigated lubrication systems are characterized. First the case study tribological system (oil) is described. Then the alternative as-received solid lubricant coatings (CrN, CrN-DLC coated dies and thin organic polymer based coated sheets) are described.

Oil

To characterize the as-received Non coated die surface, three profiles taken along the direction perpendicular to the sliding one (Figure 5.6) were measured.

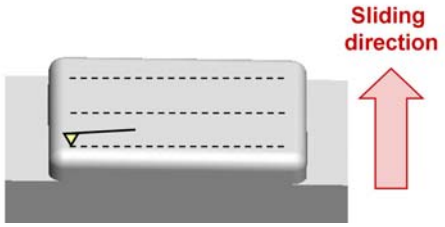

Figure 5.6. *Profile Measuring strategy.*

The experimental results are reported in Figure 5.7. The surface finishing is defined by a wavy surface probably as consequence of the last grinding operation. The average roughness Ra is of about 0.15µm.

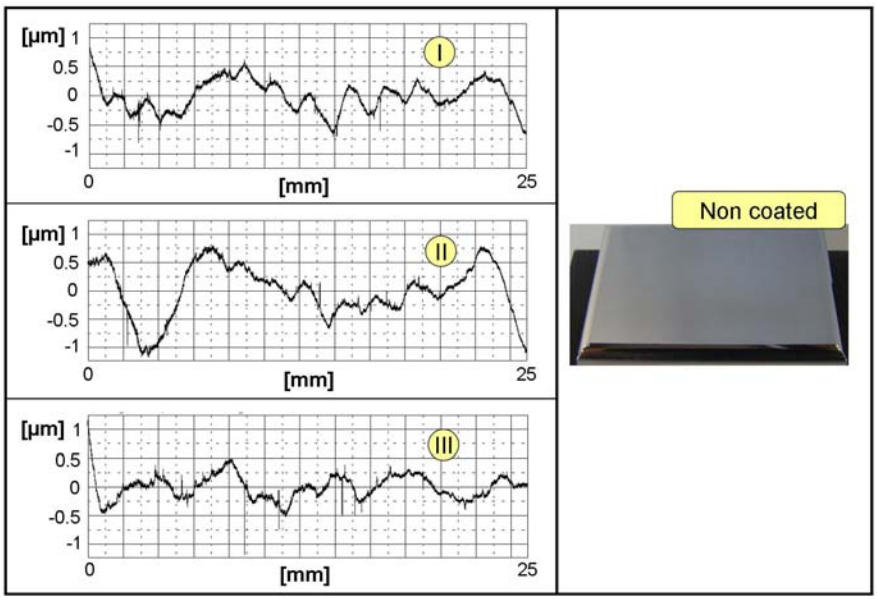

Figure 5.7. *As delivered Non coated die profiles.*

In Figure 5.8 the average over three profiles for the as delivered non coated sheet metal specimen is reported. The same measuring strategy adopted in the case of die profile recording was implemented (Figure 5.8). Only one profile is presented being the three very much the same. The specimen has an average roughness value of approximately 0.08 µm.

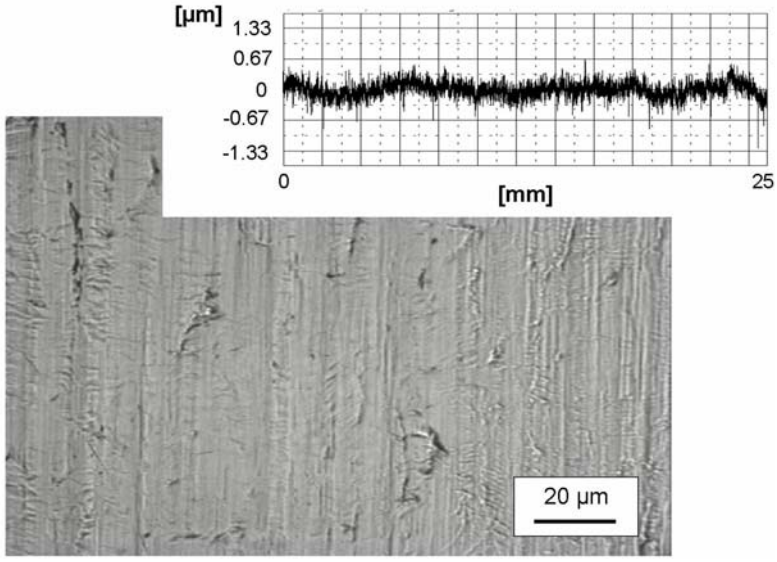

Figure 5.8. *As delivered Non coated sheet metal specimen.*

The lubrication is performed by a conventional deep drawing oil. It is a synthetic oil (OIL V031) with a density at 15°C of 1100 Kg/m^3 and a Viscosity at 40°C of 35mm^2/s.
It is suggested especially for severe stainless steel plastic deformations like deep drawing operations. Due to its high adhesiveness the oil can withstand the lubricant film shearing effect.

Inorganic coatings (Tool side)

The same measuring strategy followed for the previous surface condition (Oil) was used for characterize CrN and CrNDLC coated dies. The experimental profiles are presented in Figure 5.9 and Figure 5.10 respectively.

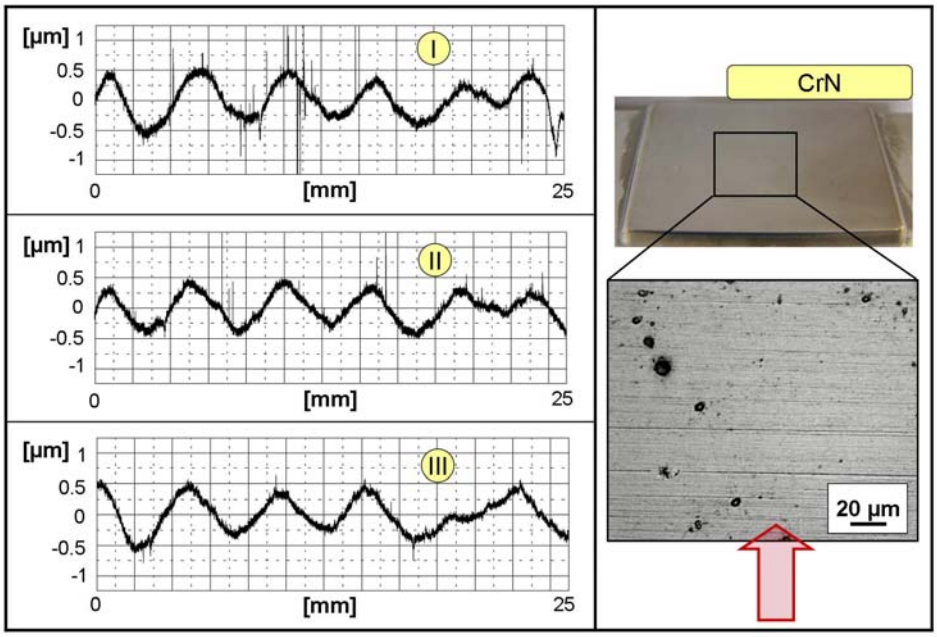

Figure 5.9. *As delivered CrN coated die profiles.*

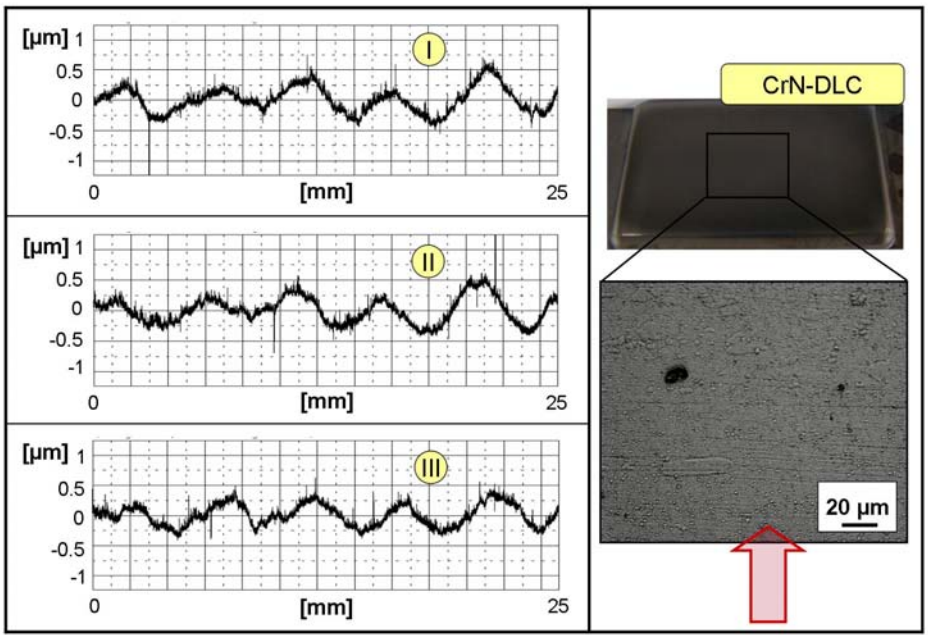

Figure 5.10. *As delivered CrN-DLC coated die profiles.*

For both the two coating the surface is defined by a wavy behaviour which replicate the one of the substrate (Non coated die). This is particularly evident if the third profile in

Figure 5.7 is consideredThe CrN-DLC coated die seems to display a less pronounced wavy surface profile. This is probably due to a higher coating thickness (with respect to the CrN one) that cause a major filling of the low level regions. Moreover the experimental profiles for the coated dies shows a bigger surface roughness if compared with the non coated one. The average roughness value (Ra) over three different die profiles, for the Non coated, CrN CrN-DLC coated dies are presented in Figure 5.11. The Ra values have been evaluated after the tip rugosimeter has been first calibrated and the correct cut-off was chosen. The Non coated surface is much smoother that the coated dies. The CrN and the CrN-DLC coatings are about 41% and 46% rougher than the Non coated one, respectively.

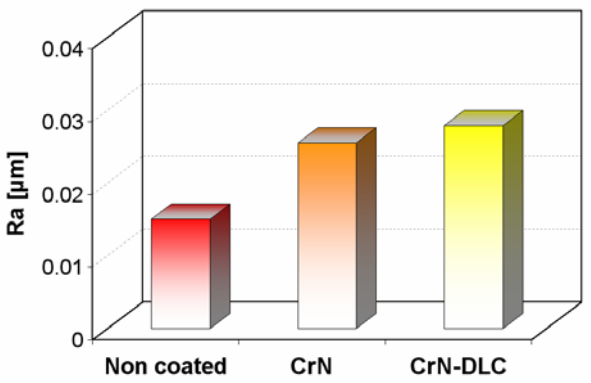

Figure 5.11. *Average roughness values for the Non coated, CrN and CrN-DLC coated dies.*

Organic coatings (sheet metal side)

Two organic coatings, namely Coating A and Coating B have been deposited over the sheet metal specimen described in the paragraph oil. They are characterized by the presence of both an organic and inorganic part. In Figure 5.12, top-down SE SEM images of the two coatings are presented. The morphology is significantly different: in the case of coating A, the presence of surface cracks is quite evident while for coating B they are not visible. On the other side Coating B is characterized by a more compact morphology and by the presence of homogeneous darker circular areas.

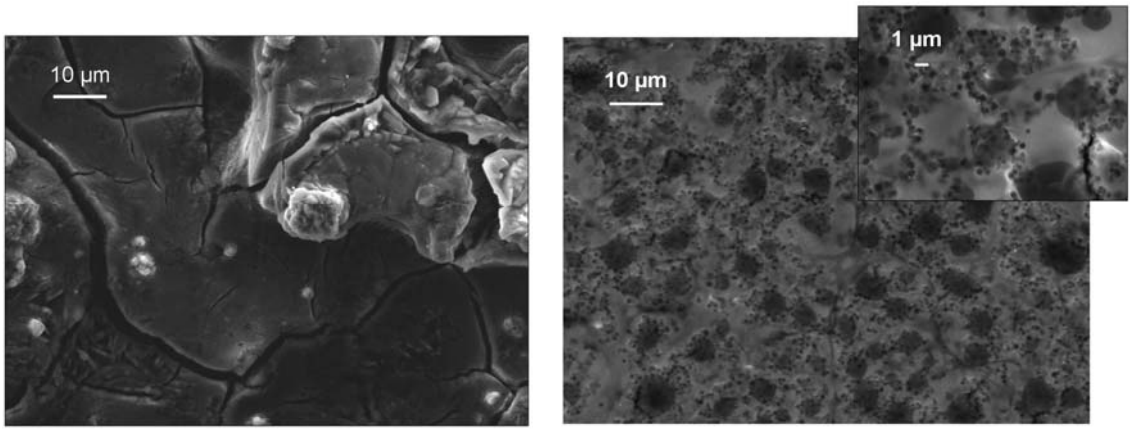

(a) (b)

Figure 5.12. *Top-down SE SEM images of (a) coating A and (b) coating B.*

The two coatings differ also for chemical composition and the mount of the organic part as well (Table 5.4). Concerning the inorganic part, coating A contains Zn, P and K while coating B contains Na and Si. The organic part is the same for both the two coating and it is made of polyethylene dispersions (wax) characterized by a meltin temperature within the range $129°C \leq T_{MELTING\text{-}WAX} \leq 139°C$. Moreover coating B has an amount of organic part five times higher (15%) than coating A (3%) thus implying that the former contains more wax.

	Inorganic components	Organic part [%]
A	Zn, P, K	3
B	Na, Si	15

Table 5.4.*vDescription of the organic coatings A and B chemical properties.*

5.2.3. Experimental set-up

5.2.3.1 Room temperature pin on disc set-up

The Pin on disc test (Chapter 3.2) at room temperature has been carried out on the Universal Mechanical Tester (UMT) by CETR Inc. The upper specimen (pin) is connected to both a vertical and lateral linear motion system while the lower specimen (disc) is fixed to a lower rotary drive (Figure 5.13, red arrows indicate the motion systems.).

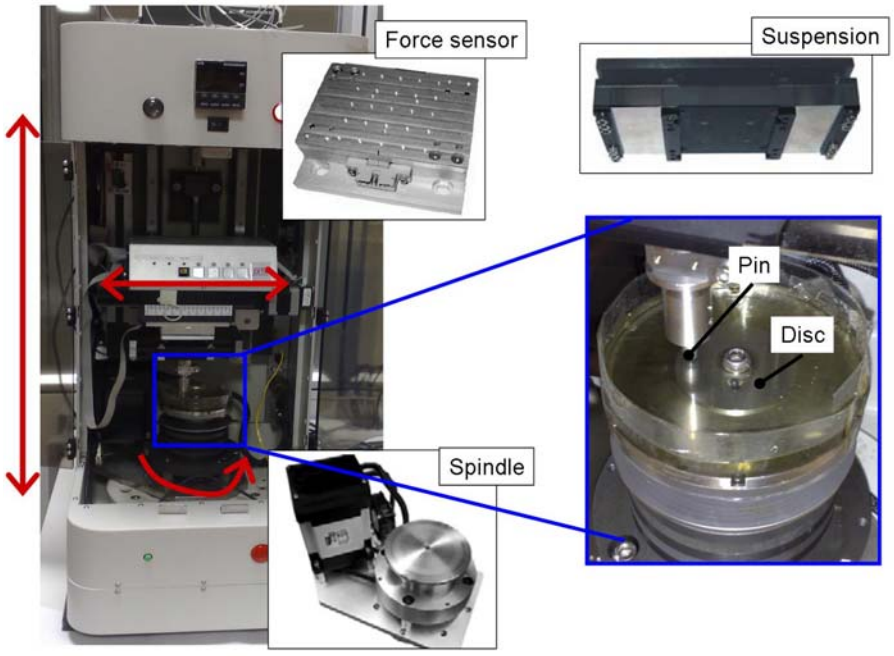

Figure 5.13. *Experimental set-up for Pin on Disc test at room temperature.*

The target characteristics of both the linear and rotary motion systems are presented in Table 5.5 and Table 5.6 respectively. In Figure 5.14 the torque versus speed characteristic for the rotary drive is presented.

	Vertical positioning system	Lateral positioning system
Position resolution [mm]	1	2
Maximum travel [mm]	150	75
Speed [mm/s]	0.001 - 150	0.01 -10

Table 5.5. *Target data of the Vertical and Later positioning system.*

	Spindle
Speed [rpm]	0.1- 3000
Maximum Load [N]	500

Table 5.6. *Target data of the lower drive spindle.*

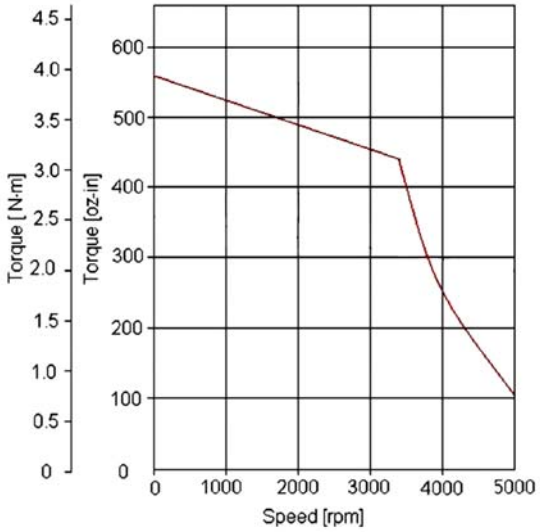

Figure 5.14. *Torque vs Speed rotary drive characteristics.*

Ultra-accurate strain-gauge sensors perform simultaneous measurements of load and torque in two axes (F_Z and F_X). A normal-load sensor provides feedback to the vertical motion controller, actively adjusting the sample position to ensure a constant load during testing. The target data of the two used force sensors are presented in Table 5.7. Mounted to the force sensor is a suspension which allows the upper specimen to follow variations in the height of the lower specimen as it rotates.

	Force sensor 1	Force sensor 2
Range [N]	0.1-10	1-1000
Resolution [mN]	0.5	5

Table 5.7. *Target data of the force sensors.*

In order to reproduce the tribological system typical of sheet metal forming operations the material used for the pin is usually the one of the tool working steel, while the counter material is a disc made of the sheet metal under investigation. It is important that the surface finishing of both the pin and the disc reproduce the one of the tool and the blank of the production environment. A planar contact must be insured. In addition any liquid/solid lubricant that need to be tested has to be present at the pin/disc interface. The test output signals are F_Z and F_X, the coefficient of friction μ is calculated as indicated in equation (3.1). The variation of the μ values give information about friction behaviour at the pin/disc interface.

5.2.3.2 Flat drawing test experimental set-up

In order to perform the Flat Drawing test an ad hoc experimental set up (Figure 5.15) has completely been realized at The Department of Manufacturing (DIMEG) University of Padova within the phd period.

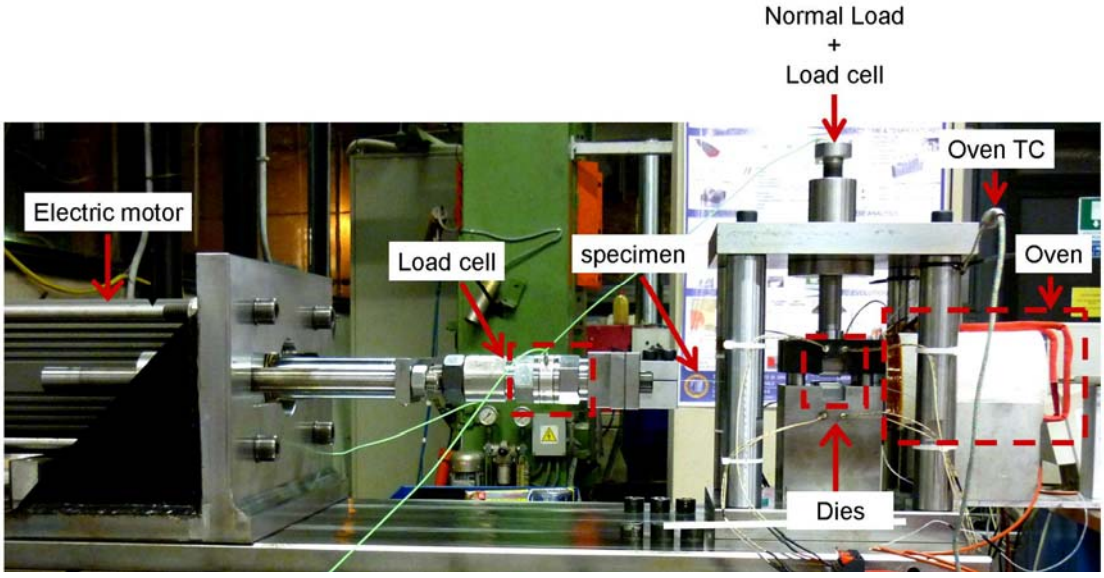

Figure 5.15. *Flat Drawing Die experimental set-up developed at The Department of Manufacturing (DIMEG), University of Padova.*

The sheet metal specimen is mechanically clamped as shown in Figure 5.16. The clamping device has an additional central hole that corresponds to an equivalent hole in the specimen in order to avoid any possible further slipping of the latter.

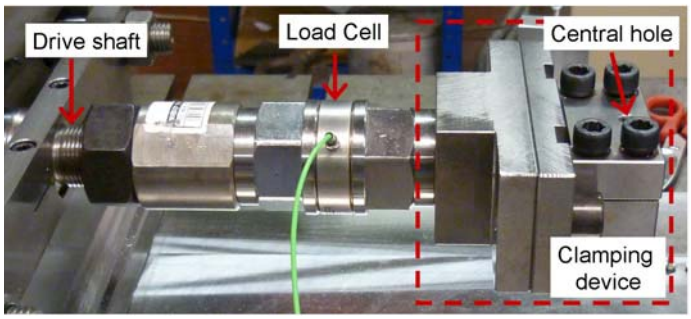

Figure 5.16. *Sheet metal specimen clamping device.*

Between the drive shaft and the clamping device a direct load sensor cell for the tangential force (F_T) measuring is located.
The normal load (F_N) is applied through a screw system (Figure 5.17) which transmits the force to a vertical punch that push the upper die holder against the lower one which is fixed. In between the screw and the vertical punch an indirect load force sensor is located. The drawing die is made of two sliding surfaces (Figure 5.18) which, as already mentioned in the previous chapter, must have the surface finishing that needs to be investigated. The dies are less wider (32mm) than the sheet metal strip (36mm) in order to avoid any contact between the sheet metal sheared profiles and the die surface. The sheared specimen profiles would indent the die surface thus increasing the tangential force (F_T) which in turn would affect the frictional behaviour.

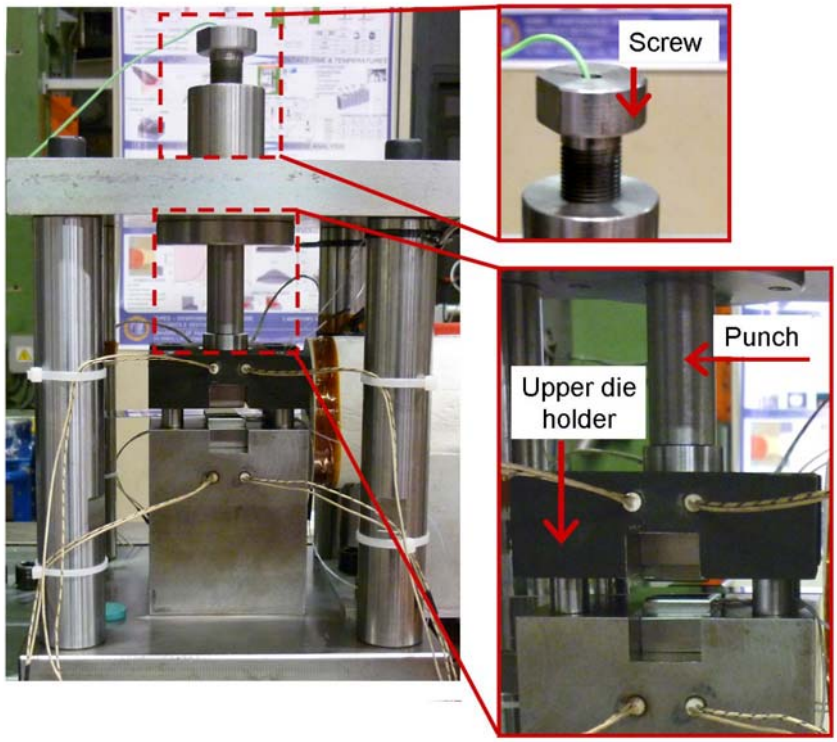

Figure 5.17. *Vertical load transmitting system.*

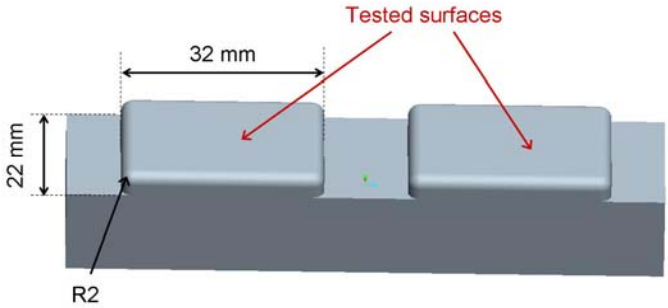

Figure 5.18. *Drawing die.*

Once the target normal load at the sheet metal/die interface has been applied the specimen is drawn by means of an electrical actuator with the desired speed and stroke values. The target specification of the linear motor are presented in Table 5.8..

Axial load [N]	50000
Stroke [mm]	250
Sliding speed [mm/s]	254

Table 5.8. *Target data of the linear actuator.*

Die heating system

In order to reproduce the tool heating taking place in the industrial environment (see chapter 5.2.1) , the dies are heated up by means of six 250 W heating cartridges (two located in the upper die holder and four in the lower one). Their temperature evolution is measured and controlled by a thermocouple spot-welded at a vertical distance of 2mm from the sliding surface (Figure 5.19).

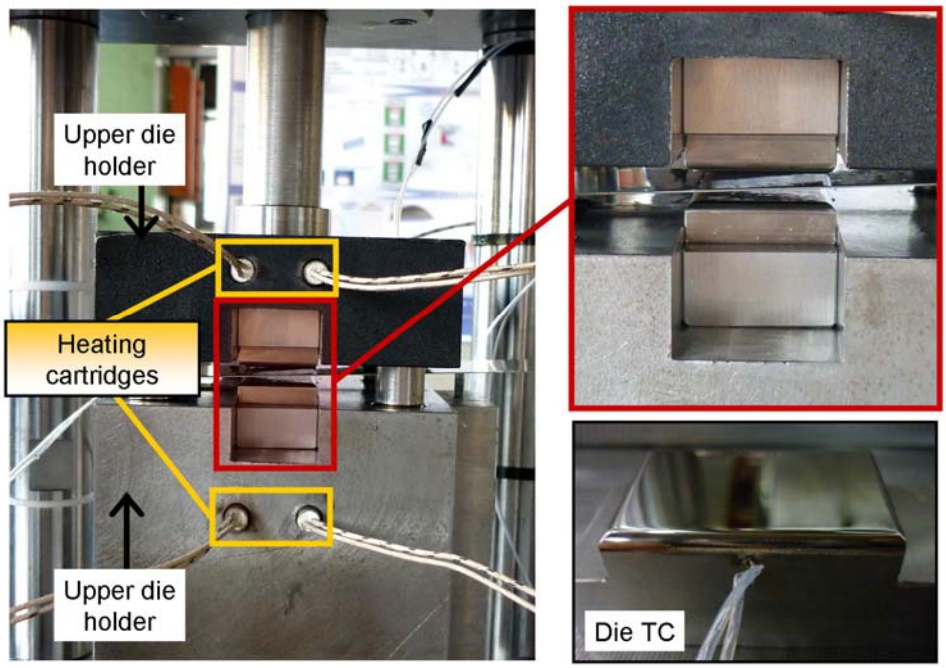

Figure 5.19. *Dies heating system.*

Once the target temperature is reached the dies are kept at the desired temperature for 10 min before starting the tests in order to get an homogeneous temperature field all over the to be tested die surface. During the die heating the sheet metal specimen is kept non in contact with the dies in order to avoid the specimen heating via conduction.

Sheet metal specimen heating system

To can reproduce the blank heating that takes place in sheet metal forming operations as consequence mainly of the material plastic deformation, friction and heating exchange with tools, the specimen is heated up with a ceramic fiber heater (Figure 5.20). The latter is made by integrating an iron-chrome-aluminium (ICA) heating

element and ceramic fiber insulation. Heating unit constructed of ceramic fiber insulation isolates the heating chamber from the outside. Ceramic fiber is an insulation made of an alumina-silica composition, held together by an inorganic binder. The specimen is heated through radiant heat transfer exclusively. The heater target data are reported in Table 5.9.

Operating temp. [°C]	20° - 1024
Watt densities [W/mm^2]	0.8 – 4.6
A [mm]	51
B [mm]	152
C [mm]	102

Table 5.9. *Ceramic fiber heating technical and geometric specifications.*

The temperature evolution is measured by a K type thermocouple radially inserted in the middle of the full heater length (B, Figure 5.20). The temperature evolution is controlled through a PID controller which uses the real time temperature value as feedback signal in order to to adjust the heating power.

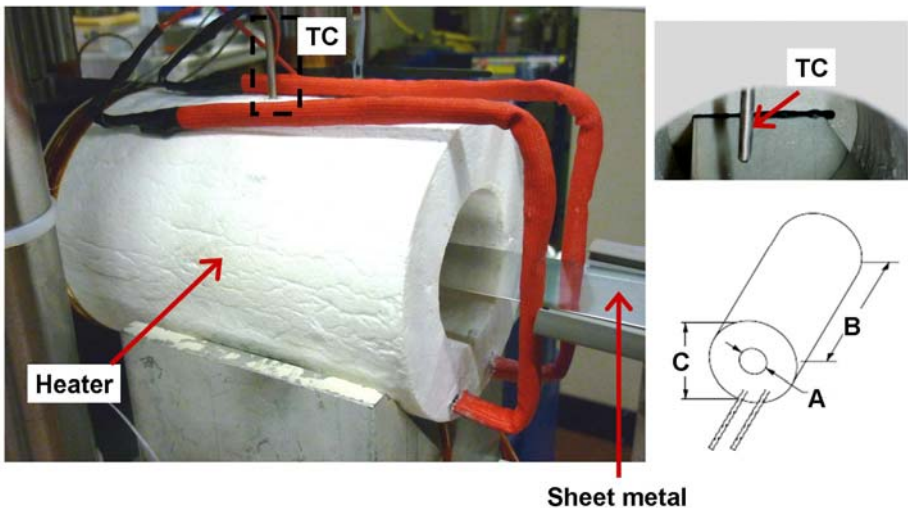

Figure 5.20. *Sheet metal specimen heating system.*

As the specimen temperature is not directly measured a calibration procedure of the sheet metal specimen temperature has been needed. As first step the nominal target temperature is set in PID controller. Once the heater reaches the desired temperature 10min were waited in order to get a complete temperature homogenization. At this point a sheet metal specimen with three thermocouples spot welded an axial distance of 50mm from each other was put inside the heater in a way that TC1 was at 25mm far from one heater ending surface, TC2 was exactly in the middle of the heater and TC3 was at a distance of 26mm from the other heater ending surface (Figure 5.21). Through a dedicated LabVIEW™ program the temperature evolution of TC1 TC2 and TC3 was recorded. An holding time of about 15 minutes it is necessary for the specimen to reach the target temperature all over the specimen and being stable. This calibration procedure has been carried out for three temperatures: 40, 80 and 120°C.

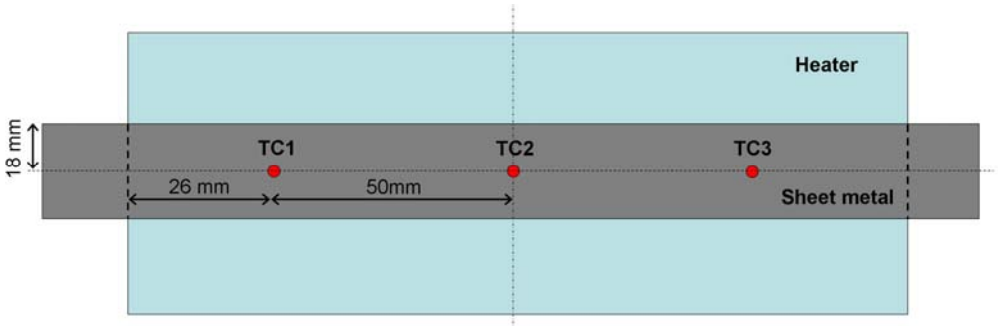

Figure 5.21. *Scheme of the thermocouple positioning for the heater calibration procedure.*

In Figure 5.22 the three thermocouple profiles as function of the holding time is presented. Once the sheet metal specimen reaches the target temperature it remains stable. While the temperature measured by TC1 and TC is the same, the temperature in the middle is higher. This temperature gradient is probably due to both the coils location and thermal losses in proximity of the heater ending surfaces. The higher the target temperature the higher the gap between the value measure by TC2 and the ones measured by TC 1 and TC3.

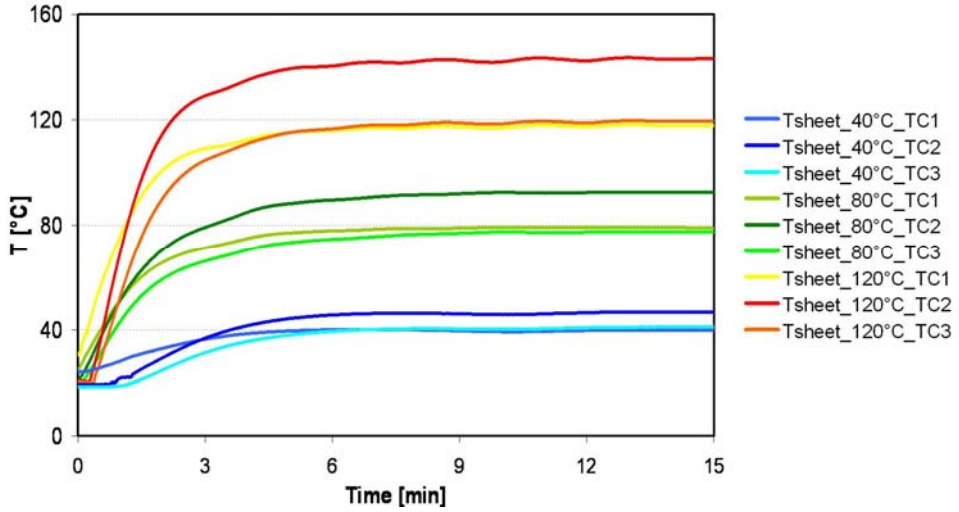

Figure 5.22. *TC1, TC2, TC3 evolution profile for target temperatures of 40, 80 and 120°C.*

In the Flat Drawing experiments the heated portion of the specimen starts to slide against the die after a stroke of 93 that correspond to a time of about 9.8sec

Experimental procedure

A dedicated LabVIEW™ program was developed to:

- acquire the forces, stroke and temperature signals
- control the shaft drive movements and activate the cartridge heaters.

In the case of the more complex test for which both the dies and the sheet metal specimen are heated, the dies heating cycle is controlled by the dedicated LabVIEW™ software while the heater is controlled by means of an external PID controller. Oce both

the die and sheet metal specimen target conditions are reached, the normal load is applied and successively the specimen is drawned by means of an electric actuator which is controlled both in stroke and speed, according to the input parameters value. The load cell monitor in a con tenuous way both the normal load and the drawing force. The steady state friction coefficient calculated as in eq. 3.2 is the main output.

5.2.4. Experimental strategy

5.2.5.1 Friction behaviour

As described in Chapter 1, the main objective of the present work consists in evaluating the tribological performance of the proposed alternative solid coating lubricants under process conditions and comparing the obtained results with the frictional behaviour of the oil lubricant. The latter represents the actual lubricating condition for the case study here considered (see Paragarph 5.2.1). In Table 5.10 the investigated tribological pairs are presented.

Lubricant type		Die material	Sheet metal
Liquid lubricant	Oil	• K340 • Grinding	• X5 CrNi 1810 • Thickness: 0.48 mm • Width: 36 mm • 2R
Solid lubricant DIE SIDE	CrN		
	CrN-DLC		
Solid lubricant SHEET METAL SIDE	Organic coating A		
	Organic coating B		

Table 5.10. *Different lubrication conditions investigated at room temperature.*

The experimental test used for evaluating the oil and the solid lubricant coating tribological behaviour is the Flat Drawing Test. It allows an independent control of the critical process parameters: Normal load (σ_N), Die temperature (T_{DIE}), Sheet metal temperature (T_{SHEET}) and sliding speed (v). The influence of each process parameter on the friction behaviour has been considered independently from the others as shown in Table 5.11.

(a)	$\mu = f(\sigma_N)$	σ_N [MPa]				T_{DIE} [°C]	T_{SHEET} [°C]	v [mm/s]
		1	3	5	25	20	20	5
(b)	$\mu = f(v)$	v [mm/s]				T_{DIE} [°C]	T_{SHEET} [°C]	σ_N [MPa]
		0.5	5	10	50	20	20	5
(c)	$\mu = f(T_{DIE})$	T_{DIE} [°C]				T_{SHEET} [°C]	σ_N [MPa]	v [mm/s]
		20	60	80	100	20	10	5
(d)	$\mu = f(T_{SHEET})$	T_{SHEET} [°C]				T_{DIE} [°C]	σ_N [MPa]	v [mm/s]
		20	60	80	120	80	10	10

Table 5.11. *Experimental strategy for the tribological evaluation of oil and alternative solid lubricant coatings under process conditions.*

The die and sheet metal heating set up has been necessary to reproduce both the tool heating only (1° deep drawing operation, see chapter 5.2.1) and the sheet metal/ tool

contemporary heating (5° deep drawing operation, see chapter 5.2.1). The stroke has been considered always equal to 100mm.
In Table 5.12 the experimental strategy for all the investigated tribological pairs is presented. In the case of the lubricant oil the dependence of the friction coefficient on the normal pressure (σ_N), drawing speed (v), die temperature (T_{DIE}) and sheet metal temperature (T_{SHEET}) has been investigated.
As the interface temperature does influence the oil lubricant behaviour mainly, the tribological performance of the CrN and CrN-DLC coated dies has been investigating as function of the normal load and the sliding speed only.
In the case of the thin organic coating, their frictional behaviour has been studied as function of the normal load (σ_N), the sliding speed (v) and of both the tool and the sheet metal temperature. The tests by heating the sheet metal specimen were of particular interests as the organic part material behaviour could be influenced by the process temperature values.
For all the different types of lubricant systems the dies were not cleaned before performing a new test in order to reproduce the industrial surface conditions of the tools.

Lubricant Type		Exp. conditions	Repeatibility
Liquid lubricant	Oil	a) b) c) d)	3
Solid lubricant DIE SIDE	CrN	a) b)	3
	CrN-DLC	a) b)	3
Solid lubricant SHEET METAL SIDE	Organic coating A	a) b) d)	2
	Organic coating B	a) b) d)	2

Table 5.12. *Experimental parameters for the different tribological pairs*.

In order to can consider the results obtained with the Flat Drawing Die experimental apparatus as reliable, they were compared with the ones obtained from the Pin on Disc test performed on the UMT apparatus. The friction coefficient values in the case of CrN coated die as function of the normal pressure were compared only (case (a) in Table 5.11).

5.3. Experimental investigation of interface conditions in hot stamping operations

5.3.1. The case study

The reference case refers to the hot stamping of quenchable Al-Si coated boron high strength steel. As already introduce in Chapter 2 the blank is heated up at its austenitization temperature and then transferred on the dies where it is contemporary formed and quenched. The quenching process is due to the fact that the dies are cooled down at room temperature (Figure 5.26).The latter are made of hardened hot working tool steel.
The process parameters in terms of normal pressure, testing tempearture and sliding speed have considered equal to the values presented in [80].

Figure 5.23. *Hot stamping of a b-pillar. [81]*

5.3.2. Material characterization

The investigated sheet specimen is a 1.5 mm thick Al-Si coated 22MnB5 commercially produced by Arcelor (USIBOR 1500^{TM}). The coating layer of the steel sheet product is what is called the Type 1 coating layer, a plating layer of aluminium containing approximately 10% to 13% Si according to SEM EDX analysis. In Figure 5.24, the coating on the sheet metal blanks as delivered at room temperature is presented.

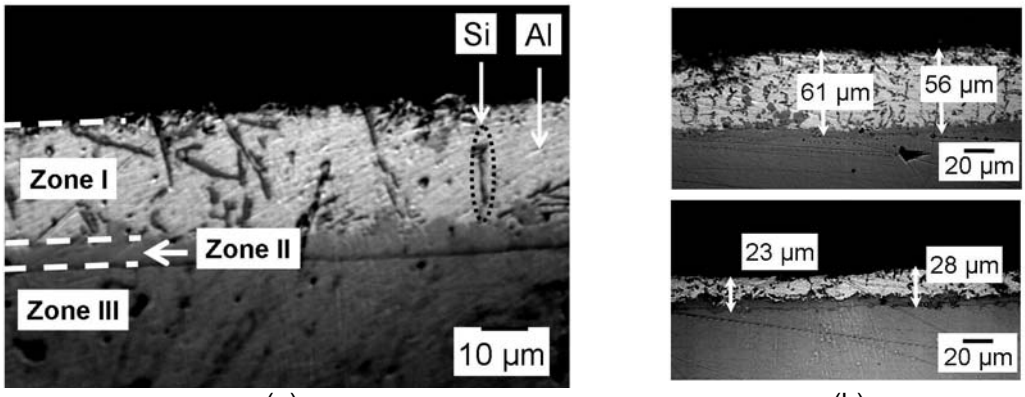

(a) (b)

Figure 5.24. *Optical image of the: (a) Al-Si coated HSS sheet at room temperature. (b) Coating thickness variation*

Three different zones can be outlined: *zone I* where Si aggregates are embedded in Al matrix, *zone II* which is the interface area between the coating itself and the steel substrate. This interface area is made of an Fe, Al and Si system having a weight percentage of 39%, 53% and 8% respectively, according to SEM EDX analysis. Eventually, there is *zone III* which is the base metal. The coating thickness can vary significantly along the sheet metal, showing the average value of 40µm. Even if the coating melting point is approximately 600°C, an Al-Fe alloy with a higher melting point forms from the interface with the base metal and quickly reaches the surface. This prevents the coating layer melting. In Figure 5.25, Backscattered Electrons (BSE) SEM

cross sections and SEM EDX analysis (measured in the thickness direction) for specimens at 20°C, 600°C and 900°C respectively, are shown.
At room temperature it is not possible to distinguish between the Al matrix and the Si aggregates because they have a very similar atomic weight. Once the heating temperature reaches the value of 600°C, the steel starts to diffuse from the interface area (zone II, Figure 5.24) to the coating surface (zones B and C) giving origin to an Al-Fe alloy. As consequence of the Fe diffusion process the further from the interface zone the lower the Fe amount ($Fe_{wt\%,B}$ = 46%, $Fe_{wt\%,C}$= 70%). Once the sheet metal is heated up to its austenitization temperature the coating layer develops a sub-layer structure made of approximately 5 zones (A, B, C, D and E). These sub-layers are characterized by an alternating variation of the Al and Fe percentages in zones A, B, C, D and by the almost absence of Al at the interface area (zone E).

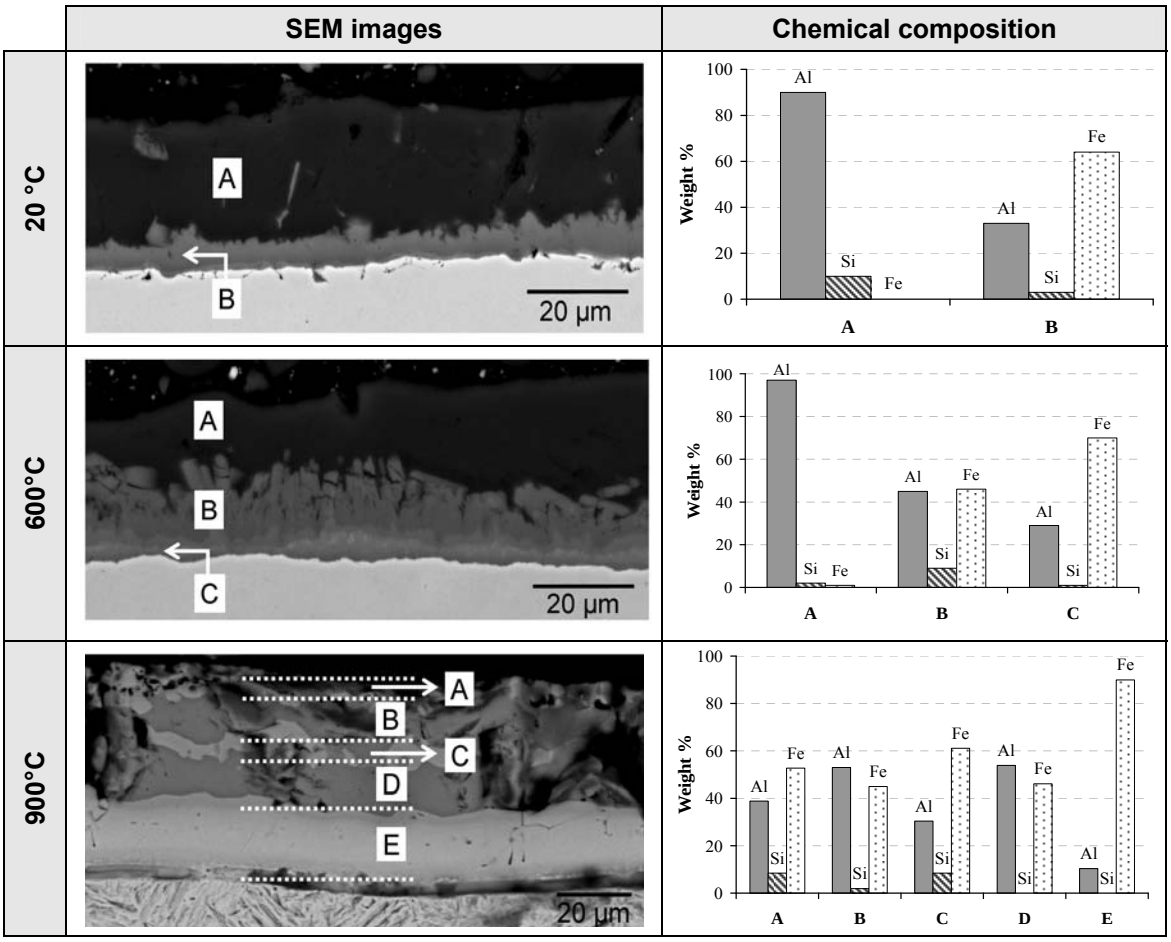

***Figure 5.25**. SEM cross sections and SEM EDX analysis for specimens at 20°C, 600°C and 900°C.*

The coating chemical evolution with the heating temperature does correspond to a topography evolution as well (Figure 5.26). At room temperature the coating surface is characterized mainly by plateau large areas and small valleys zone with an average Ra value of 1.5 µm. The plateau areas represent the Al matrix while the narrower valleys correspond to the Si precipitates.

At 600°C when the diffusion step takes place the surface topography change in a very significant way as the large plateau area convert into a small dot like surface with a higher roughness value (Ra=3.4 μm).
For a temperature equal to the asutenization one the small dots surface appears as constituted by nodules like features. It looks like the small dots have expanded into well defined nodules dimensions which present a lower roughness (Ra=2.3μm). As these nodules derive from the iron diffusion into the coating they are probably made of the AlFe intermetallic that takes origin within the diffusion step.

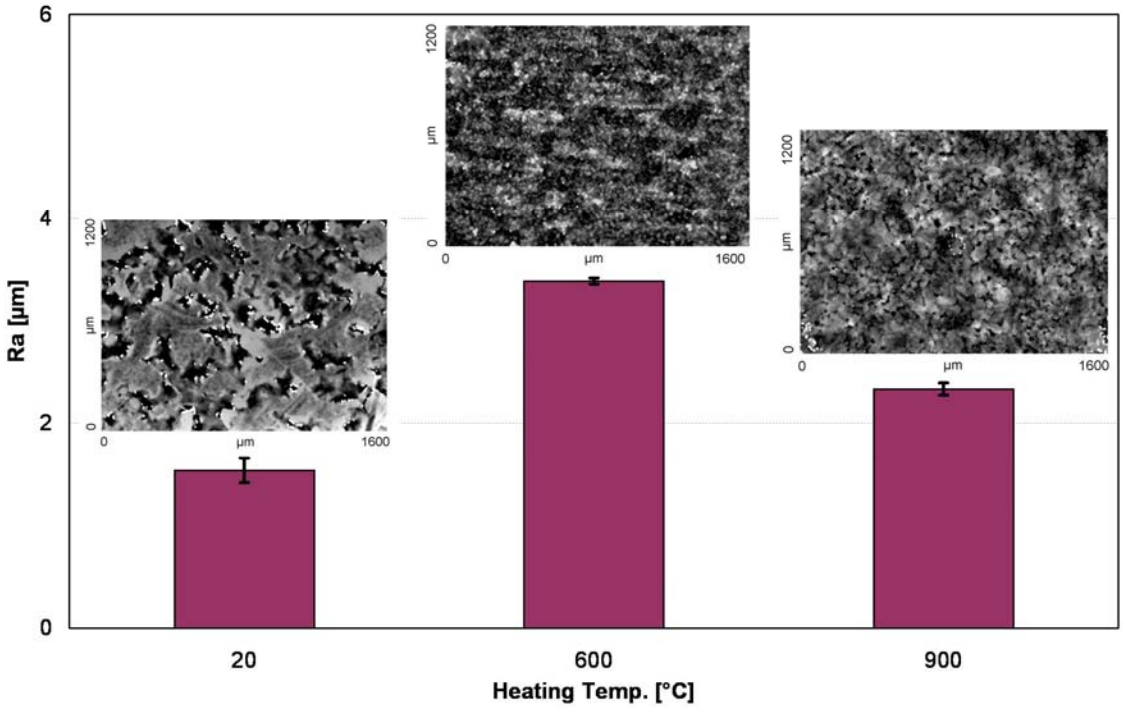

***Figure 5.26**. Al-Si coating roughness evolution as function of the heating temperature.*

5.3.3. Experimental set-up

5.3.3.1 Thermal experiments

In order to reproduce the same thermal history that occurs during the hot stamping process a dedicated experimental set-up has been developed (Figure 5.27).
The sheet metal specimens are heated by an induction furnace, and maintained at the target temperature for a certain amount of time (holding time) in order to get a complete microstructure homogenization.
The specimen is successively quenched by means of compressed air nozzles. The thermal profile used in the tests is shown in right part Figure 5.30. In order to keep both the heating and the cooling down steps under control, a thermocouple is spot-welded on the specimen at the centre of the heated zone.
The cooling system is capable to reproduce different cooling rates by means of compress air or mixed water-compress air medium in the range from 5°C/s to 50°C/s.

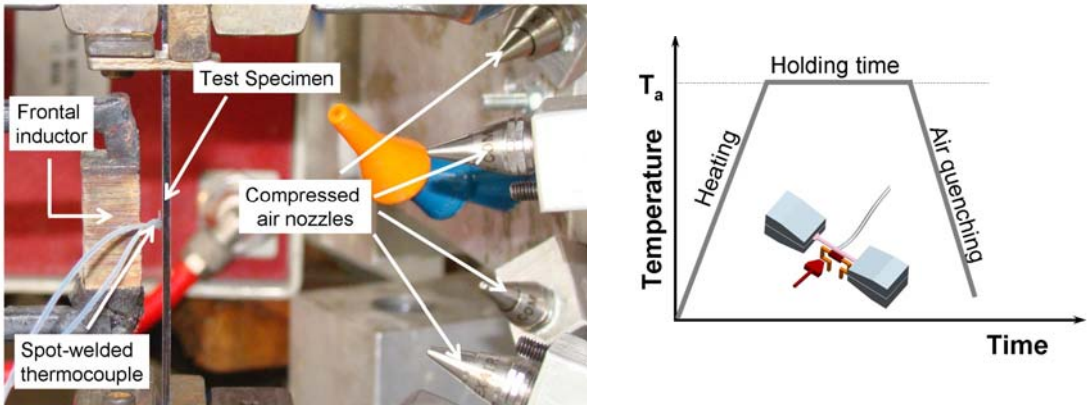

***Figure 5.27**. Experimental set-up utilized to perform the process thermal cycle.*

5.3.3.2 Surface roughness measurements

A three-dimensional investigation was carried out through White Light Interferometer (WLI) technique with a commercial instrument implementing a Michelson-type configuration, best suited for measurements with low magnification objective lenses. The instrument implements a 2.5× objective, with a numerical aperture of 0.075 and a working distance of 10.3mm. Such objective allows measurements over an area of 1654×1253 μm, with a lateral resolution of 2.2×2.6 μm. The system provides measurements over a vertical range of 100 μm, with a vertical scan speed of 2.1 μm/s and a vertical step size < 1 nm. Each sample is measured in two different positions. The measured data sets are successively post-processed in order to isolate roughness from waviness and form contributions. Extending the approach proposed by standard ISO 11562 for analysis of surface profiles, a Gaussian filter was then applied to scanned topographies.

5.3.3.3 High temperature pin on disc

In order to perform high temperature pin on disc test the UMT device is equipped with a chamber, specifically designed to assure the temperature control up to 1000°C. A heating element and a temperature sensor are located inside the chamber. A computerized temperature controller uses the output of the temperature sensor to precisely control the chamber temperature (Figure 5.28).

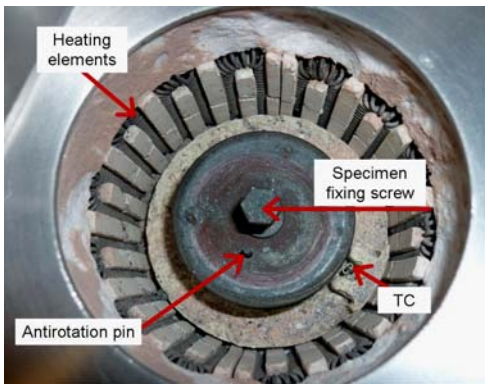

***Figure 5.28**. UMT device heating chamber.*

The chambers have an access slot on the top cover to permit coupling of the upper test specimen that is inside the chamber to a friction/load sensor. Accordingly the disc which is fixed at the lower rotary drive can be heated up inside the chamber alone or together with the pin, depending on the process conditions to be reproduced The chamber heating up rate is of about 0.43°C/s while the cooling down rate is approximately of about 0.33 °C/s.In order to avoid an excessive heating of the load sensor an heat dissipator is placed in between the suspension and the pin holder (Figure 5.29).

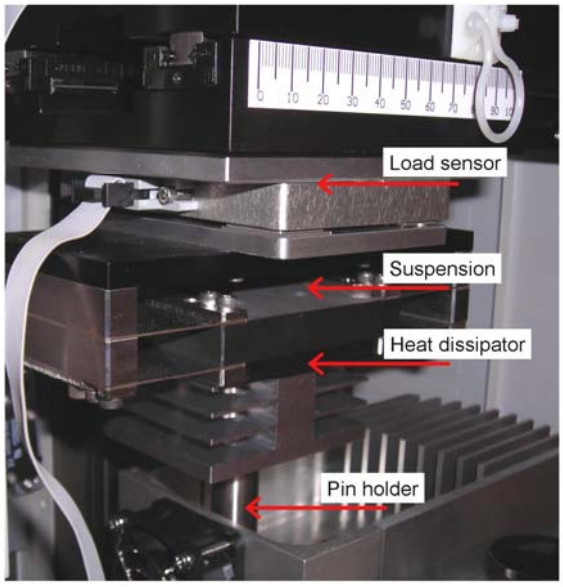

Figure 5.29. *View of the dissipator.*

The rotary drive target data are the ones presented in Table 5.7. In Figure 5.30 the complete set-up for high temperature pin on disc set up is presented.

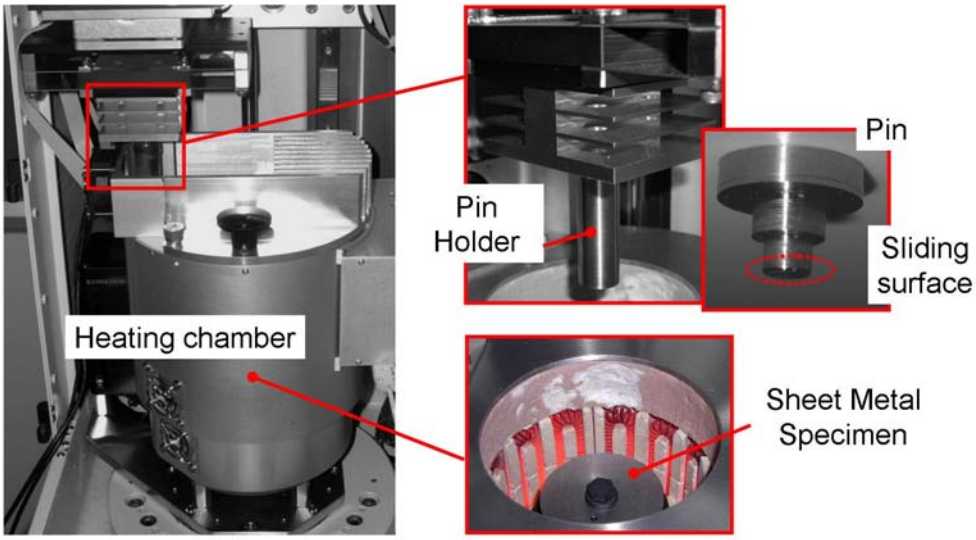

Figure 5.30. *UMT tester configured for the high temperature pin on disc test.*

5.3.4. Experimental strategy

5.3.4.1 Coating chemical evolution with critical thermal process parameters

The main objective of the present study consisted in investigating if and in which way critical process parameters like the holding time (at the austenitization temperature) and cooling rate did affect the coating evolution both in chemical and morphological terms. In Table 5.13 and Table 5.14 present the experimental plans for the analysis of cooling rate and holding time effects respectively. When analyzing the influence that the cooling rate has on the surface layer, the heating rate and holding time are kept constant according to the typical industrial process parameters [80].

	Heating Temp.[°C]	Heating rate [°C/s]	Holding time [sec]	Cooling rate [°C/s]
Specimen 1	900	7.3	180	300
Specimen 2	900	7.3	180	50

Table 5.13. *Experimental parameters to investigate the influence of the cooling rate.*

	Heating Temp.[°C]	Heating rate [°C/s]	Holding time [sec]	Cooling rate [°C/s]
Specimen 3	900	7.3	180	50
Specimen 4	900	7.3	10	50

Table 5.14. *Experimental parameters to investigate the influence of the holding time*

5.3.4.2 Friction investigation in hot stamping conditions

To investigate the influence that the process parameters, namely sheet temperature, normal pressure, sliding velocity and tool roughness, have on the friction at interface between the sheet metal blank and the dies, pin on disc tests were performed. The material used for the pin is the hardened hot working tool steel, while the counter material is a disc made of Al-Si coated HSS. The sheet metal specimen was heated up to 900°C in order to have its complete austenitization and, then, cooled down to the target temperature with a constant cooling rate of 0.33 °C/s. Even if this cooling rate is much lower than the industrial one, it has been demonstrated in [81] that the cooling rate does not influence the 5 layered structure coating formation. In order to simulate the industrial conditions of the cold dies during the stamping operations, the pin was kept outside the heating chamber when heating up the specimen. Once the sheet metal reached the target temperature, the pin was moved inside the chamber and brought into contact with the specimen.

To understand the effects of the most relevant process parameters and investigate their reciprocal influence, DOE techniques were applied to the design of the experimental plan. On the basis of the main parameters affecting hot stamping, four process parameters (factors) were considered: (i) normal pressure, (ii) sheet temperature, (iii) sliding velocity, and (iv) tool surface finishing. A full factorial plan was developed with two levels for each factor and repeatability equal to two. Low level and

high level of factors, shown in Table 5.15, were initially chosen on the basis the process conditions [80].

Factors	Low level	High level
Normal pressure [MPa]	5	50
Temperature [°C]	500	800
Sliding velocity [mm/s]	1	10
Surface condition	Turned	Polished

Table 5.15. The proposed levels of factors for pin on disc experiments at high temperature

Successively it has been necessary to verify the reproducibility of the values chosen by the UMT tester. As result of the feasibility analysis the high level value of the factor *normal pressure* as well as both the values of the factor *sliding speed* had to be changed according to what is presented in Table 5.16.

Factors	Low level	High level
Normal pressure [MPa]	5	25
Temperature [°C]	500	800
Sliding velocity [mm/s]	3	3
Surface condition	Turned	Polished

Table 5.16. *The levels of factors for pin on disc experiments carried out on USIBOR 1500^{TM}*

The friction coefficient measured during the pin-on-disk test is the response of experiments.
The steady state friction coefficient measured during the pin-on-disk test is the response of experiments.

5.4. Conclusions

For both the investigated tribological systems the starting material: sheet metal, lubricant and die material have been characterized. The experimental set up (Flat drawing and pin on disc test) to investigate the frictional behaviour taking place at the sheet metal/die interface was described.
Eventually the pursued experimental strategy was discussed.

CHAPTER 6

RESULTS AND DISCUSSION

6.1. Introduction

In the following chapters the experimental results concerning the tribological behaviour of oil, inorganic and organic type of solid lubricant coating will be presented and analyzed. In the second part of the chapter. Successively the study of the AlSi coating evolution with the holding time and cooling rate as well as the friction conditions taking place at the sheet metal/die interface as function of the main critical process parameters will be presented and discussed

6.2. Flat drawing test validation

Figure 6.1 shows the steady state average friction coefficient as function of σ_N for both pin on disc and flat drawing test. In the two different testing conditions the value of μ does not show any significant dependence on σ_N being the friction within the range $0.16<\mu<0.13$ for the pin on disc test and $0.10<\mu<0.12$ in the case of the flat drawing test. The average value of μ obtained with the pin on disc test is higher then the one obtained with the other test. The more significant difference takes place for the lowest normal pressure (σ_N=1MPa) and is equal to 37%. This difference ca be due to the surface starting conditions both in terms of topography and of sliding contact. For the highest normal pressure value (σ_N=25MPa) the difference is not significant as it is of about 7%. Being the experimental results obtained by the two different tests in agreement, it can be assumes that the frictional information given by the ad hoc experimental apparatus can be considered as reliable.

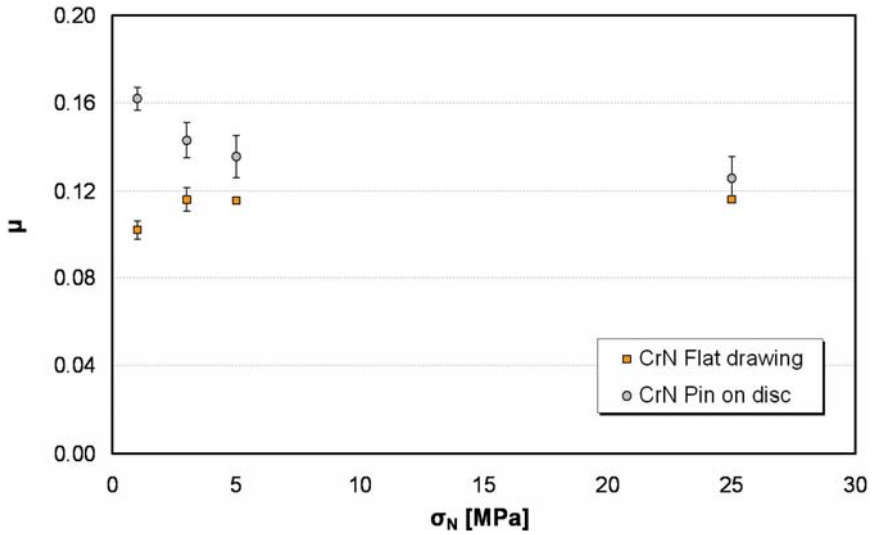

Figure 6.1. *Friction coefficient μ as function of normal pressure σ_N for both flat drawing and pin on disc test.*

6.3. Tribological performance of the conventional oil

In Figure 6.2 the friction coefficient as function of the normal load (condition (a), Table 5.12) is presented. It can be noticed that the μ value does not show any significant dependence on the normal pressure as the friction coefficient varies within the range $0.05 \leq \mu \leq 0.06$. The very low value of μ demonstrates that the lubricating property of

the investigated oil is quite high and stable as well, being the standard deviation significantly low. The lubricant mechanism taking place at the sheet metal/die interface is the mixed boundary hydrostatic one (0.03≤μ≤0.1, see Chapter 2.4.1). There are some metal-to-metal contact at the higher asperities; the load is shared by the hydrostatic pressure (lubricant pockets) and by the asperity contact pressure as well.

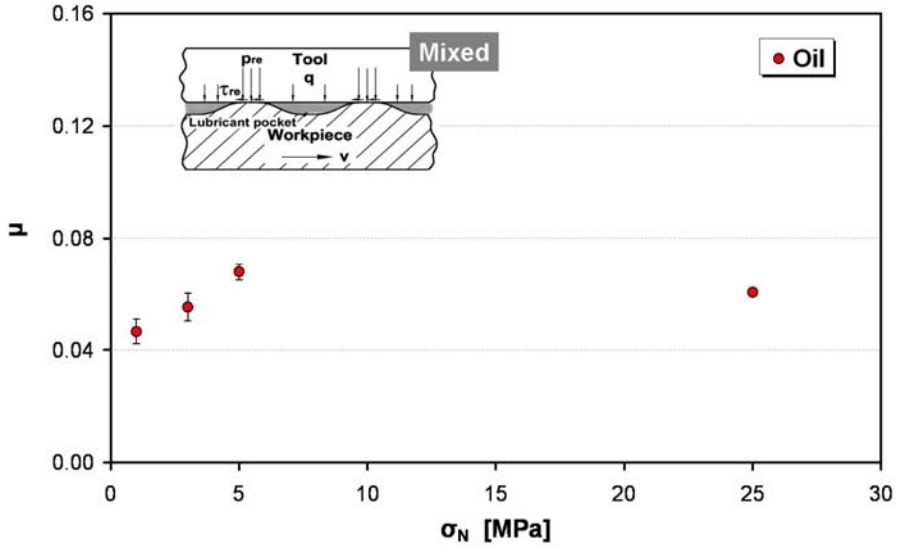

Figure 6.2. *Friction coefficient value μ as function of the normal pressure σ_N for oil lubricant.*

In Figure 6.3 the tested Non coated die profile is presented. If compared with the profile of the as-receive die (Figure 5.7), it can be observed how the die asperities have been flattened. The flattening is probably due to the asperities plastic deformation, being the load on the asperity contact much higher than the apparent value.

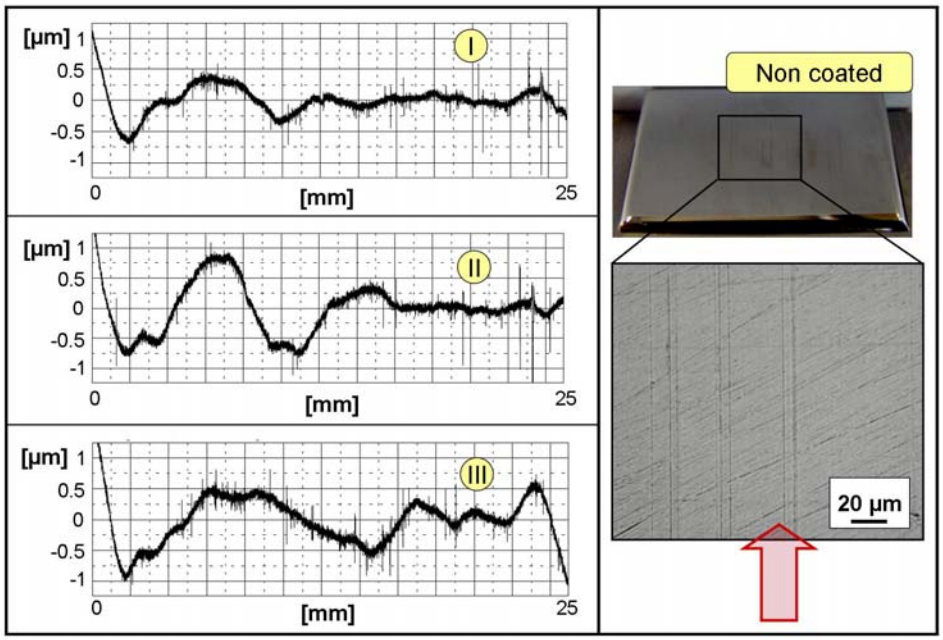

Figure 6.3. *Non coated die profiles.*

The die profile is also subjected to a roughening process as the Ra value goes from 0.013µm to 0.025 µm (Figure 6.4 (a)). This is mainly due to the material transfer from the sheet metal specimen to the die, as shown in Figure 6.4 (b) and Figure 6.5 (b).

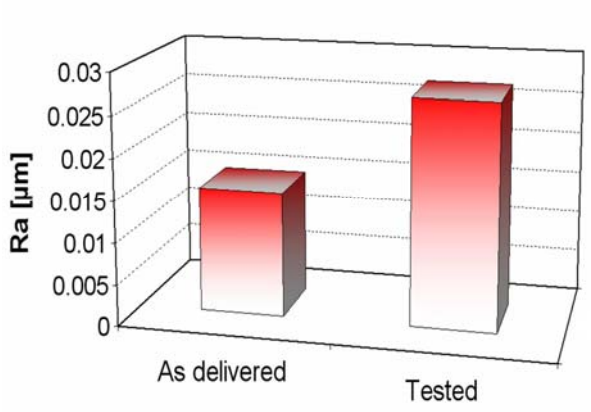

Figure 6.4. *Roughness of the as delivered and Tested Non coated die.*

Due to the material transfer behaviour the roughness of the sheet metal specimen increases as well.
In Figure 6.5 the friction coefficient value as function of the drawing speed (v) is presented (condition (b), Table 5.12).

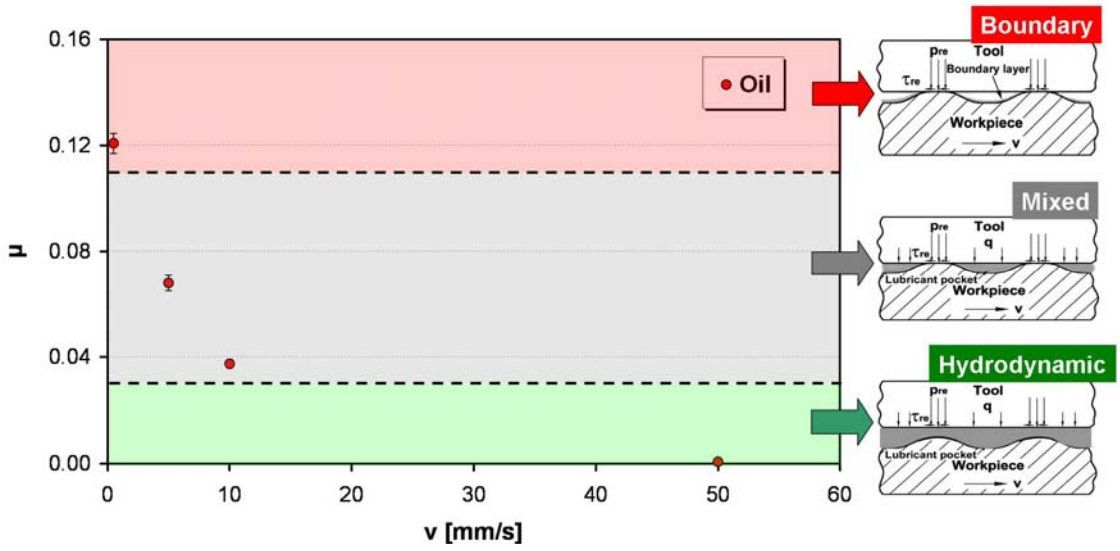

Figure 6.5. *Friction coefficient value µ as function of the drawing speed (v) for oil lubricant.*

For this testing conditions the frictional behaviour shows a significant dependence on the process parameter v: µ varies from a value of 0.12 for v=0.5 mm/s to almost 0 for v=50mm/s. This change in friction coefficient corresponds to a shift in the lubrication mechanism. By increasing the drawing speed (v) the lubricant regime goes from boundary (v<2mm/s) to the mixed boundary hydrostatic one (for 2<v<10 mm/s) to a complete hydrodynamic state (v>10mm/s). The change of the lubrication condition as consequence of an increased drawing speed where low pressure occurs is due to a large film thickness achievement (see Chapter 2.4.1). The higher the speed the more the lubricant is dragged into the gap between the dies and the sheet specimen. In case

of hydrodynamic lubricant regime the surfaces are completely separated by a fluid film, relative motion occurs by shearing of the fluid film. What previously explained finds an experimental evidence in the modification of the sheet metal specimen surface condition (Figure 6.6). For the lowest sliding speed (0.5mm/s) being the amount of contacts between asperities more significant the specimen surface is characterized by more scratches (Figure 6.6(a)) The higher contribution to the frictional behaviour is given by the ploughing effect. While for the highest sliding speed (50mm/s) the contact between the sheet metal and the die is almost prevented therefore no many scratches can be observed on the specimen surface (Figure 6.6(b)).

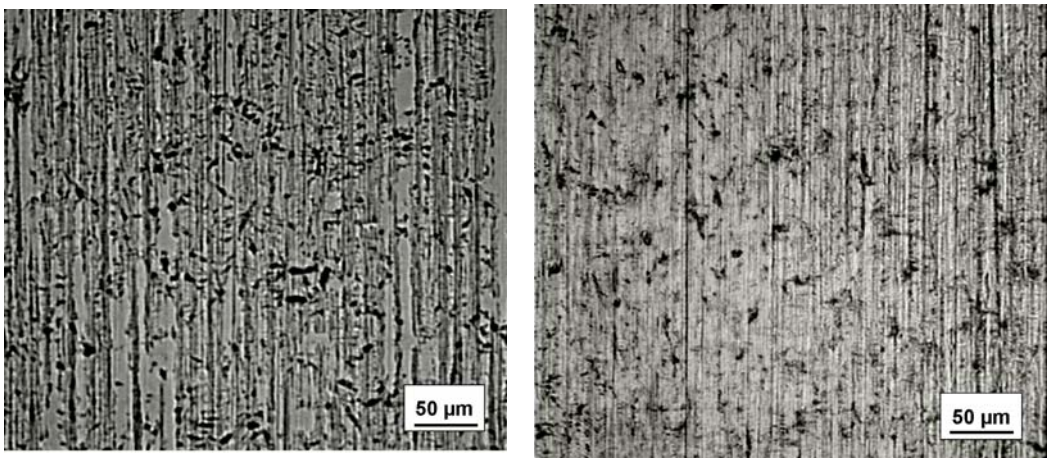

(a) (b)

Figure 6.6. *Optical image of the sheet metal specimen tested in the case of a sliding speed equal to 0.5mm/s* ***(a)*** *and to 50mm/s* ***(b).***

The influence of the tool temperature only has been investigated (condition (c), Table 5.12) in order to reproduce the process conditions corresponding to the 1° drawing operation (see Chapter 5.2.1). In Figure 6.7 the friction coefficient μ as function of the die temperature (T_{DIE}) is reported..

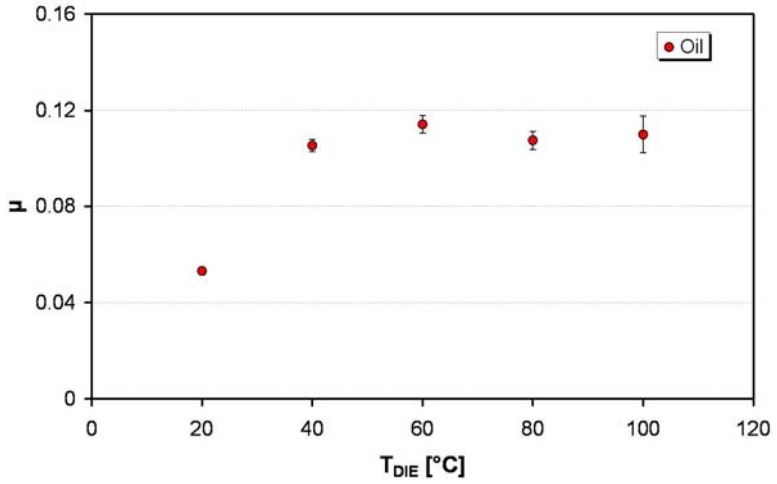

Figure 6.7. *Friction coefficient value μ as function of the die temperature (T_{DIE}).*

For a die temperature of 40°C μ becomes about twice (μ=0.11) its value at room temperature (μ=0.06). Even at higher die temperatures the friction coefficient does not significantly change showing an average value of about μ=0.11. Being a friction coefficient value of 0.11. A μ value of 0.1 represents the border between a mixed and a boundary lubrication mechanism (Chapter 4.2.1). The increasing of the die temperature up to 100°C corresponds to a local increase of the sheet metal temperature due to heat exchange with dies while sliding. This in turn provokes a reduction of the oil kinematic viscosity that means a reduced fluid lubricant film thickness. More asperities will get into contact thus increasing the frictional behaviour as the ratio between the asperity contact and pressurized oil increases.
In Figure 6.8 the friction coefficient as function of the sheet metal specimen temperature (for a constant die temperature of 80°C) is presented (Condition (d) Table 5.12).

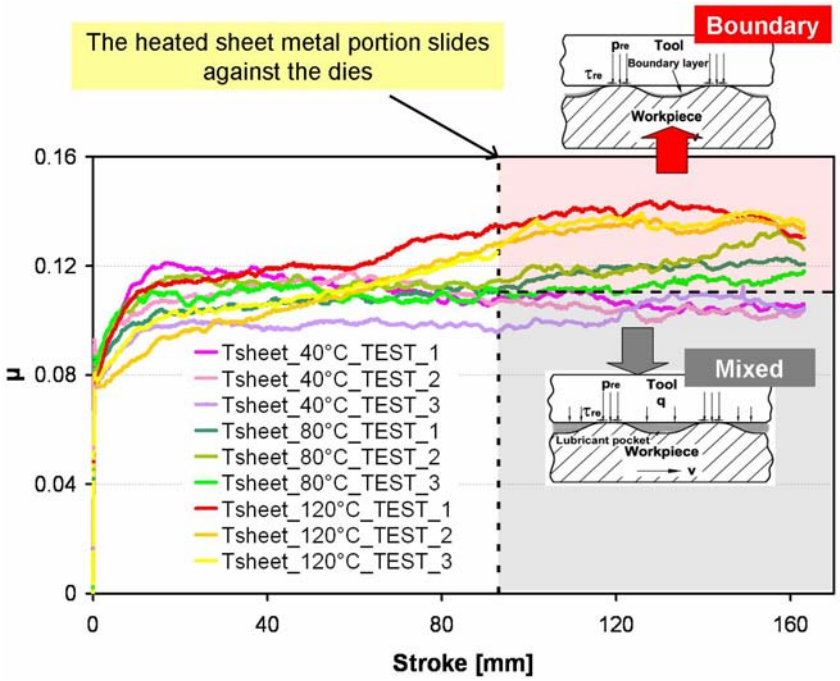

***Figure 6.8**. Friction coefficient value μ as function of the sheet metal temperature (T_{SHEET}).*

It must be kept in mind that the heated portion of the sheet metal specimen will start sliding against the dies after a stroke of about 93 mm. Consequently only the μ signal obtained for a stroke bigger than 93mm will considered as representative. As already shown in the case of the heated dies only, for a sheet metal temperature up to 80°C the friction coefficient has a stable value around 0.11 (equal to the one found on the case of a die heating temperature 40°C≤T_{DIE}≤100°C). For a specimen temperature of about 120°C, once the heated part starts sliding against the dies, the friction condition increases of the 20% being μ=0.14. In this testing condition a friction increase is due the reduction of the fluid film thickness which gives origin to a lager contact area between asperities. Due the change in friction coefficient from a value of μ=0.06 at T_{SHEET}=20°C to μ=0.14 at T_{SHEET}=120°C the lubricant regimes shift from a mixed to a boundary one. In the latter case the oil has significantly reduced its viscosity so that the load is totally supported by the asperity contact.

In Figure 6.9 an optical image of the sheet metal specimen tested at 120°C shows the presence of quite many scratches thus giving evidence of the many asperities contact taking place when the temperature of the sheet increases thus the oil viscosity decreases.

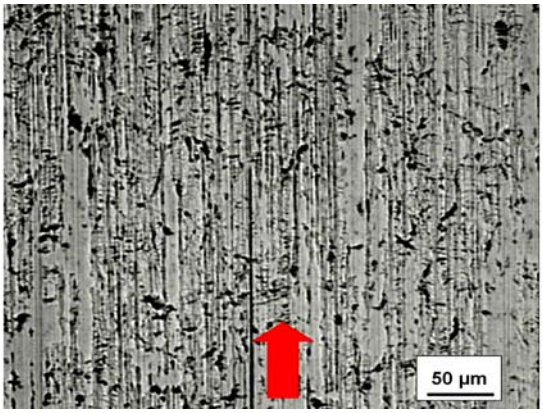

Figure 6.9. *Optical image of the sheet metal specimen tested at a temperature of 120°C.*

6.4. Tribological performance of the PVD solid lubricant coatings

For both the CrN and Cr-DLC coated dies the friction coefficient dependence on the normal load (σ_N) has been investigated (Figure 6.10).

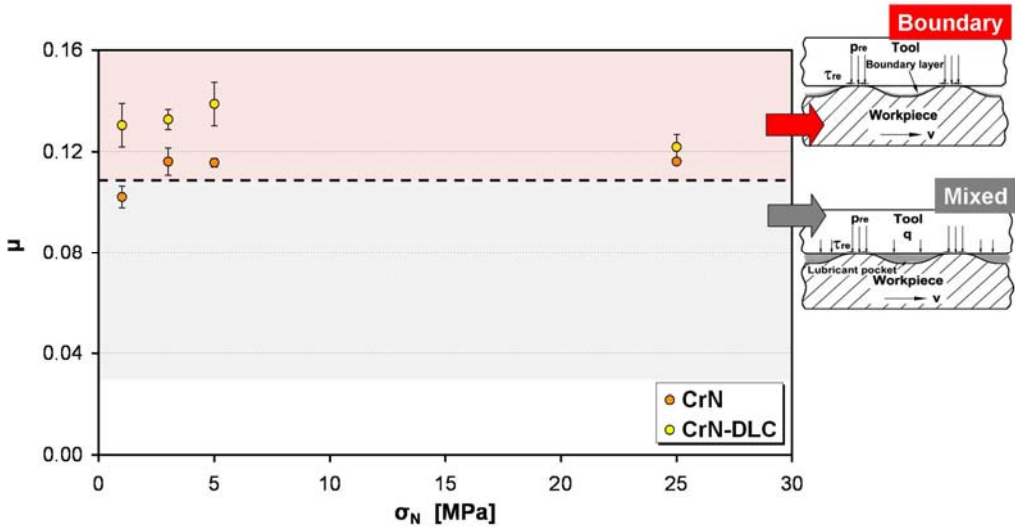

Figure 6. 10. *Friction coefficient value μ as function of the normal pressure σ_N fboth for crN and CrN-DLC coated dies.*

For both the coatings the value of μ does not show any significant dependence on the normal load (σ_N) being the friction coefficient within the range $0.10 \leq \mu \leq 0.12$ and $0.12 \leq \mu \leq 0.14$. The latter shows a worse tribological performance than the CrN one. However both the coated dies show a higher friction coefficient with respected to the oil only lubrication system. The increase in friction (Chapter 6.3) is mainly due to the

higher coating surface roughness (Figure 5.9, Figure 5.10). Being the applied amount of oil always the same, a higher surface roughness means a thinner fluid film lubricant which gives origin to a larger amount of asperity contact and a shift from a mixed to a boundary type of lubrication especially in the case of the CrN-DLC coating. By comparing the profile of the tested CrN (Figure 6.11) and CrN-DLC (Figure 6.12) with the as delivered ones (Figure 5.9 and Figure 5.10 respectively) it can be noticed that the surface profile is almost unchanged with the respected to the as-received one both in terms of morphology and surface roughness.

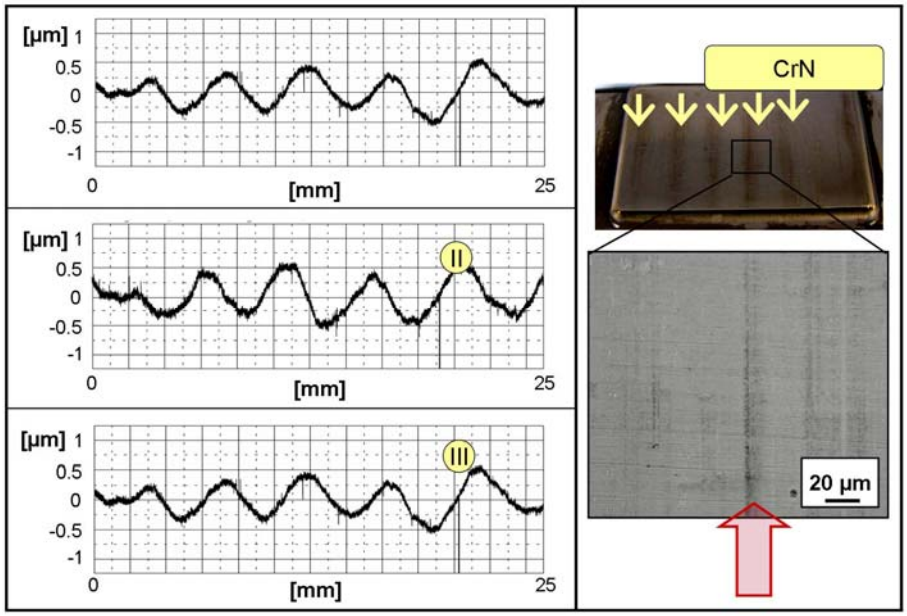

Figure 6.11. *CrN tested die profiles (Left) and image (Right).*

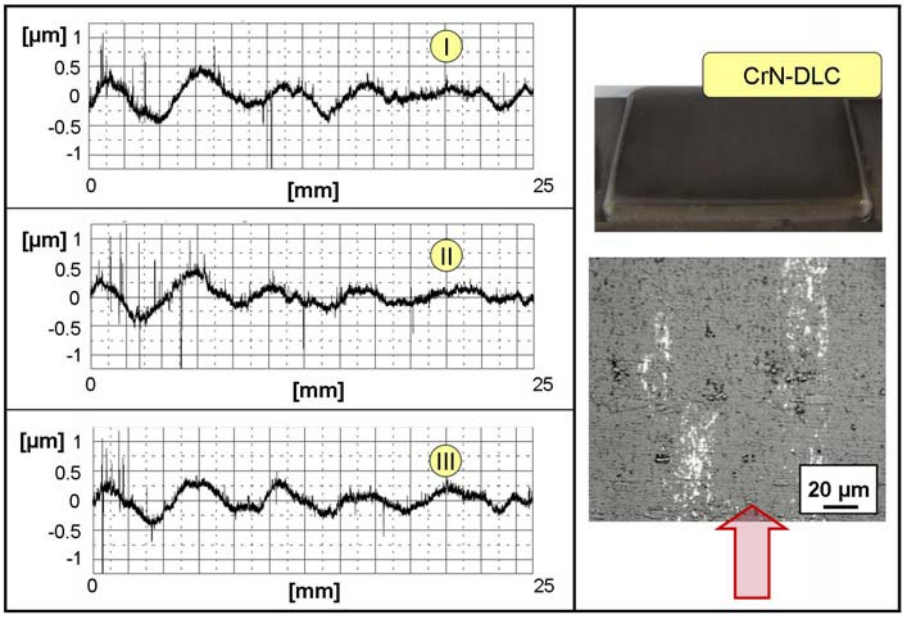

Figure 6.12*. CrN-DLC tested die profiles (Left) and image (Right).*

This is numerically demonstrated by the Ra value as presented in Figure 6.13.

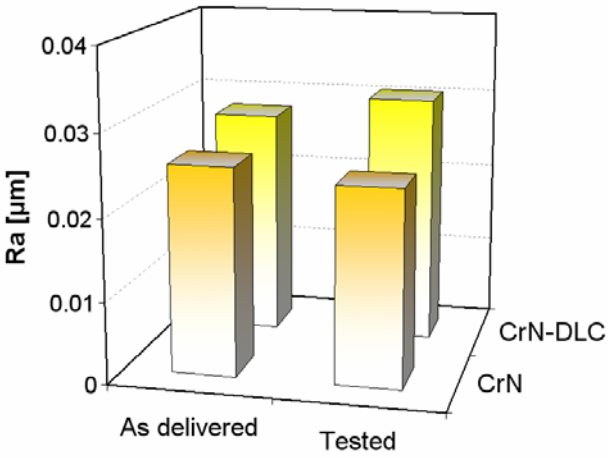

Figure 6. 13. *Roughness of the as received and tested CrN and CrN-DLC coated die.*

The prevailing frictional behaviour for both the two coating in the ploughing one (Figure 6.14). This effect is much more evident in the case of coated die because the surface of the latter is even harder than the non coated one thus the sheet metal materiual indendation is more significant.

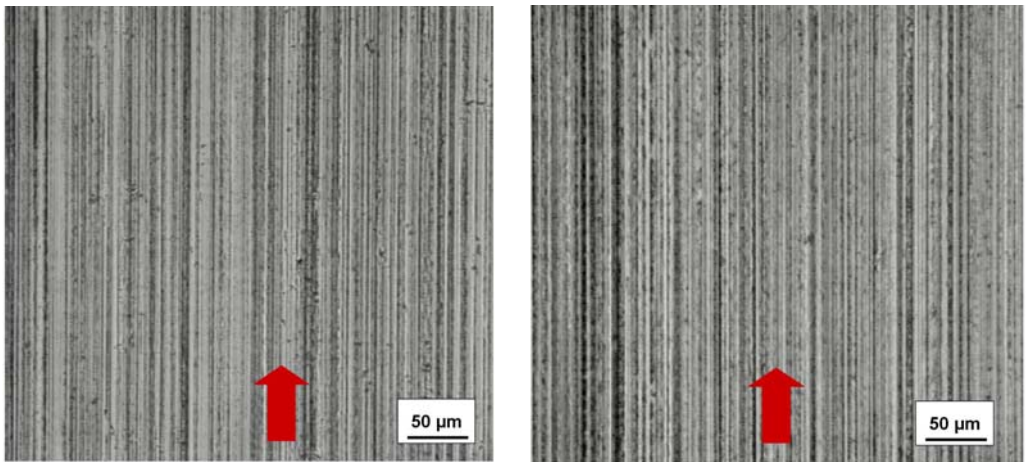

(a) (b)

Figure 6.14*.Optical image of the sheet metal specimen sliding against CrN* ***(a)*** *and CrN-DLC* ***(b)*** *coated die when a normal pressure of 25MPa is applied.*

As in the case of the Non coated die for the CrN and CrN-DLC coated dies the friction coefficient shows a significant dependence on the drawing speed v (Figure 6.15). Even if the value of μ is higher with respect the oil lubrication (because of the higher surface roughness) it goes from μ=0.16 to μ=0.06 for the CrN coating and from μ=0.16 to μ=0.08 for the CrN-DLC. A drawing speed of about 10mm represents the shift from a boundary type of lubricant regime to a mixed one for the CrN coating type, while for the CrN-DLC the speed which causes a change of the lubricant regime is higher. Moreover the hydrodynamic state is never achieved for both the two coatings probably as consequence of the high surface roughness.

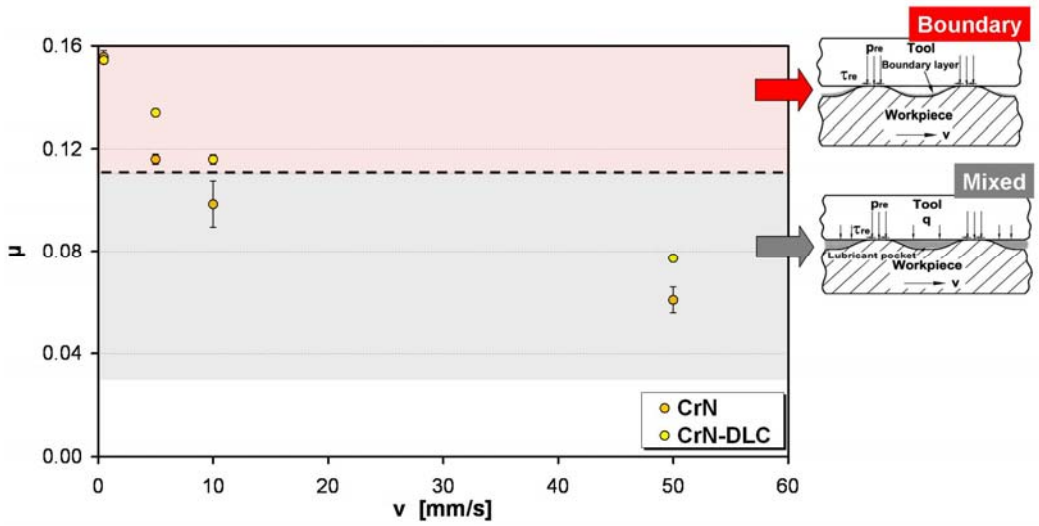

Figure 6.15. *Friction coefficient value μ as function of the drawing speed (v) for oil lubricant.*

6.5. Tribological performance of the thin organic coated sheet metal

The organic coated sheet metal specimens do not show any significant dependence of their frictional behaviour on normal pressure (Figure 6.16, condition (a), Table 5.12). Their frictional behaviour is quite stable and more over any coating delamination occurs. Coating B shows a better lubricating tendency especially in the case of higher normal pressure values as $\mu_{\text{Organic coating A}}$ (σ_N=25MPa)=0.08 while $\mu_{\text{Organic coating B}}$ =(σ_N=25MPa)=0.06. The experimental results obtained for coating B are comparable with the ones evidence by the oil lubrication only (Figure 6.17).

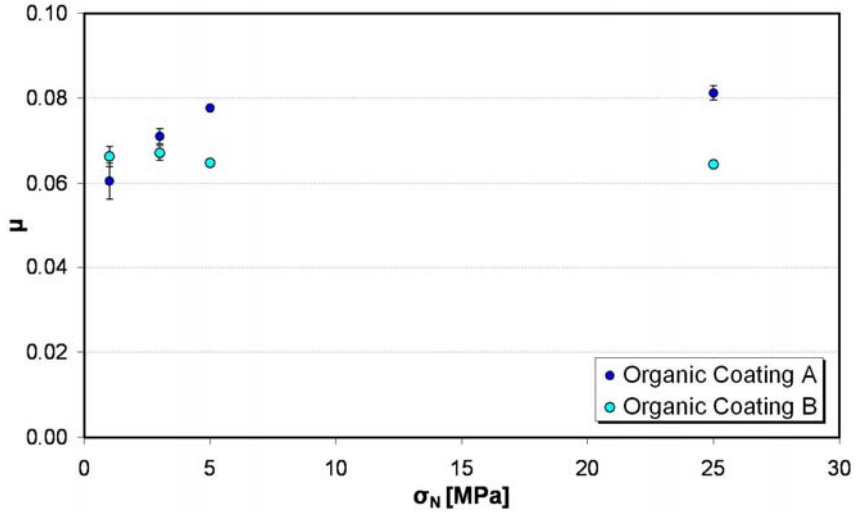

Figure 5

Figure 6.16. *Friction coefficient value μ as function of the normal pressure σ_N for both Organic coating A and Organic coating B.*

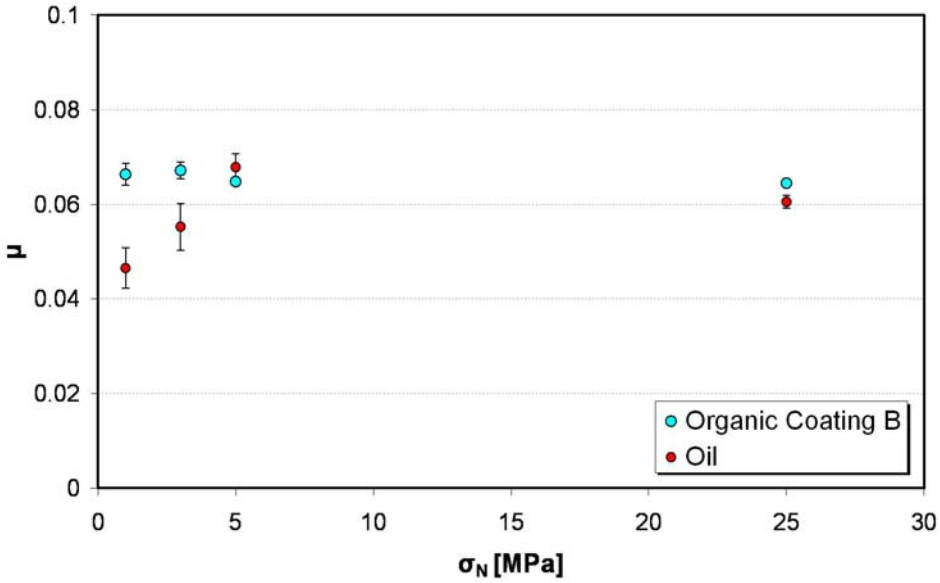

Figure 6.17. *Friction coefficient value μ as function of the normal pressure σ_N for both Organic coating A and Organic coating B.*

No significant material transfer is evidenced (dies were inspected after each test) thus implying that any adherence phenomenon did take place. This tendency supports the presence of an *interface sliding* lubrication mechanism that basically allows the die surface to slide over the organic coated one, only if there is no adhesion to the rider (Chapter 2.5.2).
The friction coefficient does not show any significant dependency on the sliding speed as well (Figure 6.18, condition (b), Table 5.12)). The value of μ does not change with respect to testes carried out varying the normal pressure (Figure 6.16).

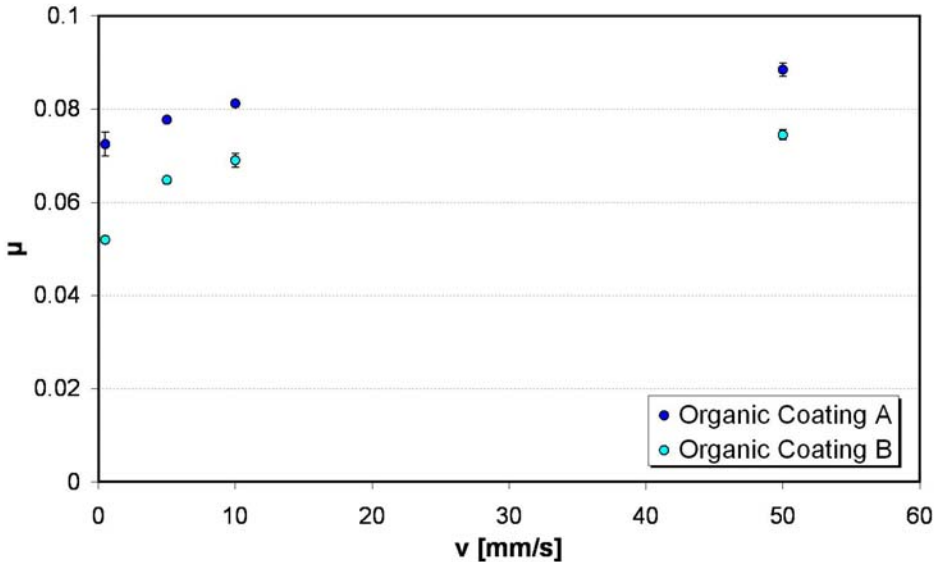

Figure 6. 18. *Friction coefficient value μ as function of the normal pressure σ_N for both Organic coating A and Organic coating B*

The results concerning the tribological behaviour of organic coating A as function of the sheet metal temperature is presented in Figure 6.19 (condition (d), Table 5.12)

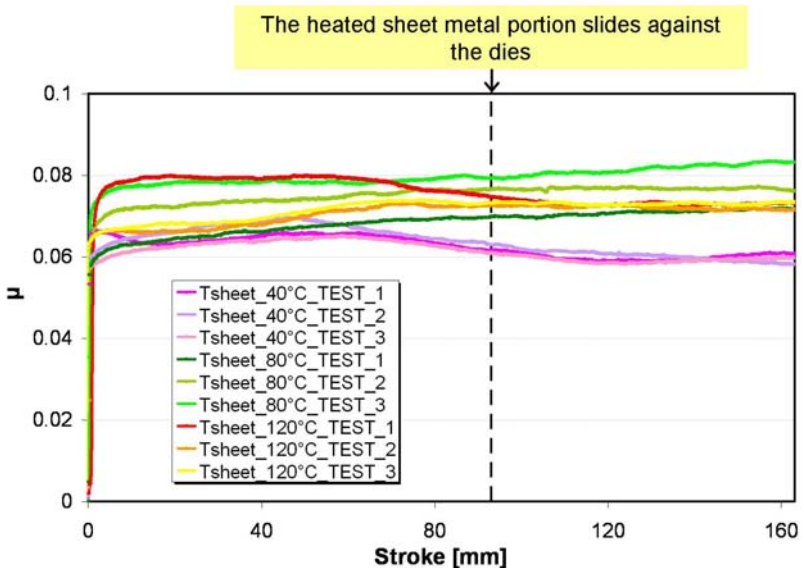

***Figure 6.19**. Friction coefficient value μ as function of the sheet metal temperature (T_{SHEET}) for Organic coating A*

At a temperature of about 40°C the friction coefficient (pink lines) tends to decrease (μ=0.06) with respect to the room temperature value (μ=0.08) probably because the organic part (wax) becomes softer thus lowering its shear stress. For the same reason explained in Chapter 6.3 there is a decrease in the μ signal starting before a stroke of 93mm. However as no material transfer takes place (Figure 6.20) the prevailing lubricant mechanism is still the interface sliding.

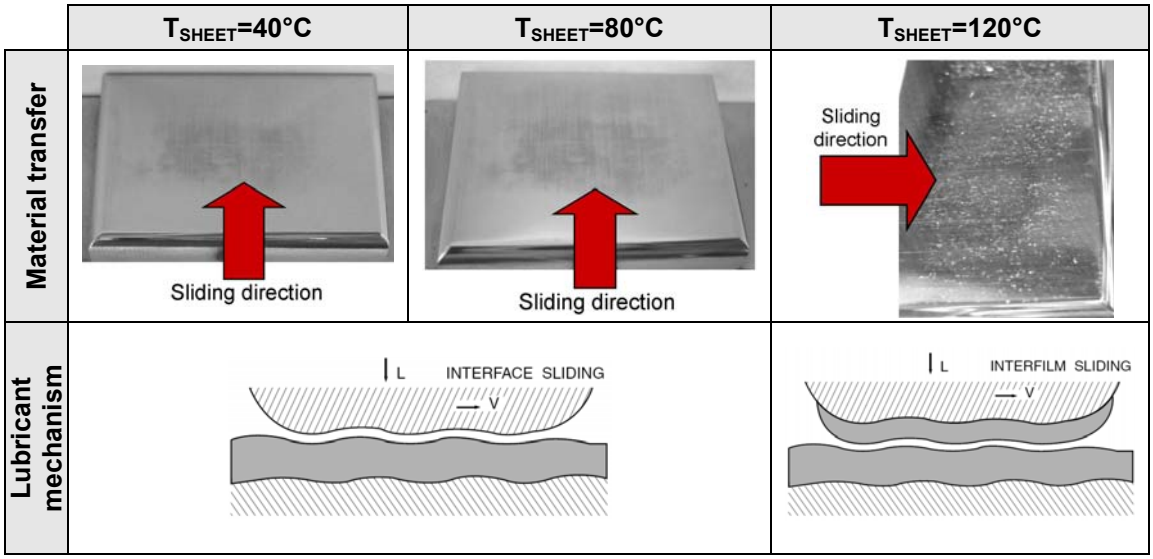

***Figure 6.20.** Lubrication mechanism for Organic coating A in the sheet metal specimen heated at 40, 80 and 120°C.*

By increasing the temperature (T_{SHEET}=80°C) the organic part becomes even softer and consequently less viscous. This decrease in viscosity can be critical in reducing the organic part thickness when a normal load is applied. This could cause a contact between the coating inorganic part and the die surface thus increasing the friction coefficient (green lines). Nevertheless no material transfer is visible on the die surface (Figure 6.20). For a sheet metal specimen temperature of about 120°C (red lines) the organic part has melted in some areas (see Chapter 5.2.3.2). Once the heated portion of the specimen starts to slide against dies the latter is transferred to the dies surface. Consequently the immediately subsequent part of the heated specimen will slide against the previously transferred wax thus causing a change from an *interface sliding lubricant mechanism* to an *interfilm* one (Figure 6.20). When the two successive tests at 120°C are performed, the non heated specimen portion will slide as well against the wax deposited by the previous test (interfilm sliding) thus causing an overall lowering of the frictional behaviour. This phenomenon is evidenced in Figure 6.21. For all the three heating temperatures the coefficient of friction is lower or comparable with the one obtained in case of tests carried out at room temperature.

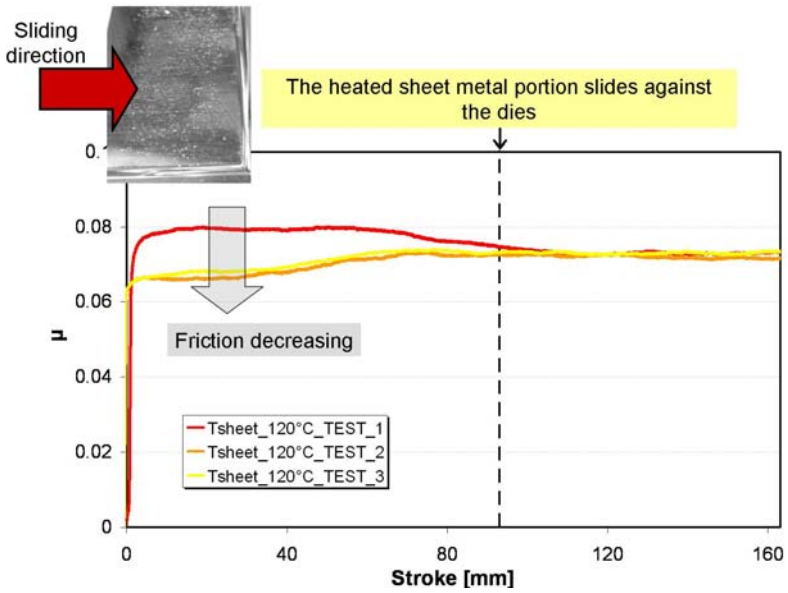

Figure 6.21. *Friction coefficient μ as function for a sheet metal temperature of 120°C (Coating A)*

The frictional behaviour of the Organic coating B as function of the heating sheet metal temperature is presented in Figure 6.22. Coating B shows the same general trend as Coating A. For a specimen temperature of 40°C the μ value decreases as conseguence of the organic part softening. When the specimen is heated up to 80°C (green lines) friction seems to increase probably for the same reasons evidenced in the case of Coating A. The main difference consists in the presence of a slope in correspondence of a 60mm stroke. Due to the significant wax softening when the heated part of the specimen slides against the dies a wax accumulation takes place thus causing a temporary increase of the drawing force. This phenomenon is particularly evident in the case of Coating B as this characterized by a higher amount of organic part (five times more with respect to the Coating A). Nevertheless no material

transfer on to the dies can be appreciated. For a sheet metal specimen is heated up to approximately 120° (red lines), as in the case of coating A, in some areas the wax will be in a melted state. This will emphasize, the slope behaviour taking place at a stroke of approximately 60mm. For the same principle explained in the case of coating A (first test) the friction coefficient will then decrease.

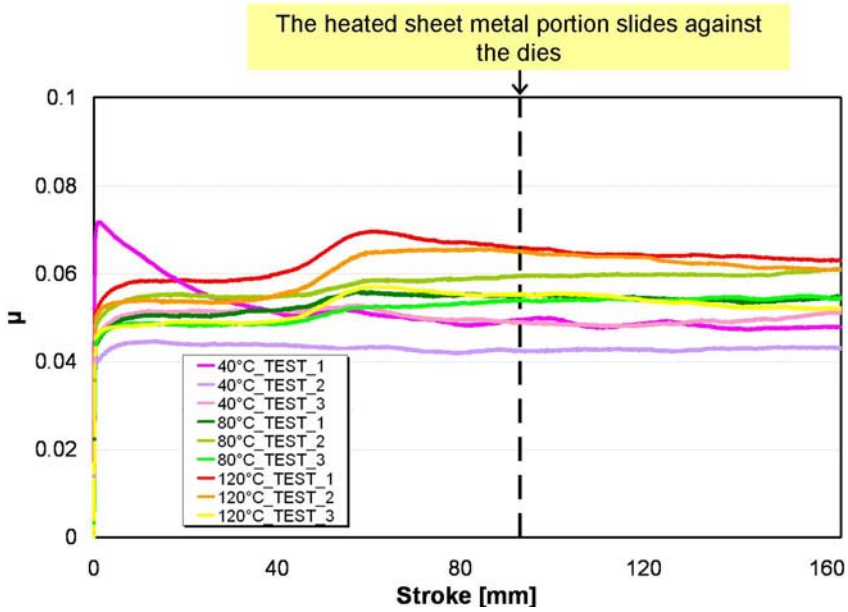

***Figure 6.22**. Friction coefficient value μ as function of the sheet metal temperature (T_{SHEET}) for Organic coating B.*

Due to the shift from an interface sliding lubricant mechanism to an interfilm one the overall friction behaviour will decrease for the second and the third test as shown in Figure 6.23 where it is visible at a glance the wax transfer.

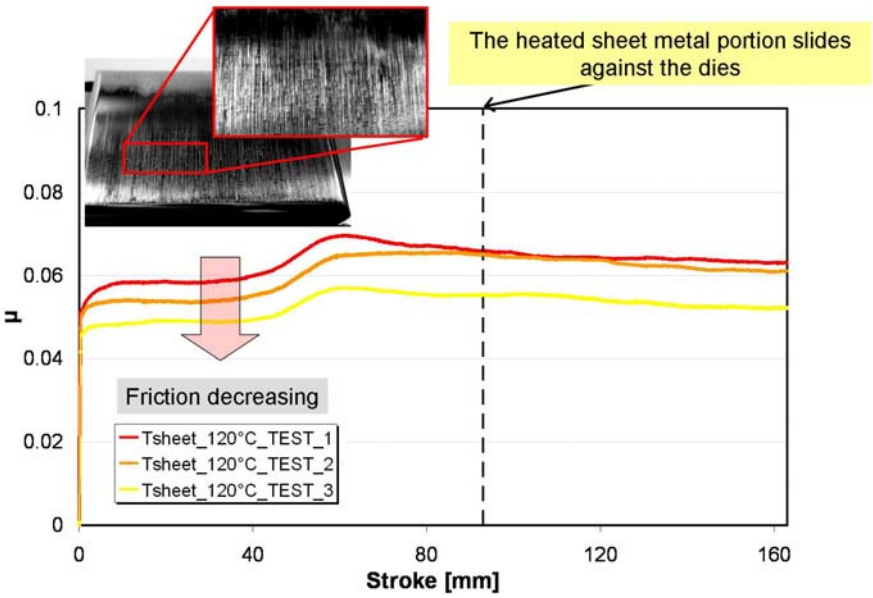

***Figure 6.23.** Friction coefficient μ for a sheet metal temperature of 120°C (Coating B)*

6.6. Friction in hot stamping operations

6.6.1. Chemical behaviour as function thermal parameters

In Figure 6.24 SEM cross sections of specimens 1 and 2 are shown. The different cooling rate does not affect the sub-layer structure that takes place when the sheet metal is heated at 900°C. The five zone indicated with the letters A, B, C, D, E, representing different concentrations of Al and Fe elements, maintain the same distribution and the same thickness in the analyzed sections. [82]

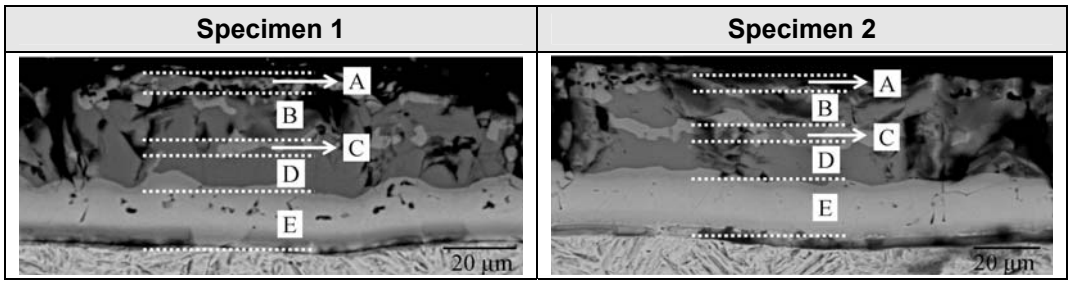

Figure 6.24. *SEM cross sections of specimens 1 and 2.*

Even the chemical composition does not significantly change for the two specimens as shown by the SEM-EDX analysis results reported in Figure 6.25.

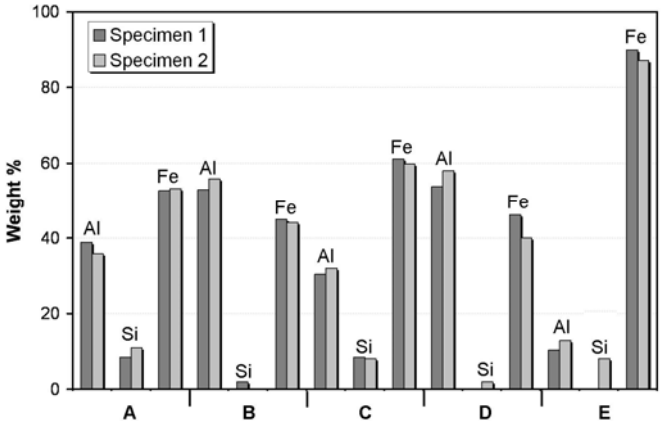

Figure 6.25*. SEM-EDX analysis for specimens 1 and 2.*

In Figure 6.26 both the SEM cross sections for specimens 3 and 4 are shown.

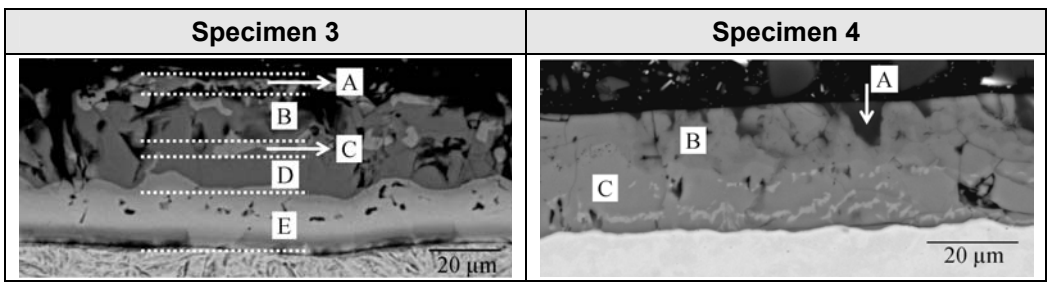

Figure 6.26. *SEM cross sections of specimens 3 and 4.*

A difference in the coating sub-layer evolution can be noticed. In the case of the shorter holding time tested in the experiments (specimen 4), the coating appears much more homogeneous: the structure made of five sub-layers does not appear as in the case of specimen 3 characterized by the higher holding time.
Considering the SEM EDX results in the case of specimen 4 (Figure 6.27) there are still some surface zones not completely reached by the steel substrate (such as zone A). The structure of specimen 4 looks like as the alternating Al-Fe alloying system does not have enough time to develop.

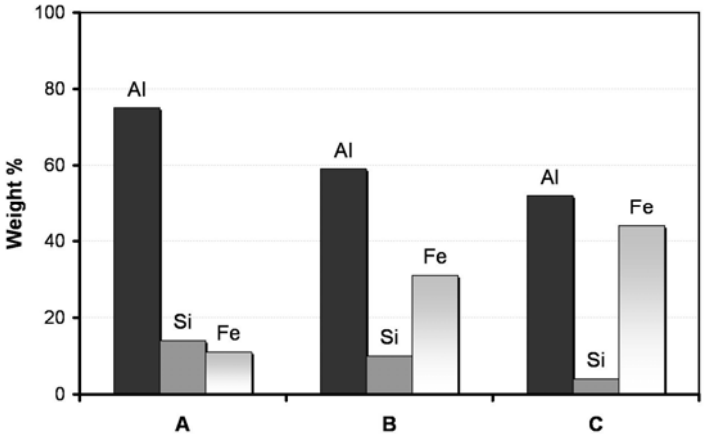

***Figure 6.27**. SEM-EDX analysis for specimen 4.*

6.6.2. Surface roughness measurements

As neither chemical nor morphological difference is observed for specimens 1 and 2, the surface roughness comparison is carried out between the two specimens heated at 900°C and kept at this target temperature for different holding times. In Figure 6.28 the White Light Interferometer images are shown, while the corresponding surface roughness parameters are reported in Figure 6.29.

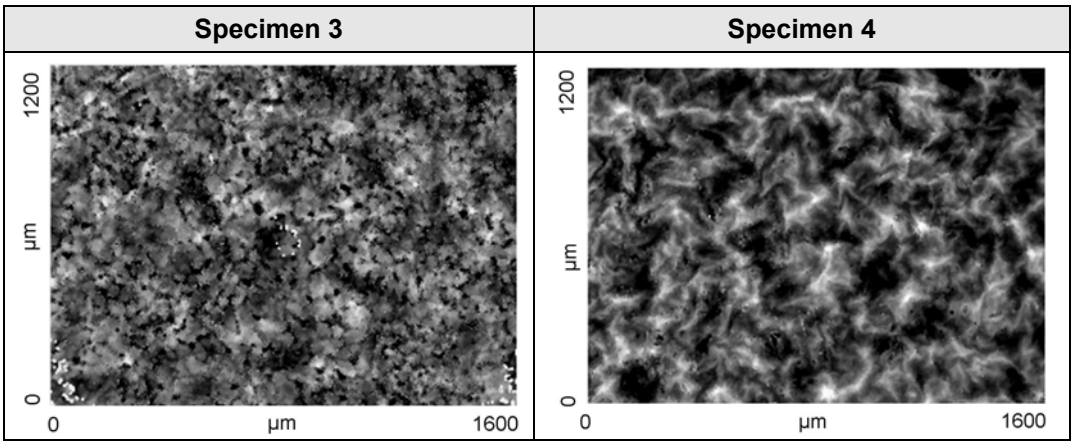

***Figure 6.28.** WLI images for specimens 1 and 4.*

Specimen 4 turns out to be less rough (Ra = 1.792 µm) than specimen 1 (Ra = 2.336 µm). Moreover specimen 1 is characterized by a Svk value which is approximately

double of the one describing specimen 4, meaning that the latter is characterized by much larger valley areas (as it is clearly evidenced by the WLI images). While the reduced summit height (Spk) is almost the same. This morphological behaviour can be attributed to the steel diffusion step, as in the case of specimen 4, Fe has not completely reached the surface yet.

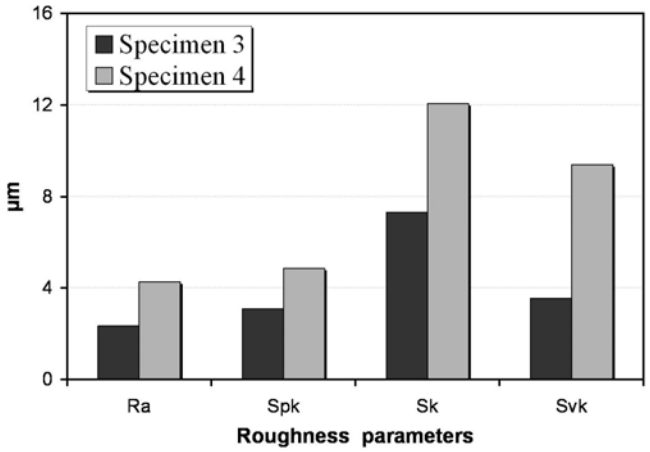

Figure 6.29. *Roughness parameters for specimens 1 and 4.*

6.6.3. Frictional behaviour as function of the main process parameters

The analysis of variance (ANOVA) has been utilized as statistical technique in order to evaluate which factors have the most relevant influence on the friction coefficient and in which way. It is verified that the assumptions of independence, normality, homoschedasticity and absence of anomalies are fulfilled (Figure 6.30), therefore, the ANOVA being the response model assumptions verified through the analysis of residuals.

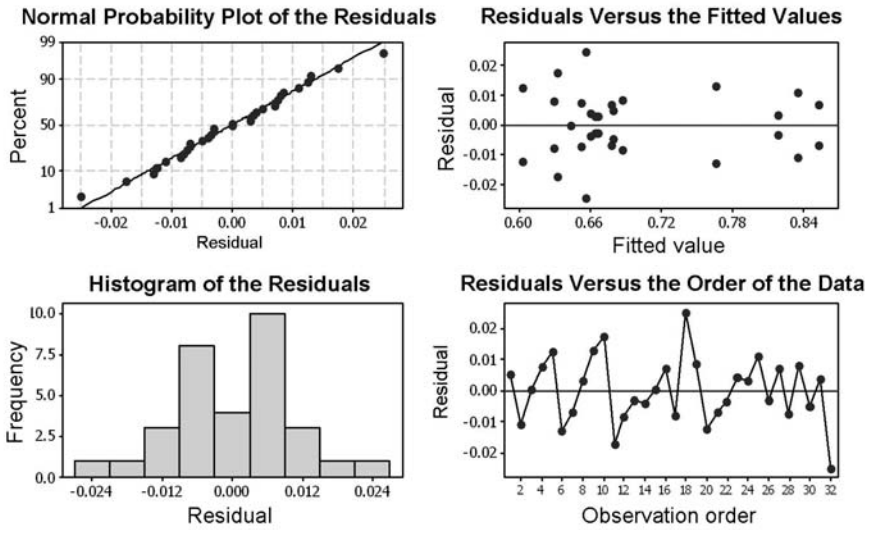

Figure 6.30. *Analysis of assumptions of independence, normality, homoschedasticity and absence of anomalies.*

The most relevant effects of the tested process parameters on friction at the sheet metal/die interface and their interactions are presented in Figure 6.31 and Figure 6.32, respectively. According to the main interaction plot, *"Normal pressure"* and "*Temperature"* are the factors mainly influencing the tribological behaviour; on the other hand, *"Sliding velocity"* and *"Roughness"* show no effect on the friction coefficient value.

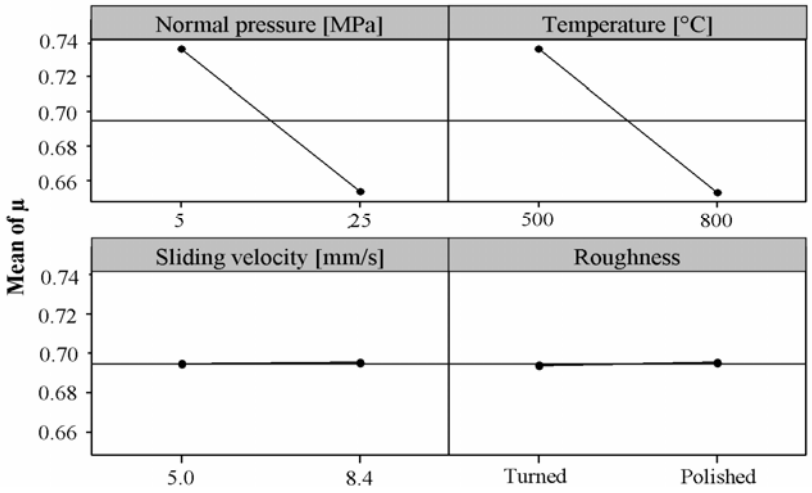

***Figure 6 31**. Main effects plot for friction coefficient.*

The interaction plot shows that the interaction between the parameters "*Temperature"* and "*Normal pressure"* is the most relevant for the friction coefficient in hot stamping. For low values of normal pressure the friction decreases as the temperature increases, while for low temperature values the μ value decreases as the normal pressure increases

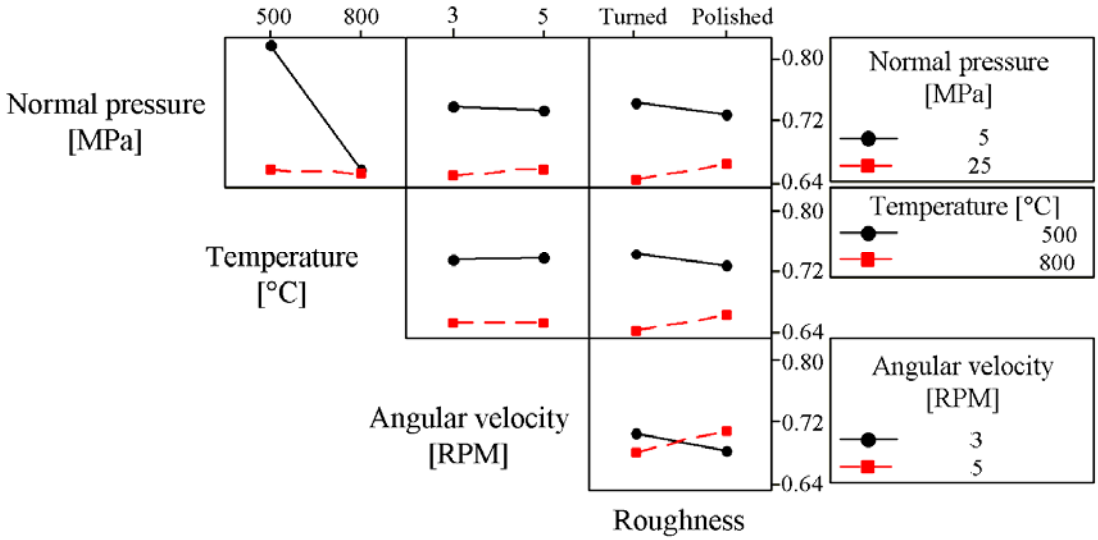

***Figure 6.32.** Interactions plot for friction coefficient.*

The dependency of friction coefficient on process temperature is shown in Figure 6.33 for low normal pressure. In Figure 6.34 the dependency of friction coefficient on normal pressure for low testing temperature is presented.
This result, in accordance with previous researches reported in [62-64], could be explained by the formation of the ternary system Al-Si-Fe on the sheet surface at elevated temperature, which could be considered responsible of the friction reduction under the application of increasing normal pressure and temperature.

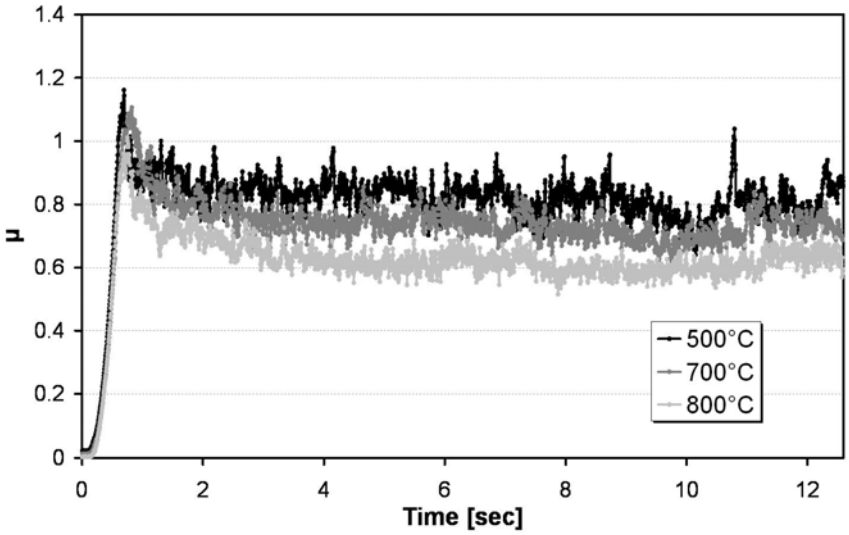

Figure 6.33. *Friction coefficient dependency on testing temperatures for low normal pressure (5MPa).*

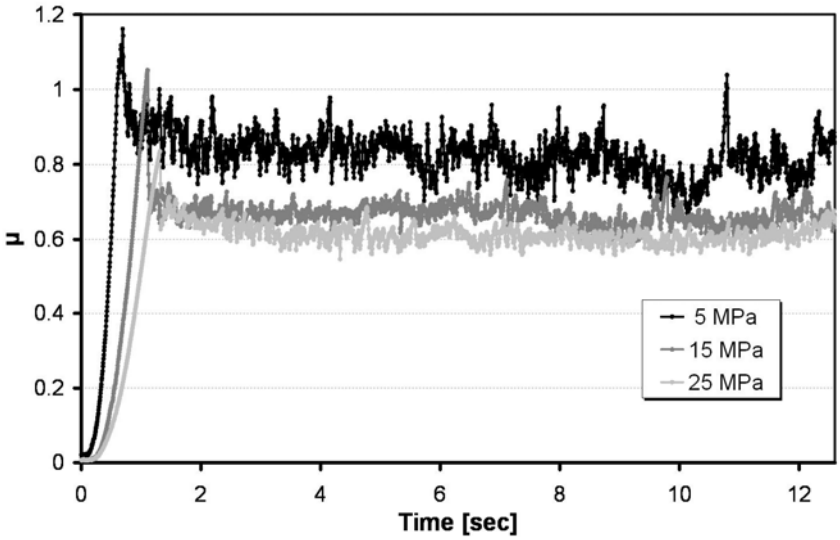

Figure 6.34. *Friction coefficient dependency on testing normal pressure for low temperature (500°C).*

To verify if any change in the coating chemical composition did happen as consequence of the different testing conditions, SEM EDX analysis was carried out on

the samples tested at different temperatures and normal pressure. The wear track and the non tested area were investigated (Figure 6.35).

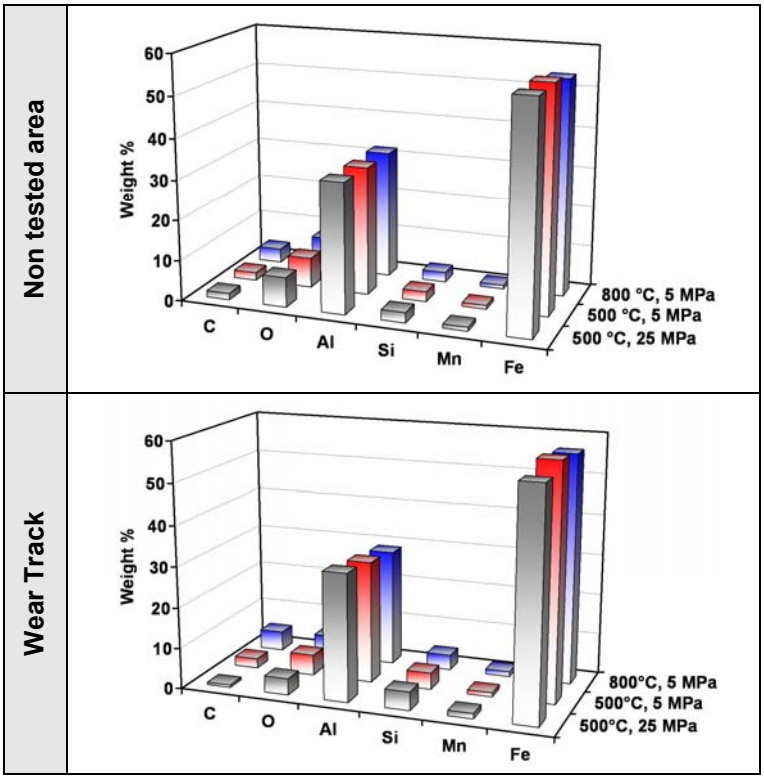

***Figure 6.35**. SEM EDX analysis carried out both on the non tested area and the wear track for different temperature and normal pressure testing g conditions.*

No chemical difference can appreciated thus implying that the coating chemical composition does not change with testing parameters. In Figure 6.36 a top down SE SEM image shows the interface between a non tested area and the wear track. The nodules like features (ternary Al-Fe-Si system) are flattened when the pin slides over.

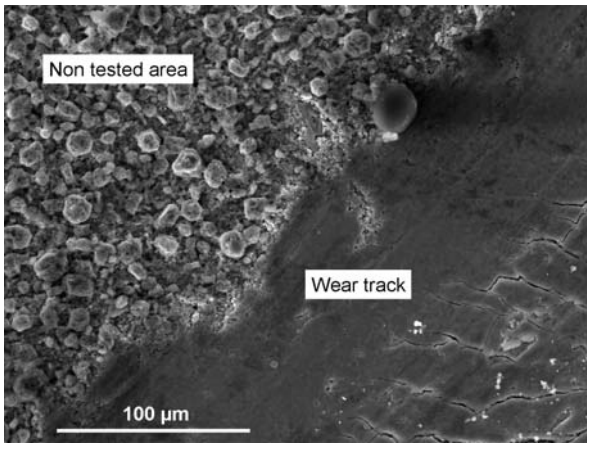

***Figure 6.36.** Top down SE SEM image.*

To give a possible explanation of the coating tribological response to the temperature and normal pressure process parameters both a macro and micro-mechanical approaches have been followed (see Chapter 2.5.2).
On a macro level the case of a soft coating on a hard substrate (Figure 2.22) has been considered as representative of the investigated tribological system. In this case friction is determined by the shear strength of the film and the contact area, which is related to the deformation properties of the substrate.
On a micro scale, the asperity deformation phenomenon turns out to be the most relevant.
In the case of low testing temperature (500°C), as consequence to an increased normal pressure, the asperities deformation and thus surface topography flattening phenomenon becomes more significant (Figure 6.37). For higher normal pressure the pin moves over a less rough surface with respect to the case of low normal load. This implies a reduction of friction.

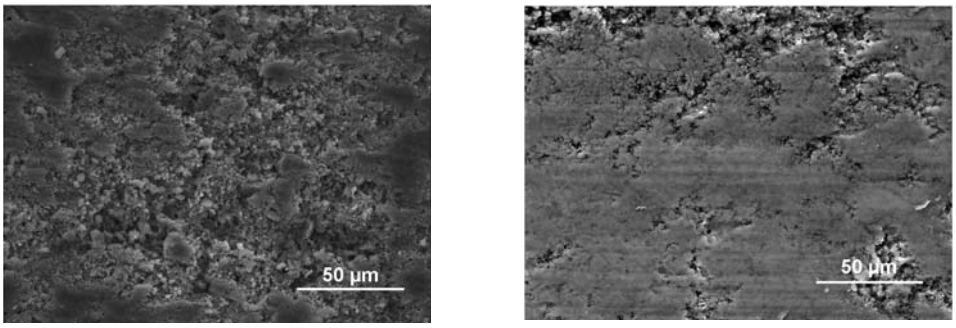

(a) (b)

Figure 6.37. *Top down SE SEM images for specimen test at (a) 5MPa and (b) 25MPa for a low temperature.*

Considering now the effect of the testing temperature on the coating tribological behavior, it can be said that the higher the sheet metal specimen temperature the softer the coating thus its shear strength is lower. When the pin slides over the coating the asperities of the latter are more easily deformed and sheared provoking a decrease of the friction coefficient.
What previously discussed explain why in the case of high testing temperatures (800°C) no friction dependency on the normal pressure is observed. In the case of low normal load even if the surface is much rough the shear stress is low while for higher normal pressure the flatting effect is the predominant one.
The same apply to high normal loads, the flattening of the surface asperities determines, thus reducing the surface roughness reduces friction.

6.7. Conclusions

The present chapter focuses on the study of the interface conditions taking place at the sheet metal/die interface for two different tribological systems:

- deep drawing of stainless steel sheet
- hot stamping of quenchable Al-Si coated HSS sheet

With respect to the first case the interface conditions actually present in the industry environment have been characterized first. Grinded non coated dies are lubricated by means of conventional oil. The starting non coated die profile is characterized by a wavy surface.
The frictional behavior has been studied as function of the main critical process parameters namely normal pressure σ_N, sliding speed (v), die temperature (T_{DIE}) and sheet metal temperature ($T_{SHEET\ METAL}$). It has been found that at room temperature the dominant lubrication regime is the mixed boundary-hydrostatic one (μ=0.06) independently of the applied normal pressure. The sliding speed has a significant effect of the frictional behavior: the higher the speed the lower the friction coefficient. For v≥10mm/s the prevailing lubrication mechanism is the hydrodynamic one with a coefficient of friction close to 0. When the dies only are heated up within a range 40°C≤T_{DIE}≤100°C the friction coefficient increases of the 50% (μ=0.11) already for T_{DIE}=40°C and it remains stable for all the testing temperatures. The increase of friction, is due to a decrease of the oil viscosity which provokes a reduced oil film thickness thus allowing more asperities getting into contact. When the sheet metal specimen is heated up within a range 40°C≤T_{DIE}≤120°C the highest temperature seems to be critical as the friction coefficient increases up to μ=0.14 meaning a shift to a boundary type of lubrication.
In order to perform dry or semidry operations solid lubricant coatings have been proposed and their tribological performance studied. The two different types of inhorganic coatings CrN and CrN-DLC gave worse results in terms of friction coefficient with respected to the non coated one, probably as consequence of the higher surface roughness. On the other hand the coated die show a higher wear resistance. Due to the wavy initial surface condition the CrN coated die show a visible wear in correspondence of the highest peaks. This does not happen for the CrN-DLC coated dies probably because the as-received surface seem to display a less pronounce wavy surface profile so the normal load is spread over a larger area.
Two different types of organic coatings namely Coating A and Coating B have been investigated as function of σ_N, v and T_{SHEET}. Coating B shows a better lubricating tendency ($\mu_{Organic\ coating\ B}$=0.06) and presents a tribological behavior comparable to the oil one at room temperature. When the sheet metal is heated up at 40°C its friction decreases, while at 80°C the friction signal increases and at 120°C due to the presence of melted wax a material transfer from the coating to the die surface takes place provoking a shift from an interface sliding lubricating mechanism to an interfilm one

Concerning the interface condition taking place during hot stamping operations of Al-Si coated boron HSS sheets first the coating both chemical and morphological evolution with the thermal parameters holding time and cooling rate has been studied. Only the former does influence the morphology of the Al-Si coating as the five layered structure does not have enough time to develop. A friction analysis based on DOE technique has also been carried out in order to study the dependency of the friction coefficient on normal pressure, testing temperature, tool surface roughness and sliding velocity. The interaction between normal pressure and temperature is the most relevant for the friction coefficient: For low values of normal pressure the friction decreases as the temperature increases, while for low temperature values the μ value decreases as the normal pressure increases. To give a possible explanation of the coating tribological

response to the temperature and normal pressure process parameters consists on the both a macro and micro-mechanical approaches have been pursued.
Consequently to the interaction between the normal pressure and the temperature parameters a contour plot can be obtained (Figure 6.38) which enable to optimize the investigated process parameters in order to reduce friction. Considering the hot stamping process area in the right side could be considered as feasible: reducing as much as possible the transferring time from to furnace to the die in order to form the blank at high temperatures

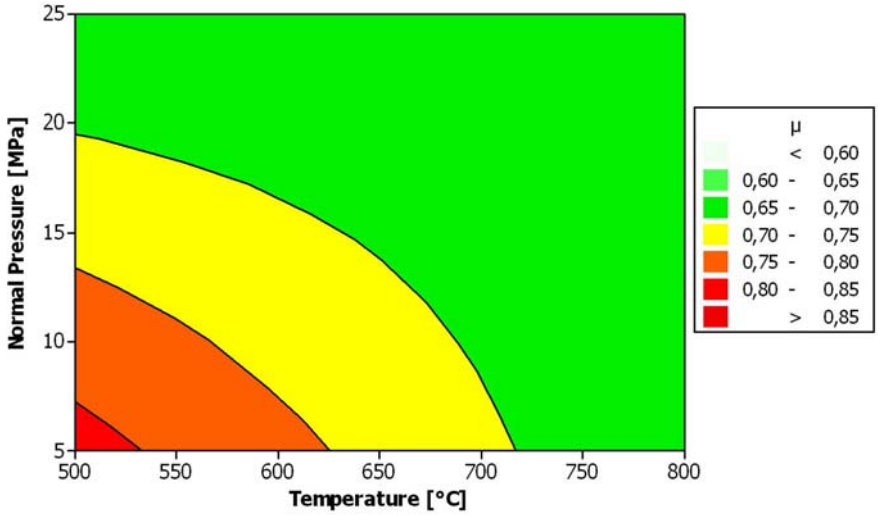

Figure 6.38. *Countour plot of μ versus Normal pressure and testing Temperature*

CHAPTER 7

CONCLUSIONS

The present work aimed at investigating the interface conditions in sheet metal forming operations with particular interest to the following tribological systems:

- deep drawing of stainless steel sheet
- hot stamping of quenchable Al-Si coated HSS sheets

To characterize the prevailing lubricating mechanism taking place at the sheet metal/die interface simulative testing approach was pursued. Post test characterization using surface analysis technique such as SEM, EDX, WLI, profilometer and optical microscopy has been necessary to evaluate the tribological properties of the tribo surfaces

The first system has been studied by means of an ad hoc experimental device, capable of performing the flat drawing test, completely design and set up at DIMEG, University of Padova within the Phd period.
The case study refers to the deep drawing operation of a 0.38mm thick stainless steel sheet (X5 CrNi 1810 – 2R) while the dies are made of K 340. In the actual process conditions the lubrication is performed by a conventional oil. The tribological performance of the oil was compared with the one of two alternative solid lubricants: PVD coatings deposited on the die side and organic coatings deposited on the sheet metal side. The following conclusions can be drawn:

- The oil lubrication is significantly affected by the sliding speed, for v≥10mm/s an hydrodynamic lubrication regime is assured. The sheet metal temperature should not be higher than 80°C in order to avoid a shift from a mixed to a boundary type of lubricating mechanism. While an increased in the tool temperature caused an increase of the 50% of the friction coefficient already for a temperarture of 40°C but for higher tool temperatures it remains stable

- The alternative inhorganic solid lubricant systems CrN and CrNDLC showed a worse tribological performance than the non coated dies. This result is mainly due to the higher coating surface roughness which causes and increases of the asperities contact thus friction. Thus the as deposited coating should be post-polished.

- The organic coatings (Coating A and Coating B) did show a great potential to perform dry sheet metal forming operations. The main difference between the two of them consists in the chemical composition of th einhorganic part and the percentage of the organic part.

- Both of them presented a quite stable frictional behavior as no significandependence of the friction coefficient on both the normal pressure and the slidingspeed was observed. Coating B was characterized by an average coefficient of friction (μ=0.06) comparable to the one shown by the oil (μ=0.06). The prevailinglubrication mechanism was the interface sliding as not material transfer from the coating to the die surface could be evidenced. Interesting results were obtained when the sheet metal specimen was heated up with the temperature range 40°C≤TSHEET METAL≤120°C. Both the coatings did show the same tendency. At the lowest temperature the friction coefficient decreased At a temperature of 80°C the friction increased while at 120°C μ decreased probably as consequence of change in the lubrication mechanism from interface sliding to intrafilm sliding. The

organic part (wax) is partially melted and transfer to the die surface thus giving origin to a self-lubricating concept which could be of great interest from an industrial viewpoint.

Concerning the hot stamping of Al-Si coated boron HSS sheets the present work gives a significant contribute in trying to understanding the lubrication mechanism taking place at the AlSi coated sheet metal/die interface:

- holding time does influence the coating morphology and chemical composition: the shorter the holding time the less the coating is able to develop the five layers structure thus its surface topography is not characterized by nodule like features. While the cooling rate does not affect at all both the coating morphology and chemical composition.

- The interaction between normal pressure and testing temperature affect the frictional behaviour: For low values of normal pressure the friction decreases as the temperature increases, while for low temperature values the μ value decreases as the normal pressure increases. This relation permitted the suggestion of a process window to reduce friction in hot stamping operations.

REFERENCES

[1]. S. Kalpakjian, “Recent Progress in Metal Forming Tribology”, J. Applied metal working, Vol. 4, N°3, July 1986.

[2]. Design of tools for deformation processes, edited by T.Z. Blazynski, Chapetr 6, “Friction and tools”, Book

[3]. ASM HANDBOOK, Friction, Lubrication and Wear Technology, volume 18.

[4]. D.D. Olsson, “Limits of lubrication in sheet metal forming of stainless steel”, Phd thesis, Department of manufacturing and Management, Technical University of Denmark.

[5]. Schey, J.A., Tribology in Metalworking. Friction, Lubrication and Wear, American Society for Metals, USA, 1983.

[6]. S. Kalpakjian, “Manufacturing processes for Engineering Materials”

[7]. http://en.wikipedia.org/wiki/Viscosity

[8]. A. Azushima, “Direct Observation of Contact Behaviour to Interpret the Pressure Dependence of the Coefficient of Friction in Sheet Metal Forming, Annals of the CIRP, Vol. 44,1, 1995, pp. 209-212

[9]. Modern Tribology Handbook, Volume two, Editor in chief Bharat bhushan

[10]. I. L. Singer and H. M. Pollock, Fundamentals of Friction: Macroscopic and Microscopic Processes, pp. 237-261.

[11]. K. Holmberg et all, K. Holmberg, A. Matthews and H. Ronkainen, “Coatings tribology-contact mechanisms and surface design”, Tribology International Volume 31 Numbers (1998) 1-3,

[12]. Ronkainen H., Holmberg K., Francey K.S, Matthews A., Matthes B. and Broszeit E., Comparative tribological and adhesion studies of some titanium-based ceramics coating, Surf. Coat. Technol., 43/44, 888.

[13]. A. Erdemir, C. Bindal, G. R. Fenske and C. Zuicker, Characterization of transfer layers forming on surfaces sliding against diamond like carbon, Surf. Coat. Technol, 1996, 86/87, pp. 692-697.

[14]. Y. Liu, A. Erdemir and E. I: Metelis, An investigation of the relationship between graphitization and frictional behavior of DLC coatings, Int. Conf. Metallurgical Coatings and Thin Films, 22-26, April 1996, San Diego

[15]. A. Erdemir, C. Bindak, J. Pagan, and P. Wilbur, Characterization of transfer layer on steel surfaces sliding against diamond-like hydrocarbon films in dry nitrogen, Surf. Coat. Technol., 76/77, 1995, pp. 559-563

[16]. Singer I.L, How third-body process affects friction and wear, MRS Bull, June, 37-40, 1998.

[17]. K. Holmberg, A. Mathews, “Coatings tribology: a concept, critical aspects and future directions”, Thin Solid Films 253 (1994) 173-178

[18]. Gee M. and Jenett N.M., “High resolution characterization of tribochemical films on alumina”, Wear, 193, 133-145, 1995.

[19]. Lin J.F., Liu M.H. and Wu J.D., “Analysis of the friction and wear mechanism of structural ceramic coatings. The effect of operating conditions and substrate material”, Wear, 198, 7-14, 1996b, Wear , 198, 7-14, 1996b

[20]. D. Nèlias, M.L: Campiot, F. Vincent, D. Girodin, R. Fougères and L. Flamand, “Role of inclusions, surface roughness and operating conditions in rolling contact fatigue”, J. Tribol. Trans. ASMR, 121, 240-251, 1999.

[21]. Oliveira S.A.G. and Bower A.F., “An analysis of fracture and delamination in thin coatings subject to contact loading, Wear, 198, pp.15-32, 1996.

[22]. Hwang, D.H., Kim D.E., and Lee S.J., “Influence of wear particle interaction in the sliding interface on friction of metals”, Wear, 225/229, 427-439, 1999

[23]. Sin H., Saka N., and Suh N.P.,”Abrasive wear mechanisms and the grit size effect, wear”, 55, 163-190, 1979

[24]. Yamada Y., Tanaka K., and Saito K., “Friction and damage of coatings formed by sputtering polytetrafluoroethylene and polymide”, Surf. Coat. Technol., 43/44, 618-628, 1990

[25]. Suh N.P., “The delamination theory of wear”, Wear, 25, 111-124, 1973

[26]. Yuan F., and Hayashi K., “Influence of the grain size of the aluminium coating crack initiation in indentation”, Wear, 225/229, 83-89, 1999.

[27]. Huang Z.P., Sun Y., and Bell T., “Friction behaviour of TiN, CrN and (TiAl) coatings”, Wear, 173, 13-20, 1994.

[28]. S. Ramalingam and Lanshi Zheng, “Film-substrate interface stresses and their role in the tribological performance of surface coatings”, Tribology Infernational Vol. 28, No. 3, pp. 145-161. 1995

[29]. J. Gunnars et all, A. Alahelisten, “Thermal stresses in diamond coatings and their influence on coating wear and failure”, Surface and Coatings Technology 80 (1996) 303-312

[30]. B. Podgornik, S. Hogmark, O. Sandberg, “Proper coating selection for improved galling performance of forming tool steel”, , Wear 261 (2006) 15-21.

[31]. B. Podgornik, S. Hogmark, O. Sandberg, “Influence of surface roughness and coating type on the galling properties of coated forming tools”, Surf. Coat. Technol., 184, 2004, pp. 338-348

[32]. B. Podgornik, S. Hogmark, “Surface modification to improve friction and galling properties of forming tools”, Journal of Materials Processing Technology 174 (2006) 334–341

[33]. K. Vercammenn, H. Haefke, Y. Gerbig, A. Van Hulsel, E. Plüger, J. Meneve, “A comparatively study of state-of-the art diamond like carbon films”, Surface and Coatings Technology 133 – 134 (2000) 466 – 472

[34]. C. Donnet, A. Grill, “Friction control of diamond like carbon coatings”, Surface and Coatings Technology 94-95 (1997)456-462

[35]. M. Murakawa and S. Takeuci, “Evaluation of tribological properties of DLC films used in sheet forming of aluminium sheet”, Surf and Coat. Technol, 163-164, 2003, 561-565.

[36]. M. Murakawa, N. Koga and T. Kumagai, “Deep drawing of aluminium sheets without lubricant by use of diamond-like carbon coated dies”, Surf and Coat. Technol, 76-77, 1995, 553-558

[37]. K. Taube, “Carbon based coatings for dry sheet metal-working”, Siurf and Coat. Technol, 98, 1998, 976-984.

[38]. P. Carlsson and M. Olsson, “PVD Coatings for sheet metal forming processes, a tribological evaluation”, Surface & Coatings Technology 200 (2006) 4654– 4663

[39]. K. Hanada, K. Hatsukano, K. Matsuzaki, K. Umeda, M. Isshiwata, M. Tsukita, “Graphite coating of tool steel by pressure spraying”, Journal of Materials Processing Technology 164-165, (2005) 856-861

[40]. C.S. Ramesha et all, C.S. Ramesha, S.K. Seshadri, “Tribological characteristics of nickel based composite coatings”, Wear 255 (2003) 893–

[41]. T. Katsumi, Y. Miyauchi, K. Saito and H. Kanai, Iron and Steel Society/AIME (USA) 1995 pp. 449-453

[42]. Clint, J.H. “Surfactants: Application in Plastics.” Chapman & Hall, London: (1998)

[43]. s. Bahadur, “The development of transfer layers and their role in polymer trybology”, Wear, 245, 2000, pp. 92-99

[44]. T. Tanaka, “Transfer of semicrystalline polymers sliding against a smooth steel surface”, Wear, 75, 1982, pp.183-189

[45]. T. C. Vaert and S. Ramachandra, “The effect of controlled counterface topography on polymer transfer and wear”, Int. J. of Machine Tools and Manufacture, 35, 1995, pp. 311-316

[46]. G. Jintang, “Tribochemical effects in formation of polymer transfer film2, Wear 245, 2000, pp. 100-106

[47]. E. Santner, and h. Czichos, “Tribology of polymers”, Tribology International, 22, 1989, pp. 103-109.

[48]. P. Carlsson, U. Bexell, M. Olsson , “Tribological behaviour of thin organic permanent coating deposited on hot-dip coated steel sheet- a laboratory study”, Surface and Coatings Technology, 132, 2000, pp.169-180.

[49]. P. Carlsson, U. Bexell, M. Olsson, “Friction and wear mechanisms of thin organic permanent coatings during sliding conditions”, Wear, 247, 2001, pp. 88–99.

[50]. P. Carlsson, U. Bexell, M. Olsson, “Tribological performance of thin organic coatings deposited on galvanized steel-influence of coating composition and thickness on friction and wear”, Wear, 251, 2001 pp. 1075–1084

[51]. U. Bexell, P. Carlsson and M. Olsson, “Tribological characterization of an organic coating by the use of ToF-SIMS”, Applied Surface Science, 203-204, 2003, pp. 596-599.

[52]. P. Carlsson, “Surface Engineering in Sheet Metal Forming”, Phd thesis, Uppsala Universitet, ISSN 1651-6214, ISBN 91-554-6136-0

[53]. R. Neugebeauer, T. Altan, M. Geiger, M. Kleiner and Sterzing A, “Sheet Metal Forming at Elevated Temperatures”, A. of the CIRP, Vol. 55, 2006, pp. 793-816.

[54]. K. Mori, S. Maki, Y. Tanaka, “Warm and Hot Stamping of Ultra High Tensile Strength Steel Sheets Using Resistance Heating”, Annals of the CIRP 54(1), 2005, pp. 209–212.

[55]. D. Lorenz and K. Roll, “Modelling and Analysis of Integrated Hot forming and quenching Processes”, Sheet Metal 2005 Conf.,Proc. (2005), pp. 787-794, 2005.

[56]. International Iron and Steel Institute, UltraLight Steel Auto Body - Advanced Vehicle Concepts (ULSAB-AVC) Overview Report (2002).

[57]. J. Wilsius, P. Hein, and R. Kefferstein, “Status and future trends of hot stamping of USIBOR 1500 P”, presented at Erlangen Workshop 2006.

[58]. D. Lorenz and K. Roll, “Simulation of Hot Stamping and Quenching of Boron alloyed Steel”, presented at 7th Int. ESAFORM Conf. on Mat. Forming, Trondheim, Norway, 2004.

[59]. T. Altan, “Hot-stamping boron-alloyed steels for automotive parts”, Stamping Journal, Part II: Microstructure, material strength changes during hot stamping, January 2007

[60]. T. Skåre, F. Krantz, “Wear and frictional behaviour of high strength steel in stamping monitored by acoustic emission technique”, Wear 255 (2003) 1471-1479

[61]. J. Hardell, B. Prakash, “High-temperature friction and wear behaviour of different tool steels during sliding against Al-Si-coated high strength steel”, Tribology International 41 (2008) 663-671

[62]. J. Hardell, E. Kossfeldt, B. Prakash, “Friction and wear behaviour of hight strength Boron steel at elevated temperatures of up 800°C”, Wear 264 (2008), pg. 788-799.

[63]. J. Hardell, B. Prakash and K. Steinhoff, “High temperature tribological studies on surface engineered tool steel and high strength boron steel”, Proceedings of The 2nd International Conference on Hot sheet Metal forming of High-performace steel (2009), CHS2, pp. 69-76.

[64]. A. Yanagida and A. Azushima, “Evaluation of coefficients of friction in hot stamping by hot flat drawing test”, CIRP Annals - Manufacturing Technology 58 (2009) 247–250

[65]. C. Dessain, P. Hein, J. Wilsius, L. Penazzi, C. Boher, and J. Weikert, “Experimental investigation of friction and wear in hot stamping of Usibor 1500P”, Proceedings of The 2nd International Conference on Hot sheet Metal forming of High-performace steel (2009), CHS2, pp. 217-226

[66]. T. Stoehr, M. Merkleín and J. Lechle, Determination of frictional and thermal characteristics for hof stomping with respect to a numerical process design, Proceedings of The 2nd International Conference on Hot sheet Metal forming of High-performace steel (2009), pp. 293-300

[67]. Geiger M., Merklein M., Lechler J., “Determination of tribological conditions within hot stamping”, Annals of the German Academic Society for Production Engineering (WGP), Vol. XVIII (2008) 2, accepted, available online.

[68]. M. Suehiro, J. Maki, K. Kusumi, M. Ohgami, T. Miyakoshi, “Properties of Aluminum-coated Steels for Hot-forming”, Nippon steel technical report N°.88, July 2003.

[69]. H. Cho, G. Ngaile, “Simulatneous Detremination of Flow stress and Interface Friction by Finite Element Based Inverse Analysis Technique”, CIRP ANNALS, MANUFACTURING TECHNOLOGY, 52, issue 1, 2003, pp. 221-224

[70]. M. Meiler, M. Pfestorf, M. Geiger, M. Merklein, “The use of dry lubricants in aluminium sheet metal forming”, Wear, 255, 2003, pp. 14551462.

[71]. S. Kataoka, M. Murakawa, T. Aizawa, H. Ike, “Tribology of dry deep-drawing of various metal sheets with use of ceramic tools”, Surf. and Coat. Technol, 177,-178, 2004, 582-590.

[72]. H. Kim, J. H. Sung, R. Sivakumar, T. Altan, “Evaluation of stamping lubricants, using deep drawing test”, Int. J. of Machine Tools and Manufacture, 47, 2007, pp. 2120-2132.

[73]. H. Cho, T. Altan, “Detremination of flow stress and interface friction at elevated temperatures by inverse analysis technique” J. of materials processing Technology, 170, 2005, pp. 64-70.

[74]. J. L. Andersen, N. Bay, M. Andersen, E. Christensen, N. Bjerrum, “Screening the performnce of lubricants fort the ironing of stainless steel with a strip reduction test”, Wear, 207, 1997, pp. 1-5

[75]. R. J. M. Sniekers, H. A. A. Smits, “Experimental set-up and data processing of the radial strip drawing friction test”, J of Materials Processing technology, 66, 1997, pp. 216-223

[76]. K. R. Gilmour, S. Paul, A. G. Leacock, “The influence of lubricant film thickness on friction coefficients during slow speed deep drawing operations”, J. of tribology, 124, 2002, pp. 846-851

[77]. P. Pesch, S. Sattel, S. Woestmann, P. Masarczyk, K. Herden, T. Stucky, A. Martens, S. Ulrich, H. Holleck, “Performance of hard coated steel tools for sheet drawing”, surface and Coating technology, 163-164, 2004, pp. 739-746

[78]. M. P. F. Sutcliffe, H. R. Le, D. Farrugia, “Simulation of transfer layer formation in strip drawing of stainless steel”, Wear, 354, 2003, 523-531.

[79]. J. L. Andreasen, D. D. Olsson, K. Chodnikiewicz, N. Bay, “Bending under tension test with direct friction measurement”, Proc. IMechE, Vol. 220 Part B, J. Engineering Manufacture, 2006, pp. 73-80.

[80]. A. Turetta, “Investigation of thermal, mechanical and microstructural properties of quenchable High Strength Steels in hot stamping operations”, Phd Thesis, 2008, university of Padova.

[81]. B. Griesbach, B. Oberpriller, “Simulation in tool and die shop”, Proceedings of Numisheet 2008, Interlaken, Switzerland

[82]. F. Borsetto, A. Ghiotti, S. Bruschi, “Investigation of the High Strength Steel Al-Si coating during hot stamping operations”, Key Engineering Materials Vols. 410-411 (2009) pp 289-296.